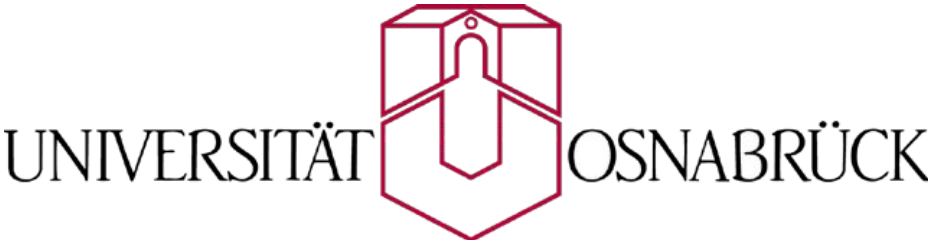

Photopatterning for probing protein-protein interactions in artificial model systems and live cells

Dissertation

Presented to the department of Biology/Chemistry, University of Osnabrueck in partial fulfillment of the requirements for the degree of *'Doctor Rerum Naturalium'*

Sharon Waichman

Osnabrueck
June 2012

…to my parents

Table of Contents

1 Introduction

1.1 General overview

Proteins are biological macromolecules that have versatile functions. These include the catalysis of chemical reactions, the transport of cellular cargos, the control over growth, proliferation and differentiation of cells and the communication across the plasma membrane. Proteins also have diverse functions in analytical and biotechnological applications. For instance, proteins are used as biological components in biosensors, as biomaterials for medical applications and as cargos in drug delivery systems. Proteins are polymers that are comprised amino-acids as monomeric units. The sequence of amino-acids constitutes the primary structure of a protein. However, most proteins do not exist as linear polymers but instead undergo folding into intricate three dimensional structures which ultimately determine their functions and properties. These structures can be organized in the following hierarchical order: (i) secondary structure, which is the organization of the polypeptide chain into helices structure, beta sheets or random coils, (ii) tertiary structure, which is the organization of different secondary structures present in a sequence of amino acids into a globular fold and (iii) quaternary structure, which is the organization of multiple folded proteins (tertiary structures) into a functional protein complex.

In spite of the tremendous advance in techniques available for characterization of protein functionality and interactions, there are still a vast number of proteins and processes that remain obscure. In this work, I established tools that assist in studying interactions and cellular mechanisms induced by cell surface receptors. These are proteins that are embedded in the plasma membrane (PM) through which information is transferred from the extracellular matrix into the interior of the cell and vice versa. Binding of extracellular proteins such as growth factors, cytokines and adhesion molecules to their cell surface receptors triggers different reactions across the plasma membrane and elicit cellular responses. Therefore, cell surface receptors play a key role in molecular recognition and signal transduction. For this reason, cell-surface receptors play a major role in drug discovery as evident from the fact that they function as targets of more than 60% of the drugs today [1]. Cell surface receptors are mostly

transmembrane proteins that span the membrane either once as in the case of cytokine receptors and receptor tyrosine kinases (RTKs), or several times for G protein-coupled receptors (GPCRs). In this thesis, cell surface receptors that contain a single α-helix were studied. These receptors are composed of three main parts as depicted in Figure 1-1:

(I) Extracellular (EC) domain – The part of the receptor that extends beyond the PM and exposed to the extracellular matrix (ECM) for interacting with its ligand.

(II) Transmembrane (TM) domain – This is an α-helical segment which exhibits hydrophobic nature. This segment is embedded in the PM and is responsible for the diffusion and interactions with the membrane.

(III) Intracellular (IC) domain – this part interact with species at the cytoplasm (such as effector proteins) through which downstream signaling is induced.

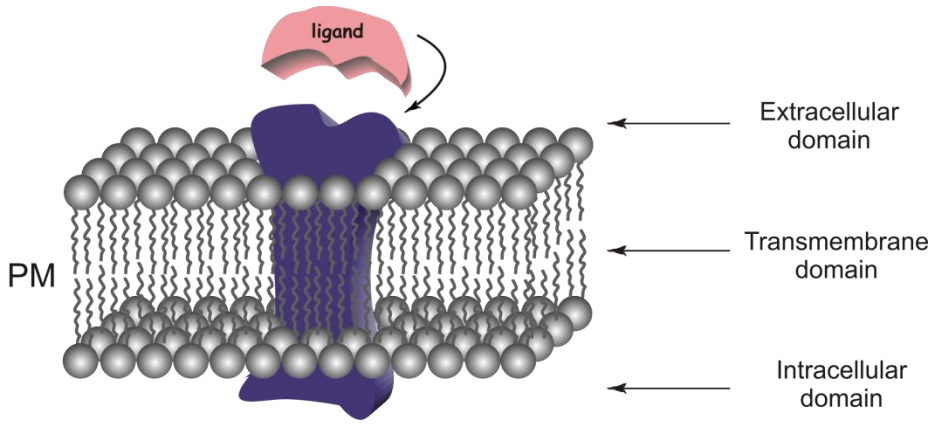

Figure 1-1. Cell surface receptor. The structure of a transmembrane protein can be divided into three parts: extracellular domain, transmembrane domain and intracellular domain.

1.1.1 Aims

It is a very challenging task to study the properties of entire cell surface receptors due to their complex structure. Therefore, by exploiting the modular structure of these proteins, I aimed at developing generic methods for analyzing functional aspects of the three domains separately. Towards this end, I devised techniques which could be used for the immobilization of the different protein domains on suitable solid supports and moreover, could be readily combined with state-of-the-art microscopic and spectroscopic methods. The fundamental requirement from such methods is that they preserve the functionality of the investigated proteins to a high

degree. Thus the protein immobilization methods devised were based on (i) biocompatible polymer coatings that abrogate non-specific protein interactions with the support and ensure the structural integrity of the immobilized proteins and (ii) efficient chemistry for site-specific protein immobilization through proteins or peptide tags which can be genetically fused to the proteins of interest. Moreover, these methods were amenable to photolithographic micropatterning allowing biophysical analysis using ensemble and single molecule techniques.

These methods were customized for probing different functions of the three domains of a transmembrane protein:

(I) Artificial model systems:

- Site-specific protein immobilization system for probing interactions between the extracellular domain of receptor subunits and their ligand (Figure 1-2a) which is presented in chapter 2. In addition, such biocompatible systems were coupled with selective chemistry for targeting proteins into micrpatterns and will be discussed in chapter 3.
- Lipid membrane based system, in which recombinantly expressed cell surface receptor segments consisting of their extracellular and transmembrane domains could be accommodated for characterization of protein diffusion and interactions in micropatterns (Figure 1-2b). This system is introduced in chapter 4.

(II) Live cells based system, from which selective capturing of cell-surface receptors in micropatterns was carried out for probing interactions with their extracellular and intracellular binding partners (Figure 1-2c). The system is demonstrated in chapter 5.

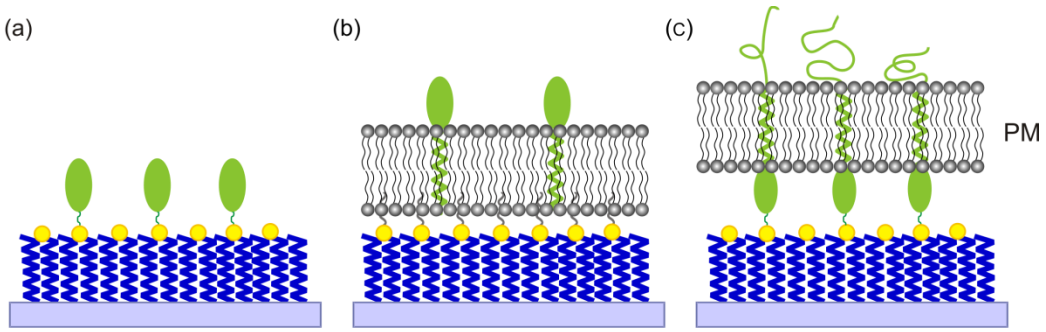

Figure 1-2. Versatile biocompatible systems employed for probing protein-protein interactions where (a) the extracellular domain of the receptor was immobilized; (b) the transmembrane domain was incorporated into a lipid-bilayer; and (c) full length cell surface receptors were captured onto surfaces directly from live cells.

1.2 Protein immobilization

Immobilization of proteins on solid supports is highly essential for different purposes in fields including biotechnology [2], biomedical engineering [3], drug development and delivery [4], energy storage systems [5, 6], electronic devices [7] etc. A fundamental criterion which determines the applicability of the immobilization method is to retain protein functionality. Thus, the challenge of immobilizing proteins on solid supports is to preserve their structural integrity and therefore to prevent loss of function. Hence, rendering surfaces biocompatible is a prerequisite for their application with proteins. To this end, different approaches employing flexible compounds and polymer cushions were developed. These include the utility of dendrimers [8], hydrogels [9, 10] and poly(ethylene) glycol (PEG) coatings [11] as biocompatible scaffolds. In addition to a biocompatible layer, functionalizing surfaces with chemical moieties presenting selective groups for site-specific attachment is necessary in order to ensure optimal orientation of the immobilized proteins. In this fashion, conformational changes of proteins due to immobilization are efficiently reduced and the protein active site is freely accessible to interaction partners. The conditions for an adequate protein immobilization approach as mentioned above are summarized in Figure 1-3.

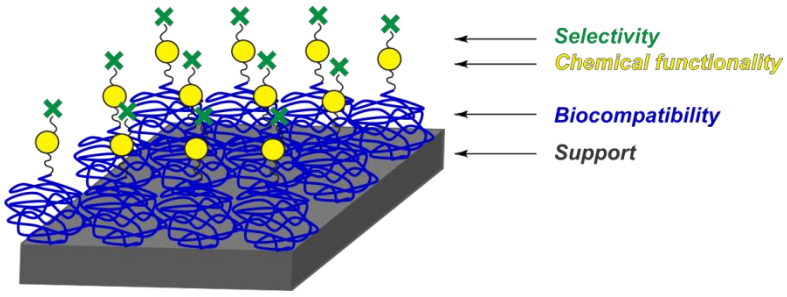

Figure 1-3. Prerequisites for site-specific immobilization of proteins: A solid support compatible with the detection techniques applied (grey), a biocompatible scaffold (blue), chemical moieties (yellow) with selective groups (green) for protein immobilization.

Exploiting an efficient protein immobilization method which enables capturing of proteins from cell lysates is an eminent advantage solving the need for protein purification. In this regard, efficient immobilization techniques must be bioorthogonal [12] in order to reliably probe interactions between proteins. Moreover, bioorthogonal strategies allow the investigation of biological processes considering selective attachment of membrane proteins onto surfaces directly from live cells. This way we can avoid purification and conduct functional studies in the native environment of the proteins.

1.2.1 Substrates

Detection of materials on solid supports can be carried out using a variety of techniques. The fundamental requirement for surface detection and characterization is the utility of a substrate that has compatible properties with the technique applied. The following substrates are commonly employed using detection techniques:

Silica-based substrates

- Glass – a noncrystalline material, transparent to visible light and have high surface homogeneity. Thus compatible with techniques such as optical microscopy, atomic force microscopy (AFM) and reflectance interference spectroscopy (RIfS).
- Quartz – a crystalline substance which has a very low absorption at the ultra-violet (UV), visible and near infra-red (NIR) range. Compatible with optical techniques and with AFM.
- Silicon – a crystalline material which absorbs light in a wide range of wavelengths: UV, visible and near NIR. Silicon surfaces are homogeneous and hence they are suitable with

techniques such as atomic force microscopy and ellipsometry. Due to the high transparency at the middle IR (MIR) region, it is also suitable for characterization using Fourier transform infra-red (FTIR).

- Mica – silicate-based crystal presenting a layered structure. Highly suitable using AFM due to its flatness and smoothness.

Gold-based substrates

A transition metal, stable under harsh conditions and interact in a semi-covalent manner with thiols. Alkyl-thiols (up to ~20 carbons) react with gold substrates to form self-assembled monolayer (SAM), a stable and highly ordered layer. Utilizing their electrical properties, gold surfaces are highly compatible with techniques such as surface plasmon resonance (SPR) and scanning electron microscopy (SEM). Other techniques include atomic force microscopy and FTIR.

1.2.2 Biocompatibility

The concept of biocompatibility was frequently associated with implant technology for which biomaterials with specific properties were developed and integrated into medical devices. These materials must be non-toxic, non-immunogenic, non-carcinogenic and must be free of hazard risks in order to be in contact with a biological system [13]. Nowadays the concept of biocompatibility has greatly expanded to include a wide variety of applications, which utilize synthetic materials such as polymers that maintain the biological integrity of the investigated system. Polymer chains that are densely tethered to a solid-support can induce the formation of a polymer 'brush' layer. Beyond a certain density, a force is exerted on the chains to stretch away from the surface and to avoid overlapping, a process which is accompanied with the loss of entropy. This effect is similar to bristles in a brush and is therefore denoted as 'brush' conformation [14]. The following requirements for a polymer brush conformation [15] are depicted in Figure 1-4:

(a) The height of the brush has to be larger than the end-to-end distance of the polymer in its free confirmation.

$h > \langle r^2 \rangle^{\frac{1}{2}}$ Where *h* is the 'brush' height and *r* is the end-to-end distance.

(b) The distance of two tethering points is smaller than the end-to-end distance of the polymer.

$d < \langle r^2 \rangle^{\frac{1}{2}}$ Where *d* is the distance between tethering points and *r* is the end-to-end distance.

In case that the density of the polymer is not sufficient to fulfill these requirements two conformations are possible [16]:

- 'Pancake' conformation, in which the polymer presents attractive forces with the surface.
- 'Mushroom' conformation, in which the polymer-surface interactions are non-attractive.

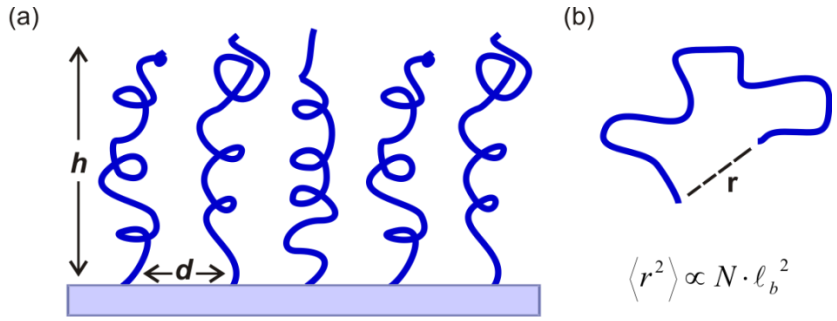

Figure 1-4. Schematic representation of polymer in its free and brush conformations. (a) Polymer brush tethered to a solid support. *h* – height of the polymer brush, *d* – distance between two tethering points. (b) Polymer conformation according to the freely jointed chain model. *r* – distance between the end points, *N* – number of bonds and ℓ_b – length of the bond.

A polymer that meets the requirements for biocompatibility is PEG, which comprises ether moieties as building blocks. PEG is soluble in aqueous solutions as well as organic solvents, which therefore designate PEG as a suitable material for surface modification. The solubility of PEG in aqueous solutions is not a common feature of polyethers and was assigned to the ability of the ether oxygen in this case to form hydrogen bond with the water molecules. The role of water in such systems was analyzed using a structural model, in which the entropy and enthalpy change of the system were explained by the enhanced water structure around the polymer chain [17]. In the context of protein immobilization, PEG layers provide an adequate support for biological molecules due to their protein repulsive properties. Thus, PEG inhibits non-specific interactions of proteins with the support. Investigation of the unique protein-

repellent feature presented by PEG coated substrates, brought up several hypotheses. For instance, the hydrated polymer hampers the adsorption of proteins, considering water displacement from the polymer as energetically unfavorable [18]. Several models were used to explain the parameters that affect biocompatibility in order to allow suitable modification of surfaces for studying biological systems [19, 20]. A recent model suggests that interaction of a particle (protein) with a polymer brush is accompanied by a loss in conformational entropy, which leads to an increase in interaction energy (the energy required to move the particle into the polymer chains). Therefore, the major effect contributing to protein resistivity is the polymer flexibility, which provides higher degree of freedom and thus high conformational entropy [21].

1.2.3 Chemical functionality

Strategies for stable surface functionalization on biocompatible supports have a great importance in probing biological systems. In contrast to chemical reactions carried out in solutions, the degrees of freedom of the interacting molecules are reduced on the surface and therefore the efficiency of the reaction is reduced. By applying selective and covalent coupling of chemical functionalities, we introduce not only diverse protein capturing groups but we also ensure specific protein orientation for increasing the reaction efficiency. An example for such method relies upon the utility of azides: the 1,3-dipolar cycloaddition that was meticulously studied by Huisgen and afterwards was acquainted as “click” chemistry [22]. The term “click” refers to reactions that occur specifically and rapidly to obtain a stable linkage between chemical moieties under ambient conditions. In addition to the conventional “click” chemistry, nowadays “click” based reactions also include the interaction of thiols with maleimide groups, [23] the thiol-ene reaction [24] (olefin groups are coupled to thiol functionalized surfaces by a photochemical reaction) and the Diels-Alder ligation[25] (the cycloaddition of a conjugated diene to a dienofile). The chemical strategies discussed are highly efficient for surface functionalization and can be utilized for direct protein immobilization as well.

1.2.4 Protein immobilization strategies

It is possible to classify the main protein immobilization approaches into two categories: (I) random and (II) site-specific immobilization.

Random immobilization

Immobilization of proteins in a non-specific fashion can be carried out via:

(i) Physical adsorption of proteins to surfaces by hydrophobic or electrostatic interactions. These forces are essential for preserving the structural integrity and the conformations of the proteins and therefore non-specific adsorption to the support may cause protein denaturation and loss of function.

(ii) Chemical coupling of proteins to surfaces through exposed amino acid residues such as lysines and cysteines. This is not performed in a controlled fashion, suffers from instability, and may increase the probability for randomly oriented proteins. In this case, the proteins may be attached to the support by reactions with their active sites which are required to carry out their functions and therefore result in the reduction of their biological activity [26, 27].

For this purpose, efficient immobilization strategies, which are based on stable and selective binding approaches, are required in order to retain the structural integrity and functionality of the immobilized protein.

Site-specific immobilization

The pivotal principle standing behind the utility of highly selective protein immobilization methods is the site-specific protein attachment, which plays a key role in preserving protein functionality [28]. A traditional method for protein immobilization is based on attachment of monoclonal antibodies (mAbs) to surfaces as capturing groups for targeting proteins. In addition to their highly stable nature, mAbs specifically recognize their substrate proteins. However, applications based on mAbs for protein immobilization require the production of mAbs to each target protein which is a highly demanding task. Thus, the availability of mAbs is limited and therefore the applicability of this strategy as a generic approach is restricted. In addition, mAbs are large in size (~150 kDa) and therefore may hamper further interactions with

the binding partners of the proteins attached to the Abs. Hence, other strategies based on selective biochemical functionalities were developed. For instance, small proteins (~20-35 kDa) fused to the target protein can be used for site-specific attachment. Such methods include the cutinase protein which is a serine esterase [29]. The catalytic serine residue in the cutinase attacks phosphonate moieties immobilized on a solid support following by the covalent attachment of the protein of interest [30, 31]. SNAP-tag [32], is the human DNA repair O^6-alkylguanine-DNA alkyltransferase that forms a covalent adduct with O^6-benzylguanine (BG) substrate [32-34]. An alternative approach is based on the HaloTag protein (HTP), a haloalkane dehalogenase, which will be discussed later on. However, these proteins are still large when comparing to peptide tags such as His- and ybbR- tags that will be discussed in more detail later in this chapter. The benefit of using short peptide tags emanates from the necessity to preserve the biological activity of the target proteins. In order to maintain the active site of the protein freely accessible for further interactions it is important to avoid any possible hindrance. To this end, the design of short peptide tags is of a great importance. In the current work, I employed protein immobilization methods based on biomolecular interactions for selective coupling of proteins to a solid-support. The methods can be applied via two types of interactions: (I) non-covalent (affinity) and (II) covalent based- immobilization.

Non-covalent immobilization

This type of interactions depends on the degree of attraction between the moieties involved in the bond formation which determines the possibility for the binding to occur in a reversible manner.

Tris- nitrilotriacetic-acid

A highly attractive method for reversible immobilization relies upon the interaction of nitrilotriacetic-acid (NTA) as a chelator head to a polyhistidine peptide (His-tag) mediated by Ni^{2+}. Transition metal ions form a coordination complex with atoms/molecules denoted as ligands. Four of the six coordination sites of Ni^{2+} can be filled by NTA leaving two coordination sites free for other ligands such as histidine residues from proteins (Figure 1-5a). A common

utility of this interaction was the purification of recombinant proteins with oligohistidine tags [35, 36], which has been extended for protein immobilization as well [37, 38]. Further addition of one (bis-NTA) or two NTA (tris-NTA) moieties, as demonstrated in Figure 1-5b, to obtain multivalent chelator heads (MCH) emerged to result in increased binding stability of the immobilized protein [39]. Association rate constant of $\sim 10^{5}\ M^{-1}s^{-1}$ and dissociation rate constant of $\sim 10^{-5}\ s^{-1}$ were determined for a tris-NTA chelator head and a decahistidine complex. In Figure 1-5c, His-tagged protein is specifically captured onto a tris-NTA functionalized solid support. A subsequent removal of a stably bound protein is carried out using buffer containing imidazole as a competitor. Furthermore, displacement of metal ions is performed by introducing ethylenediaminetetraacetic acid (EDTA) to the system. Hence, a complete regeneration of the tris-NTA moieties can be achieved. Several applications using MCH, particularly tris-NTA were shown to be highly suitable for probing protein interactions [40], conformational studies [41] and surface properties [42] by employing different techniques.

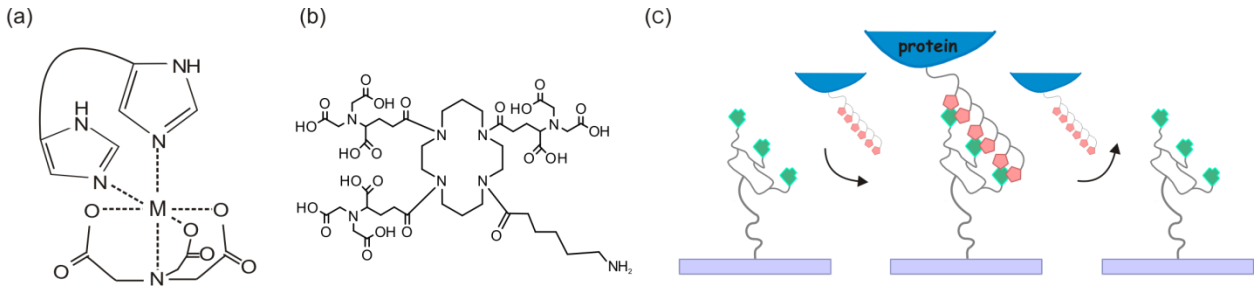

Figure 1-5. Reversible protein immobilization based on NTA chelator head and His-tagged protein. (a) NTA chelator head selectively binds to His-tag in the presence of metal ions. (b) Structure of tris-NTA. (c) Protein immobilization on a surface functionalized with tris-NTA. Protein removal is possible through imidazole wash.

Biotin-streptavidin

An immobilization strategy which is considered almost irreversible is based on biotin/(strept)avidin interactions. Streptavidin (SAv) is a tetrameric protein (each monomer has a beta barrel structure) that was isolated from *Streptomyces* culture and can bind biotin (BT) in a very strong manner with molecular binding ratio of four BT molecules to one SAv [43]. An association rate constant of $3\times10^{6} - 4.5\times10^{7}\ M^{-1}s^{-1}$ was previously reported [44] and a dissociation rate constant of $\sim 10^{-6}\ s^{-1}$ [45]. It was recently demonstrated that it is possible to

break the interaction in conditions that prevent the SAv from denaturation, thus allowing reversible protein capture using this strategy [46]. The tight interaction of BT/SAv is mainly attributed to the formation of hydrogen-bonding network between the urea moiety in the BT and several residues in SAv that induce the polarization of the ureido group. This leads to a cooperative effect that provides the unique stability of the interaction [47, 48]. Additional effects that might contribute to the strong BT/SAv interaction can be related to the van der Waals forces formed due to the contact with tryptophan residues in the binding pocket and the presence of a flexible 3-4 loop that assists in removing water molecules from the binding site [47]. This loop is tightly closed on top of the biotin binding pocket preventing it from escape and therefore contributing to the complex stability [49]. SAv is highly resistant to degradation by proteolytic enzymes and is stable at broad pH and temperature ranges [43]. For this reason, many applications relying upon the interaction of BT and SAv have been developed. A common application of BT/SAv complex is the immobilization of proteins on solid supports as illustrated in Figure 1-6 [50-52]. For this purpose, a site-specific biotinylation of the protein of interest is required. This can be carried out by enzymatic ligation of biotin to an 'acceptor peptide' (AP) tag which is fused to the protein of interest. The biotin moiety is then attached to the amine of the lysine residue in the AP tag to form an amide bond via the catalysis of the biotin ligase BirA [53].

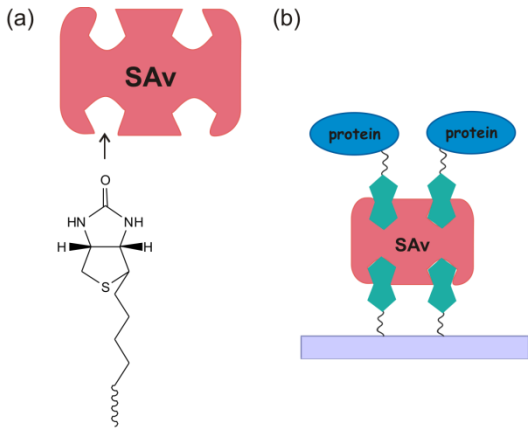

Figure 1-6. BT/SAv high affinity interaction. (a) Tetrameric SAv can accommodate four molecules of BT. (b) Protein immobilization on solid support through BT/SAv complex formation.

Covalent immobilization

Owing to the growing demand of covalent strategies for stable and reliable attachment of proteins on biocompatible supports yet maintaining their activity, site-specific immobilization methods were developed. Protein immobilization that is mediated by biomolecular interactions can be carried out through a small protein or a peptide 'tag' which is fused to the protein of interest as discussed in the introduction of this section.

HaloTag

HaloTag protein (HTP) is an engineered 34 kDa haloalkane dehalogenase from *Rhodococcus* (DhaA). Haloalkane dehalogenases are responsible for halogen abstraction from a molecule/compound. The reaction mechanism is based on a nucleophilic attack of an aspartate residue (Asp^{106}) of the protein, on a chloroalkane substrate which causes the removal of the chloride from the alkyl chain and the formation of an ester bond. In order to avoid a base hydrolysis mediated by the histidine residue (His^{272}) located near Asp^{106} in the enzyme, DhaA was mutated (DhaA.H272F) to stabilize the bond. Further mutations were needed to in order to improve binding kinetics. Eventually, an on rate constant of ~ 10^6 $s^{-1}M^{-1}$ using haloalkane-TMR ligands was obtained. Moreover, the chloroalkane - HaloTag ligand (HTL) was designed according to the structural constraints of the HPT. The catalytic site is located 15 Å away from the protein surface therefore a flexible linker 14 atoms long including 6 carbon atoms directly connected to the terminal chlorine was synthesized [54]. The chemical reaction is shown in Figure 1-7.

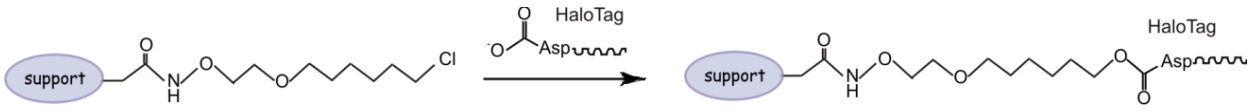

Figure 1-7. Chemical reaction of HTP with HTL functionalized solid support to give a stable covalent adduct.

The HTL can be conjugated to a variety of functional groups such as fluorescent probes, affinity handles and solid supports [54]. This labeling and immobilization method was utilized for *in vitro* labeling of proteins with quantum dots [55] or *in vivo* targeting of proteins in live cells with fluorescent nanoparticles [56]. During the investigation of the latter it was observed that the

association kinetics strongly depends on the nature of the functional group conjugated to the HTL. Utilizing groups containing hydrophobic and positively charged residues lead to an increase of the association rate constant [56].

Phosphopantetheinyl transfer reaction

This approach is based on phosphopantetheinylation, a reaction which is essential for the synthesis of fatty acids, polyketides, non-ribosomal peptides etc [57]. The activation of fatty acid synthases, polyketide synthases and non-ribosomal synthetases is based on the modification of their acyl carrier protein (ACP) domains (for fatty acids and polyketides formation) or peptidyl carrier protein (PCP) domains (for non-ribosomal peptides). In nature, carrier protein (CP) domains are subjected to the catalysis of phosphopantetheinyl tranferases (PPTases), through which the prosthetic group 4'-phosphopantetheine (P-pant) is transferred from coenzyme A (CoA) to a hydroxyl group of a specific serine residue at the protein. This results in the conversion of the protein from its inactive apo-form to an active holo-form (Figure 1-8). Subsequently, a nucleophilic reaction takes place via the thiol of the cysteamine group at the P-pant which results in acylation [58].

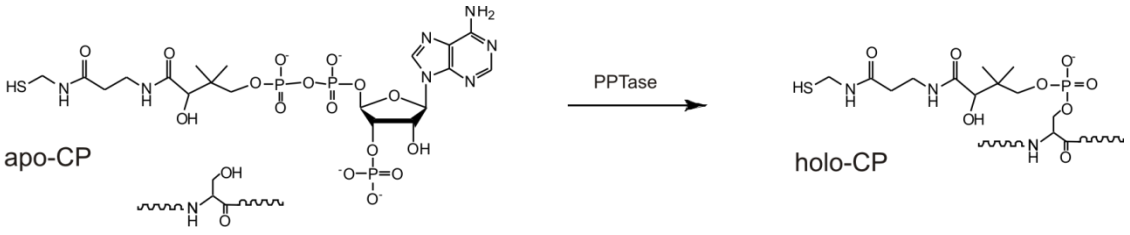

Figure 1-8. Phosphopantetheinylation reaction. The conversion of a protein from its apo-form to holo-form is mediated by a PPTase.

Different PPTases were discovered and characterized. At first the ACP synthase (ACPS), which is responsible for posttranslational modification in *Escherichia coli (E.coli)* was investigated. ACPS unveiled high selectivity to ACP domains and could not activate PCP domains. Therefore another family of PPTases was studied and EntD from *E.coli* and Sfp from *Bacillus subtilis* (*B. subtilis*) were discovered [58]. PPTases were classified into three groups [59]: (i) ACPS, which is involved in the synthesis of fatty acids of prokaryotes. (ii) FAS2, which is the fatty acid synthase in eukaryotes and (iii) Sfp, which catalyses the posttranslational modification in surfactin

synthetase and is able to recognize different carrier protein substrates at the presence of divalent metal ions. The name Sfp is derived from the gene *sfp* which is responsible for *sur*factin *p*roduction [60, 61]. A suggested hypothesis for the difference in CP substrate recognition of ACPS and Sfp results from structural and mutational analyses from which it was claimed that Sfp can bind to different substrates by means of a flexible loop through which the protein can be accommodated. In contrast, ACPS contains a rigid helix that is exclusively suitable for ACP recognition [59]. These enzymatic reactions have been employed for selective labeling of cell surface proteins with diverse compounds [62-65]. In spite of the small size of CPs (8-10 kDa) as compared with other protein tags, as discussed at the introduction of this section, the CPs are still large enough and may hamper accessibility for the interaction of the fused protein with its substrate by steric hindrance and may affect the biological activity. For this purpose, a short peptide tag comprising 11-residues was developed. This tag is fused to the protein of interest and exhibits high efficiency reaction with CoA in the presence of Sfp and divalent metal ions. The N-terminal half of the tag was derived from a certain sequence called *ybbR* at the open reading frame (ORF) of the *B. subtilis* genome and therefore the peptide was also named ybbR-tag. Labeling with small molecules using this technique has been shown to be efficient when the tag is fused to the N and C termini of several proteins. Moreover, labeling was even possible when the tag was inserted into a flexible loop at the middle of a protein [66]. The peptide sequence identified is DSLEFIASKLA with the conserved serine residue underlined. The tripeptide DSL was identified as a significant unit for Sfp recognition. It exists in the PCP sequence as well, however additional residues which are considered to be essential, are missing in the ybbR. The catalytic efficiency observed using this tag is $\sim 1.5 \times 10^3\ M^{-1}s^{-1}$ [66]. This labeling technique was successfully utilized for site-specific immobilization of proteins on solid supports [67]. Additional short peptide tags A1 and S6 were developed for orthogonal labeling. A1 and S6 are composed of 12 residues each, and can be recognized by ACPS and Sfp, respectively. The DSL sequence was preserved, however with an additional glycine at the N-terminus. Using S6 as a tagging system in the presence of Sfp the catalytic efficiency observed is twice as high as for the ybbR [68]. Labeling of proteins fused to S6 and A1 were successfully employed on different proteins [69]. The size of the peptide tag necessary for Sfp recognition was further decreased

and the minimal tag obtained- A-4, was constructed of 8 residues which is very similar in size to the His-tag and the FLAG-tag.

Based on the diverse methods and strategies discussed previously, we devised a bottom-up surface chemical approach for selective immobilization of proteins as demonstrated in Figure 1-9. Activation of glass substrate was carried out through silane compounds containing epoxide groups, followed by surface passivation using PEG in order to obtain a biocompatible system (I) [11]. Since PEG inhibits interactions of proteins with the support, chemical functionalities for efficient coupling of proteins and for surface photopatterning (as will be discussed later in this chapter) are required. For this purpose, surfaces were functionalized with maleimide moieties for further reaction with highly selective thiol-functionalized capturing groups in a "click" chemistry manner (II).

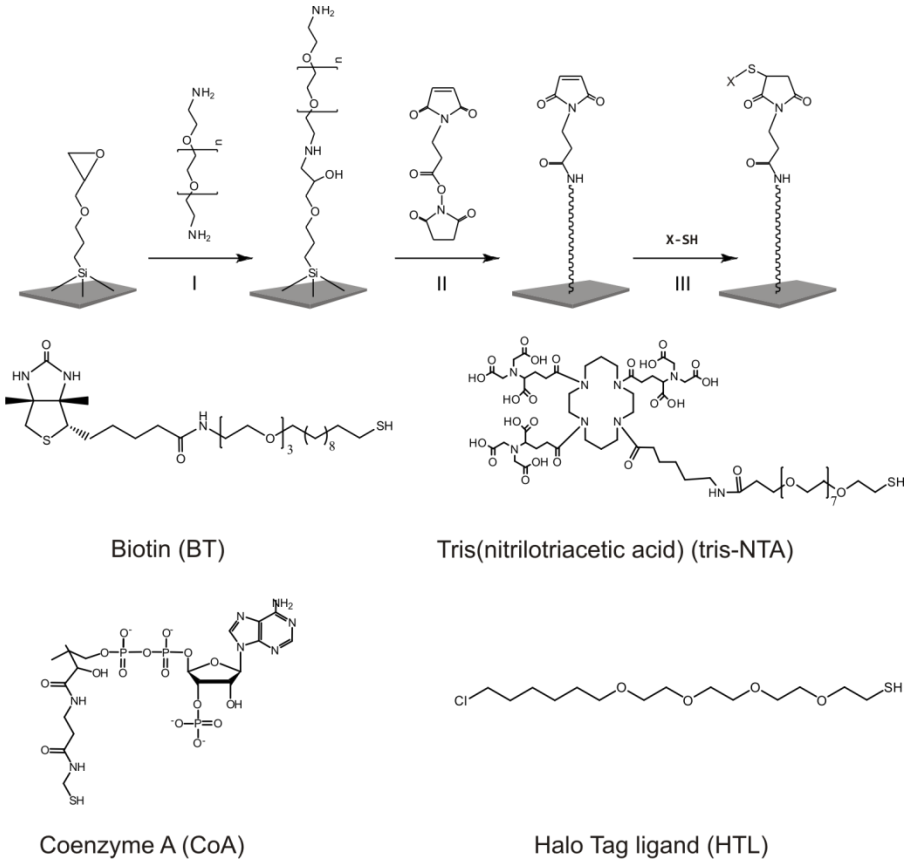

Figure 1-9. Surface modification and functionalization. After activation of a glass support, surface rendered biocompatible using PEG (I). Subsequently, the surface was reacted with MPA-NHS (II) for further functionalization of various selective groups for site-specific immobilization.

1.3 Polymer-supported membranes

The cell is the basic entity of a living organism. Its boundary is given by the plasma membrane which is composed of a lipid matrix and proteins. The plasma membrane plays a key role in regulating the entrance and exit of substances from the external environment into the cell and vice versa. The lipids of the plasma membrane are self-assembled into a fluid sheet comprising two lipid layers and is therefore termed lipid bilayer. The major lipid constituents of plasma membrane of mammalian cells are glycerophospholipids, sphingolipids and cholesterols [70] as depicted in Figure 1-10. These are asymmetric elements that contain a hydrophilic 'head' and hydrocarbon(s) as hydrophobic 'body' and therefore present amphiphilic properties. The lipid head group follows the external polar environment, while the apolar lipid body is located further away from the polar surroundings.

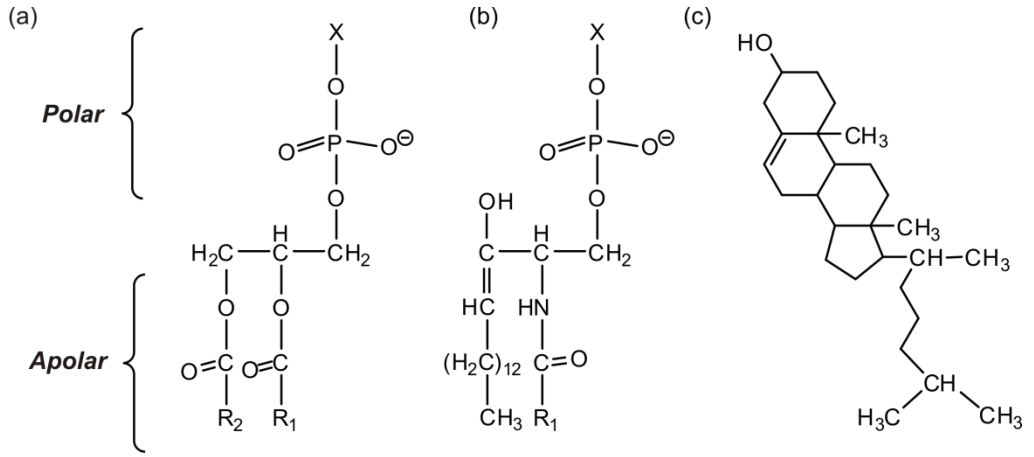

Figure 1-10. Lipids comprising the plasma membrane. Chemical structures of a glycerophospholipid (a), a sphingolipid (b) and a cholesterol (c). X is alcohol based polar group. R1, R2 are the hydrocarbon fatty acid tails.

The arrangement of proteins that associate with the membrane relies on their nature. Peripheral membrane proteins interact with lipid head groups through hydrogen bonds and electrostatic interactions, while integral membrane proteins interact with the membrane by hydrophobic interactions as well. Transmembrane proteins are integral membrane proteins that span the membrane and contain part(s) that is exposed to the extracellular matrix (ECM) and part(s) that access the cytoplasm (as mentioned in 1.1). A model suggested by Singer and Nicolson for the organization and structure of lipids and proteins in cell membranes is the fluid mosaic model [71] as shown in Figure 1-11a. According to this model, the membrane is a two-

dimensional matrix of proteins in a phospholipid bilayer. With the development of powerful tools that provide the ability to detect features beyond the optical resolution limit, it is possible to investigate processes occur in the plasma membrane at the nanometer scale. Using such methods the heterogeneity of the plasma membrane could be observed. A recent model for the organization of the plasma membrane was suggested by Kusumi *et al*. [72] The model proposed is based on the concept of the hierarchical three-tiered meso-scale domain architecture of the plasma membrane (Figure 1-11b): (1) Cortical actin skeleton-based organization into 40-300 nm domains. The plasma membrane interacts with the actin cytoskeleton and the TM proteins anchored to it ("picket and fence" model). (2) Liquid ordered lipid domains of 2-20 nm ("raft" domains) enriched in cholesterol, glycosphingolipids and GPI-anchored proteins. (3) Dynamic protein complexes domains at the scale of 3-10 nm that are induced by protein-protein interactions.

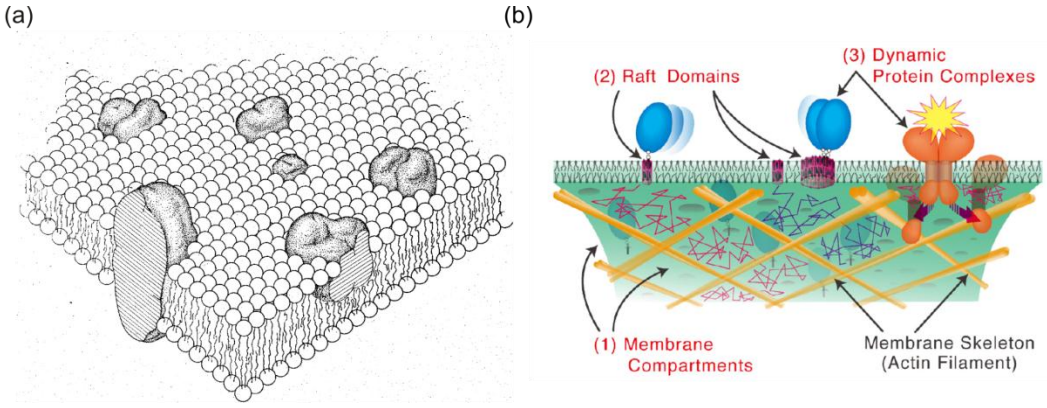

Figure 1-11. Early and recent models suggested for the organization of the plasma membrane. (a) The fluid mosaic model (Taken from ref[71]). (b) The hierarchical three-tiered meso-scale domain architecture of the plasma membrane. (1) Actin-based membrane cytoskeleton partitioning, (2) "raft"-domains and (3) dynamic protein complex domains. (Taken from ref[72]).

Thus, the lipids comprising the plasma membrane are not only the fluid platform that accommodates proteins. They also play a significant role for protein functions through (i) lipid composition (lipid domains):[70] sorting proteins and controlling their function, (ii) membrane trafficking [73, 74]: transport of lipids and proteins to distinct places inside or outside the cell in order to carry out particular functions and (iii) protein-lipid interactions [74]: activation and regulation of proteins by signaling lipids.

1.3.1 Artificial model systems

The plasma membrane contains a wide variety of lipids and proteins that stimulate different events at the membrane simultaneously, which therefore makes the investigation of membrane proteins in such complex systems highly challenging. For this purpose, artificial model systems for *in vitro* characterization of proteins are required. Probing protein functionalities and interactions *in vitro* is possible using soluble proteins after their transmembrane (TM) domain was truncated (the TM domain assists to embed the protein in the membrane, but makes it insoluble in the absence of the membrane). This can be carried out through site-specific immobilization on biocompatible solid-supports as discussed in 1.2. In this case, only the extracellular part of the protein can be studied. Another possible approach is to solubilize the proteins (including their TM domain) in detergent-lipid micelles. However, the presence of detergent may affect the stability of the proteins and can impair protein functionality. The TM domain in context with the membrane has diverse functions: it is responsible for protein mobility across the membrane, it associates with TM domains of other proteins, undergoes conformational changes and has a significant role in signaling. Therefore artificial model systems composed of lipid bilayers, which can incorporate complete membrane proteins, provide an essential tool for probing the behavior of membrane proteins *in vitro*. This has to be carried out in a manner that closely mimics their natural environment and notably, meets the needs for the investigation of membrane proteins.

Model membrane systems

A recent model membrane approach for probing membrane proteins *in vitro* is the nanodisc based system [75]. Nanodiscs are formed by self-assembly of phospholipids together with two membrane scaffold proteins (MSPs). MSPs are derived from the apolipoproteins A-1, which transport lipids by the formation of high density lipoprotein (HDL) [76]. The MSPs encircle the hydrophobic alkyl chains of each leaflet in a disc-shaped manner, which is freely accessible from both sides of the membrane formed and hence is suitable for integrating membrane proteins. After nanodiscs formation they can be also selectively tethered on solid supports via incorporation of tags to the MSPs [75]. The diameter of a nanodisc is ~10-13 nm and thus

imposes difficulties in integrating and probing diffusion properties of very large and complex proteins. Another model membrane implemented was the black lipid membrane (BLM) system, in which a membrane is generated across a small opening in a Teflon partition embedded in a chamber containing aqueous solution. Lipids dissolved in an organic solvent are applied across the opening, followed by a lipid monolayer formation and a subsequent fusion to a bilayer. The BLM obtained is free from both sides and therefore highly beneficial for studying membrane proteins. However, because of the fragile nature of BLMs and the difficulty to incorporate membrane proteins, a robust system that preserves membrane stability is highly essential. Alternative model membrane approach is the giant unilamellar vesicles (GUVs). These vesicles can have a size of ~1-100 μm in diameter and therefore are compatible with conventional optical microscopes. They can be utilized in their free-standing form or tethered to a solid-support. Using GUVs, it has been possible to perform *in vitro* studies of different lipid mixtures with reconstituted membrane proteins [77, 78]. However, GUV preparation is not straightforward and it also requires a dehydration step for the incorporation of membrane proteins, which may affect their functionality. Efforts are being made to overcome problems regarding GUV preparation and to achieve a robust approach for the reconstitution of membrane proteins into the system [79, 80].

An approach for obtaining planar lipid bilayers is the supported lipid bilayer membrane (SLB) (Figure 1-12a). Methods for lipid bilayer assembly on glass, quartz and silicon surfaces include the transfer of lipid monolayers from air-water interface to the support by Langmuir trough and Langmuir-Blodgett deposition [81, 82] or the direct fusion of lipid vesicles on supports [83-89]. Employing such methods, versatile lipid vesicle, monolayer and bilayer characterization via a wide variety of techniques has been possible [86, 87, 90, 91]. However, in spite of the high fluidity and uniformity that these supported bilayers present, a prominent deficiency is the direct coupling of the membrane to the substrate – the distance between the 'head' domain of the lower leaflet and the support is only ~10 Å. Thus, incorporating proteins with their transmembrane domain is limited because of possible interactions with the support [92, 93]. To address this issue, approaches relying on surface tethered bilayer lipid membranes (t-BLMs) were evolved (Figure 1-12b).

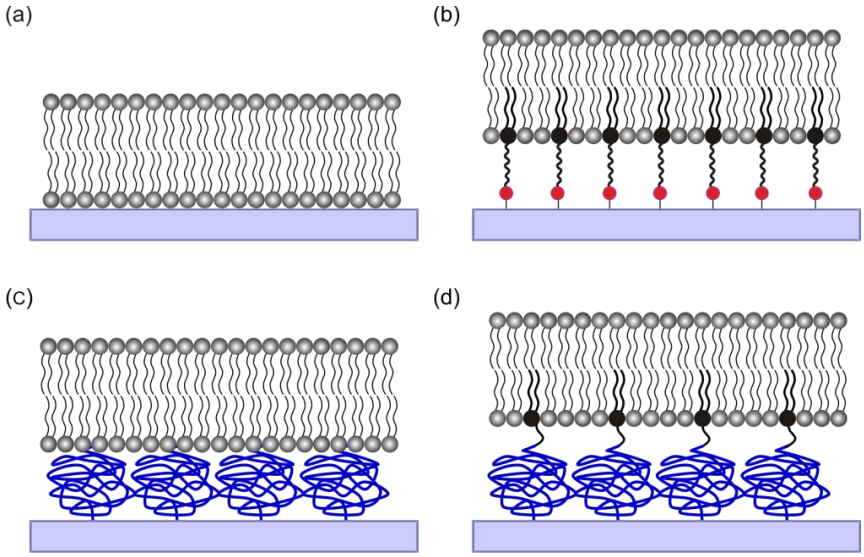

Figure 1-12. Solid-supported membranes, different approaches. (a) SLB, (b) tBLM, (c) PSM and (d) polymer-tethered membranes. (The tethered lipids in (b) and (d) are shown in black).

In this strategy, lipids are selectively attached to chemically modified substrates [94-97]. This can provide the distance necessary for integrating membrane proteins into the system but does not supply adequate biocompatible surroundings. Introducing a soft and flexible polymer layer to obtain polymer-supported membranes (PSMs) (Figure 1-12c) or polymer-tethered membranes (Figure 1-12d), prevents direct contact of the proteins with the substrate and therefore reduces non-specific binding and protein denaturation yet preserves the properties of the bilayers [98-104]. Such polymer cushions can be formed of PEG [105-112] and dextran based compounds [98, 113] among others [114-117].

Within addition to the demand for highly specific immobilization methods and fabrication of synthetic membranes on surfaces that mimic the native environment of membrane proteins, the necessity to spatially control organization of proteins and confine their diffusion into minute structures has witnessed a massive growth over the past years. Patterned surfaces presenting membrane proteins arrays such as cytokine receptors, tyrosine kinases, G-protein-coupled receptors (GPCR) or ion channels for high-throughput screening and analysis of drug targets can be a significant mean for drug discovery and diagnostics [118, 119]. Moreover, surface patterning techniques utilizing artificial model membranes can be highly beneficial for fundamental biophysical research towards the elucidation of the initial steps of signal transduction. Reduction in spatial dimensions of membrane compartments into the

submicrometer regime will have a great impact on the ability to study dynamics of proteins and processes at the single molecule level. In chapter 4, PSM was utilized as a biocompatible, fluid platform with reconstituted TM proteins. Further control of spatial distribution of lipids and TM proteins by means of micropatterns was carried out. Lateral diffusion of lipids and TM proteins was probed and interaction studies of the reconstituted protein with its ligand were carried out in micropatterns.

1.4 Cells adhesion on solid supports

Cell adhesion refers to affinity-based contact either between two cells or between a cell and the extracellular matrix (ECM). There adhesive interactions are vital for diverse processes in multicellular organisms including the construction and conservation of multicellular structures and signal transduction. Cell adhesion also affects processes such as proliferation, differentiation and migration [120]. Without cell adhesion apoptosis occurs and malignant tumors can grow and spread [121]. Cell adhesion is mediated by cell surface proteins that create contacts with other cells or with the ECM. The adhesive interactions can be carried out either through homophilic binding in which the same kind of adhesion transmembrane proteins on two cell surfaces interact with each other, or via heterophilic binding in which the adhesion transmembrane proteins bind to molecules at the ECM [120]. Cell adhesion molecules (CAMs) include integrins, selectins, cadherins and immunoglobulin (Ig) superfamily and their interaction is mediated by divalent cations (except for the Ig superfamily based-adhesion). Relying upon cell adhesion, the controlled manipulation of cells on planar supports has been utilized in diverse biophysical and biotechnological applications. Here I will briefly introduce different approaches for cell adhesion and their applications:

Glass-type substrates:

- Adsorption of ECM proteins with or without prior chemical modification of the substrate with hydrophobic polymers [122-124]. This approach was mainly used for studying cell adhesion.

- Site-specific attachment of synthetic peptides for cell adhesion. Using this method, controlling the organization of neuronal cells on various chemically modified substrates attached to laminin-derived peptides, was possible [125].
- Supported lipid bilayer as a platform for cell adhesion [126, 127]. Utilizing this approach, it was shown that signaling of receptor tyrosine kinase EphA2 could be regulated by physical barriers fabricated on surfaces [128].

Gold substrates:

- Adsorption of ECM proteins on SAMs of alkyl chains mixed with ethylene glycol groups. Cell adhesion, spreading and migration were studied using this approach [129].
- Selective attachment of the synthetic peptide arginine-glycine-aspartic acid (RGD), which will be discussed in the following subsection, using similar surfaces as described in the last bullet point [121, 130]. Using this approach, it was possible to control cell shape and function [131], cell migration by imposed polarization [132] or by utilizing a dynamic adhesive substrate [133].

  Adhesive peptides containing RGD-thiols coupled to gold nanoparticles were utilized to investigate the $\alpha_v\beta_3$ integrin-based adhesion [134]. Also specific attachment of CAMs to gold nanodots was carried out to study adhesion and neurite formation of neurons and neuroblastoma cells [135].

Hence the development of strategies to control cell adhesion plays a key role towards understanding mechanisms that are indispensable for the normal functions of cells.

1.4.1 Integrin-RGD based adhesion

Integrins are cell surface receptor proteins that play a significant role in cell adhesion. Integrins are composed of two subunits α and β, which are linked together to form a heterodimer. Some integrins can have a particular function and therefore bind to specific extracellular ligands while others are promiscuous and can bind different substrates. Moreover, integrins associate with the cytoskeleton, cluster into focal adhesion (FA) assemblies and activate signaling pathways. ECM proteins such as fibronectin and vitronectin have versatile functions. One of the very

important functions is to mediate cell adhesion through binding of integrins. However, ECM proteins impart adhesion properties to surfaces by adsorption, as mentioned above. This may lead to protein denaturation, unstable protein binding and desorption or randomly oriented protein attachment, which impair protein activity. For this purpose, synthetic peptides containing the cell adhesive sequence - RGD, were developed. This amino acid sequence was derived from ECM proteins that mediate cell adhesion. An example for an integrin-RGD complex is demonstrated in Figure 1-13. By employing a short peptide tag the need for isolation and purification is abolished and a wide range of conditions such as temperature, pH and storage can be applied due to their stability [136]. Therefore, systems comprising RGD recognition sites together with integrins are essential for applications exploiting cell adhesion [137]. In chapter 5, integrin-RGD based coupling for selective cell adhesion is demonstrated for probing protein-protein interactions in surfaces adhered live cells.

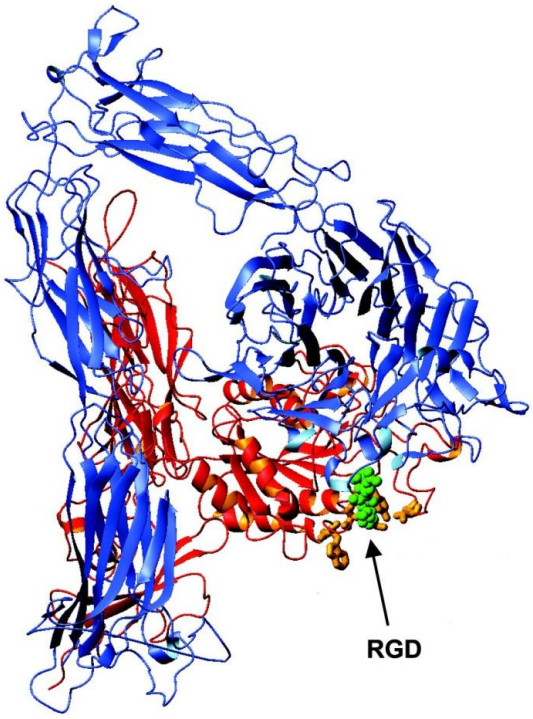

Figure 1-13. Crystal structure of the EC domain of $\alpha_V\beta_3$ integrin. RGD is shown in green. Modified from ref[138].

1.5 Patterning

Reducing dimensions of components down to the nanoscale regime is well established for electronic devices and for applications in the semiconductor industry. Suitable fabrication techniques were developed as a tool box for the construction of well defined features on solid supports at the micro- and nanometer scales that meet the needs for different applications such as sensors [139, 140], microelectromechanical systems (MEMS) [139] among others [141-143]. In recent times, fabrication techniques for the construction of micro- and nanopatterns have paved the road for biological applications. Initially, protein patterning technology was applied for creating bio-electronic microcircuits [144] and shortly after, DNA and then protein microarrays were developed. This enabled the examination of a wide number of interactions simultaneously and ensured much lower sample consumption as compared with traditional techniques [145, 146]. By utilizing this technique not only known interactions could be studied but also novel binding proteins and activities were unveiled on a proteome chip [147]. Thus, microarrays technology has proven to be a powerful tool for studying a wide variety of biological interactions that have a great impact on diagnostic assays and drug discovery [148] and in general has been highly beneficial for pharmaceutical studies on the large scale [149]. Following the trend for miniaturization, the development of nanoarray technology allows the reduction of proteins and analytes quantities and shows increase in sensitivity [150, 151]. This opened a window of opportunities for the investigation of protein functionalities and interactions on solid supports by means of a large diversity of patterning techniques.

An efficient protein patterning technique must fulfill requirements such as biocompatibility and selectivity in order to preserve protein functionality, as discussed in section 1.2. In addition, protein coupling and analysis has to be carried out in physiological conditions. Moreover, patterns should present high contrast and fidelity for good quality assays and reliable analysis.

Nowadays, there is tremendous progress in developing patterning techniques most of which are derivatives of lithographic approaches. Lithography (*lithos* = stone, *grafein* = to write),

which was invented by Alois Senefelder in 1796,* summarizes methods for printing on surfaces. Thus, fabrication techniques at the micro- and nanoscale are denoted as lithographic.

Patterning techniques can be classified into two main categories: (i) Printing-based technology, which includes soft lithography and scanning probe microscope (SPM)-based lithography and (ii) optical lithography.

Here I will introduce commonly used approaches based on printing technology:

"Soft" lithography

A method suitable for micro- and nano-fabrication which is based on an elastomeric stamp for transferring patterns to surfaces. A prominent approach for pattern transfer is microcontact printing (μCP) in which an elastomeric stamp containing molecules of interest comes into contact with a substrate and creates patterns [152-154]. Improving the elastomeric stamps and using higher molecular weight species for deposition, patterns presenting sub-100 nm features could be obtained [155, 156].

SPM-based lithography

The ability of atomic force microscope (AFM) tip to selectively deposit molecules in specific regions was applied to generate patterns on surfaces in a "dip-pen" manner, therefore introduced as "dip-pen" nanolithography (DPN) [157]. In this technique an AFM tip is used as a writing instrument to deliver molecules as 'ink' to a solid support as a 'paper' by capillary forces to generate patterns with resolution of sub-50 nm [40]. A major challenge using DPN was the ability to utilize this technique for a large capacity surface pattern production. For this purpose a new method based on DPN was developed. In this approach elastomeric tips (polymer pens) were used to transfer 'ink' to substrates in a technique denoted as polymer pen lithography (PPL) that produced patterns with sub-100 nm resolution over a whole wafer as large as 3-inch [158]. Other scanning probe microscopy (SPM) methods employed for protein patterning on surfaces include nanografting [159, 160] and nanofountainpen [161].

However, there are still several obstacles for DPN and related SPM-based lithography techniques on the way to achieve robust, high-throughput protein patterning methods and continuous efforts are being made for improvements [162].

* Wikipedia

1.5.1 Optical lithography

Lithography which is carried out by light is described as optical lithography or photolithography. This is considered to be one of the most common technologies used for constructing micrometer features on solid supports. In this method a photosensitive surface is exposed to light (ultraviolet, visible or infra-red) in a spatially defined manner leading to the execution of photochemical reactions selectively in the exposed regions only. As a result of this the exposed regions may be either become activated for further reactions or lose their ability to react, depending on the functional groups involved and the photochemistry which occurs. According to the first law of photochemistry, photochemical reactions can occur only when photons absorbed by the irradiated compound. The energy carried by the photons is described by:

$$E = h\upsilon$$

Where *E* is the energy of a photon emitted/absorbed, *h* is Planck constant ($6.63\times10^{-34} J\cdot s$) and ν is frequency.

Prior to light exposure electrons will occupy the ground singlet state (S_0) in which they are fully paired. Upon light exposure an electron is transferred to the first singlet excited state (S_1) from which there will be a chance for spin inversion and a transition to a triplet state (T_1). $S_1 \rightarrow S_0$ transitions have a very short lifetime of 10^{-8}-10^{-9} s, while $T_1 \rightarrow S_0$ are spin-forbidden transitions and therefore are several order of magnitude slower. The lifetime of excited states plays an important role in photochemical processes. Hence, excited triplet states have a great impact on photochemical processes because species in excited triplet states can undergo a large number of collisions with other molecules and induce cascade of different chemical redactions before deactivation [163].

The electronic states and the transitions are illustrated in the Jablonski diagram in Figure 1-14.

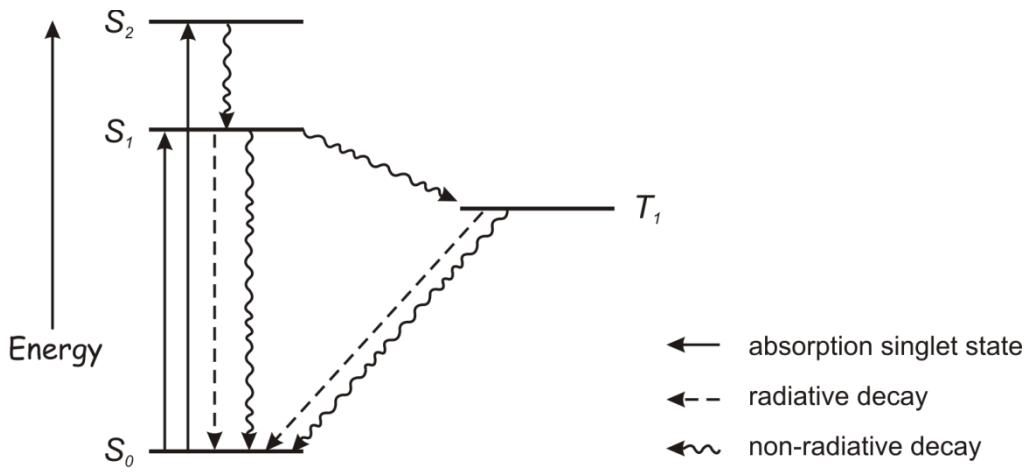

Figure 1-14. Jablonski diagram presenting radiative and non-radiative transitions between electronic states. (Taken from ref[164]). The full arrows represent transitions from the ground state to excited states. The dashed arrows represent radiative decay processes such as fluorescence and phosphorescence and the wavy arrows represent non-radiative processes such as internal conversion (transition between two electronic states with spin conservation) and intersystem crossing (transition between two electronic states with spin inversion).

The resolution *R* of an optical system is limited because of diffraction. This follows the Rayleigh criterion:

$$R = 0.61\frac{\lambda}{NA}$$

Where λ is the wavelength of the irradiating light source and *NA* is the numerical aperture. The numerical aperture is defined as $NA = \eta \sin\theta$, in which η is the index of refraction of the medium between the lens and the sample and θ is half angle of the maximum cone of light that can exit the lens as illustrated in Figure 1-15.

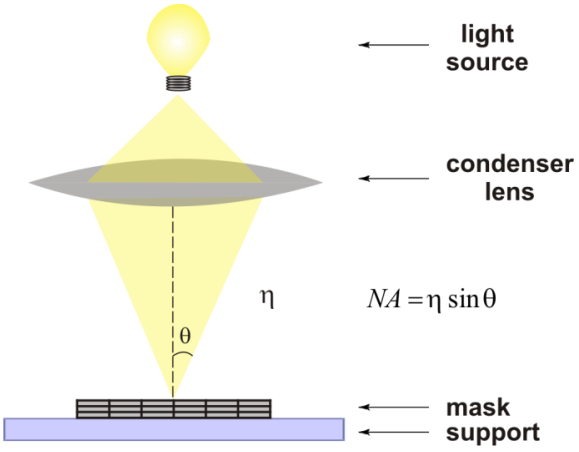

Figure 1-15. Optical system constructed of a UV lamp as a light source and a condenser lens. Light is irradiated directly on a mask which is placed on a chemically modified support.

Although optical lithography is limited by diffraction, reducing lateral dimensions to the nanometer regime has been shown to be possible by scanning near field photolithography (SNP), using a scanning near-field optical microscope (SNOM) coupled to a UV laser [165]. Moreover, advanced lithographic patterning techniques that proceed beyond the diffraction limit were developed. These include electron-beam lithography (EBL) [166] and focused ion beam (FIB) writing [167] that can generate patterns in the order of a few nanometers. However these techniques are very costly and time consuming and can not be employed for a high throughput.

In the following part I will present versatile protein patterning approaches based on optical lithography:

- Photodeprotection of caged functional groups

  This type of patterning is carried out by utilizing photosensitive molecules (molecules that experience electronic transitions upon light exposure). Nitro-substituted aromatic compounds are well established as photosensitive amine protecting groups and denoted as 'caged' amines. Nitroveratryloxycarbonyl (Nvoc) chloride is an example for a commonly used amine protecting group. Upon UV irradiation, the amide bond between the caged amine and the Nvoc moiety is cleaved, then amine groups are freely exposed and can be further functionalized [168, 169]. In addition to Nvoc, 3-amino-3-(2-nitrophenyl)-propionic acid (*Anp*) as an amine caging group was successfully applied. Photocleavable peptides carrying *Anp* were utilized for protein patterning on solid supports. The *Anp* moiety was attached either to a tris-NTA group for site-specific immobilization of proteins [170] or to a polyhistidine peptide chain [171]. The utility of nitro-substituted aromatic compounds for patterning can be extended to the protection of versatile nucleophiles [172, 173]. Moreover, photosensitive protection groups other than aromatic nitro compounds have been employed [174].
- Photocoupling of chemical functionalities or proteins

  Well established methods include patterning using photoresist technology [144], "click" chemistry [175] and thiol-ene reaction [176, 177].

- Photodeactivation of functional groups

  The photodestruction of active moieties [178] or cross-linking of polymers [179] through light irradiation.

I have discussed here a variety of patterning techniques. Some present patterns fidelity and high selectivity on the micro- and nanometer range, while others offer high patterning capacity. Nevertheless optical lithography still dominates applications for patterning of biological molecules due to low cost, high-throughput and the ease of handling required yet remains robust and reliable patterning technique.

The photopatterning technique presented in this thesis was further extended for constituting lipid bilayer in minute structures as presented in chapter 4. Moreover, controlling spatial arrangement of cells and capturing transmembrane proteins directly from cells into surface architectures is demonstrated in chapter 5.

1.6 Maleimide as chemical functionality for patterning

Maleimide is an unsaturated imide in a cyclic form that can selectively react with thiols in a "click" chemistry fashion through Michael addition. With a strong absorption in the wavelength range of 300 nm, maleimides were shown to polymerize under UV irradiation using photoinitiators [180, 181]. Photoinitiators are photosensitive molecules that upon light absorption, generate high energy species such as radicals which can initiate chemical processes. However, using such molecules has several drawbacks including their contamination in the final polymer or unwanted side products that can be obtained in addition to radicals formation [182]. Later on it was discovered that maleimide and its derivatives can undergo homopolymerization upon exposure to UV light even in the absence of a photoinitiator [183]. However, the requirements for inducing photopolymerization are the presence of a solvent that can donate hydrogen (H) [184] or maleimide derivatives containing labile hydrogens that can undergo inter- or intramolecular H-abstraction. The triplet state species formed upon UV irradiation, initiate the polymerization process via H-abstraction from aliphatic ethers and alcohols and proceed through a chain transfer reaction mechanism (a polymer chain reacts with

a molecule and is subsequently terminated while a new radical is formed) as illustrated in Figure 1-16 [185-187].

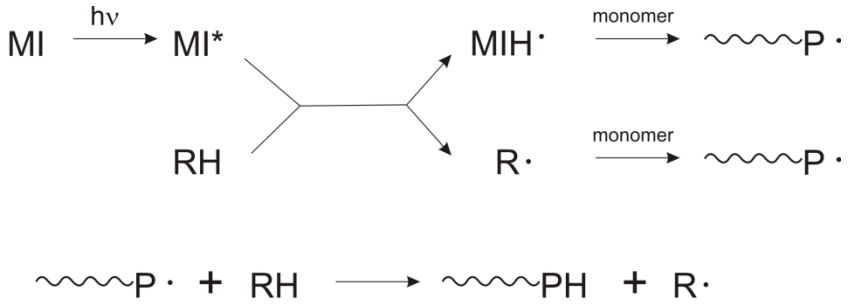

Figure 1-16. Schematic of the photopolymerization process which is carried out through H-abstraction. MI-maleimide, R-alkyl group and P-polymer. (Taken from ref[187]).

The chemical reaction based on H-abstraction from *N*-alkylmaleimide is demonstrated in Figure 1-17.

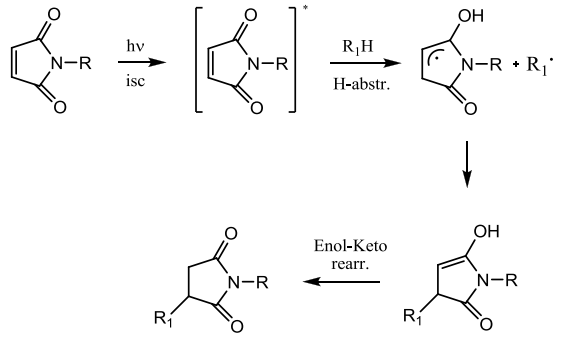

Figure 1-17. H-abstraction from triplet *N*-alkylmaleimide species. (Taken from ref[186]).

A prominent advantage of using maleimides is that the radical initiating species form without any harmful side products [182]. Hence, maleimide and its derivatives play different yet complementary roles in the polymerization process as monomers and catalysts simultaneously. For this reason, in addition to photopolymerization of maleimide derivatives, maleimide was further utilized for the polymerization of different systems. The cross-linking of maleimide/vinyl ether for example, is possible upon UV irradiation [182]. Vinyl ether is rich in electrons due to its C=C bond and therefore functions as electron donor while maleimide, which is poor in electrons, is the acceptor. The process is mainly initiated through H-abstraction as for

maleimide homopolymerization but it can also be induced via electron transfer from the vinyl ether followed by proton transfer as presented in Figure 1-18.

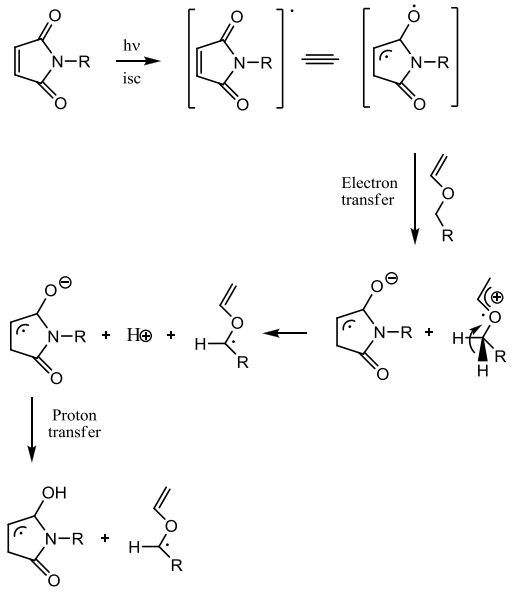

Figure 1-18. Electron transfer reaction mechanism as initiation step of polymerization .(Taken from ref[187]).

Furthermore, for acceptor/donor systems dissolved in apolar solvents, which do not present labile hydrogens, the initiation step is still possible and the polymerization is carried out through an electron transfer mechanism [188, 189]. Concerning the propagation step, in addition to H-abstraction another mechanism suggested relies upon the homopolymerization of the acceptor-donor complex [187].

The UV light source and the photoinitiator play a major role in the rate of initiation according to the following equation [190]:

$$r_i = \Phi_i I_0 \left(1 - e^{-\varepsilon l[PI]}\right)$$

Where I_0 is the incident light intensity, l is the sample thickness, ε is the absorptivity, *[PI]* is the concentration of the photoinitiator (in our case maleimide) and Φ_i is the quantum yield of initiation, which is the number of initiating species generated per photon absorbed.

The UV light source also plays an important role in the propagation of the polymerization process. Stronger intensity leads to faster polymerization and higher conversion. In addition to the increase in the rate of initiation in accordance with the above equation, higher irradiation intensity results in increase in temperature, which leads to higher molecular mobility [190].

Additional benefit of using stronger intensity is the less sensitivity of the polymerization process to oxygen inhibition [186]. Thus utilizing an intense light source yet preserving surface biocompatibility is a prerequisite for optimal cross-linking of chemical functionalities. In the current work I developed different strategies based on the ability of maleimide moieties to undergo polymerization upon UV irradiation for surface patterning, allowing biophysical analyses in micropatterns (Figure 1-19). The strategies employed are as follows:

(I) Maleimide photodestruction - surface maleimides are cross-linked.

(II) Maleimide polymerization - maleimide moieties in solution are cross-linked with surface maleimides.

(III) Maleimide-vinyl ether polymerization - alkyl chains carrying vinyl ether functionalities are cross-linked with surface maleimides.

These photochemical strategies in combination with maleimide-thiol coupling were utilized to pattern surfaces with bio-chemical moieties needed for the quantitative biophysical analysis of different model systems as introduced previously in Figure 1-2.

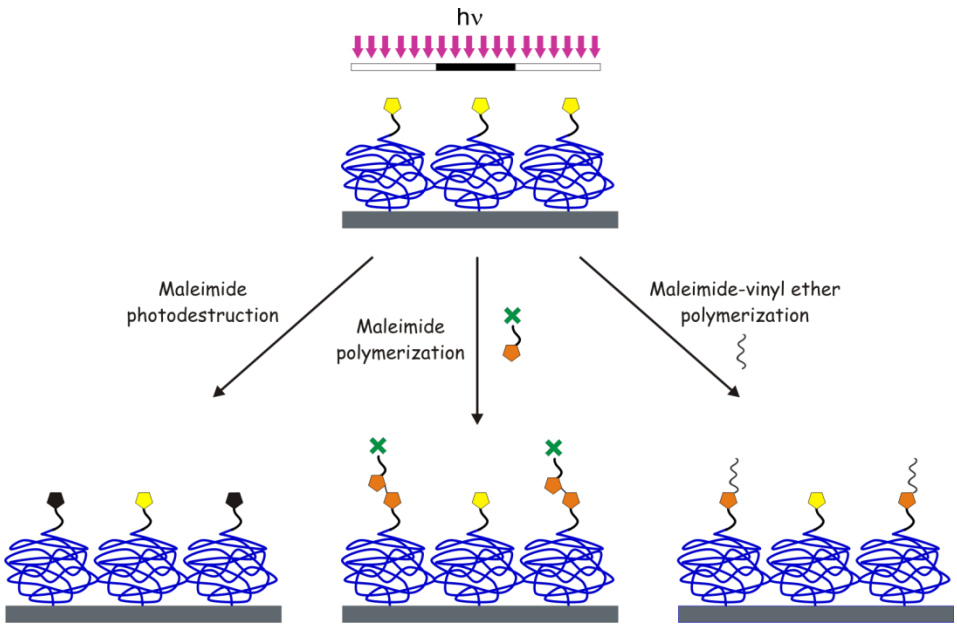

Figure 1-19. Photochemical strategies based on maleimide groups: maleimide photodestruction, maleimide polymerization and maleimide-vinyl ether polymerization.

1.7 Biological model system

Interferons (IFNs) are glycoprotein cytokines that are secreted in cells upon viral invasion and function as antiviral agents. Apart from their antiviral activity, IFNs exhibit antiproliferative and antitumor effects. Binding of IFN to its cell surface receptor impair the replication of RNA and DNA molecules of the invaded species. The IFN was discovered in the course of the investigation of interference with the growth of live influenza virus in chick chorio-allantoic membrane. Upon incubation of inactivated virus with the membrane, an interfering agent was released and caused an interference activity [191]. IFNs can be classified into three main types based on their interaction with specific receptors: IFN type I, II and III that stimulate various signaling pathways in which specific genes are then transcribed. In this work we employed type I IFN as our biological model system. All type I IFNs share a specific cell surface receptor complex IFNAR, which consists of two subunits IFNAR1 and IFNAR2 [192]. This group of IFNs comprises different subtypes of IFNα proteins including IFNα2, a protein which is encoded by the gene *IFNα2.* IFNα2 binds to IFNAR2 and induces association of IFNAR1 to form a ternary complex with subnanomolar affinity [193], presenting a 1:1:1 stochiometry. While IFNAR2 has nanomolar affinity towards IFNα2 [194, 195], the affinity towards IFNAR1 is in the micromolar range.[193] Despite its lower binding affinity to IFNα2 alone, IFNAR1 recruitment to form a ternary complex stabilizes the interaction of all three partners [196]. Upon binding of IFNα2 to its transmembrane receptor subunits, a specific signaling cascade is triggered through the cell [197]. Janus-activated kinases (JAKs) are involved in transmitting signals. They were found to be constitutively preassociated with IFNAR subunits in a non-covalent fashion [198]. Through ligand stimulation, JAKs undergo cross-phosphorylation and activation followed by IFNAR subunits phosphorylation. While the signal transducer and activator of transcription STAT2 is constitutively preassociated with IFNAR2 [199], a docking site for the Src homology 2 (SH2) domain of STAT2 is created on the phosphorylated IFNAR1. Subsequently, STAT2 is phosphorylated, thus creating a docking site for the SH2 domain of STAT1 which is then phosphorylated [200]. STAT1-2 heterodimer and p48 form the IFN-stimulated gene factor 3 (ISGF3) complex, a transcription factor [201]. Subsequently, ISGF3 complex translocates to the

nucleus and binds to IFN-stimulated response elements (ISRE) for gene transcription as illustrated in Figure 1-20.

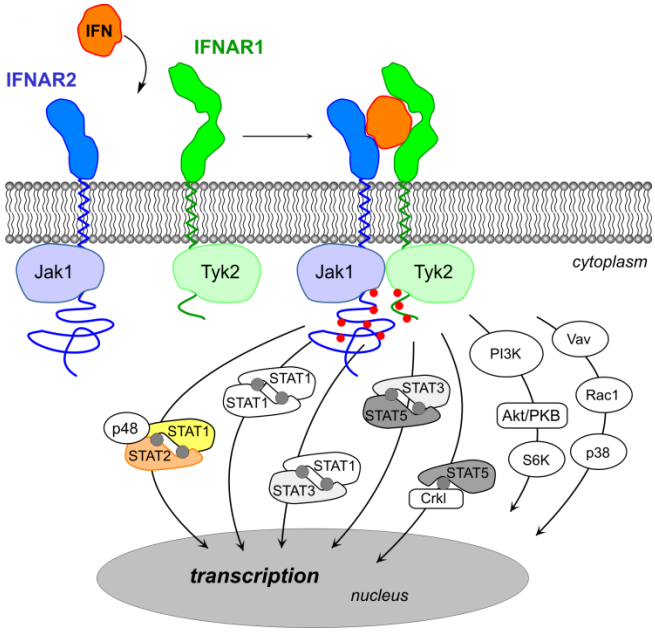

Figure 1-20. Type I IFN signaling pathway. Upon IFN binding, association with IFNAR1 and IFNAR2 induce signal propagation across the cell for gene transcription.

Additional mechanisms involved in IFNα2-mediated signaling include the activation of STAT3 and STAT5. Moreover, type I IFNs stimulate the phosphatidylinositol 3-kinase (PI3K)/AKT (protein kinase B) signaling pathway and the Ras-related C3 botulinum toxin substrate 1 (RAC1)/mitogen-activated protein kinase (MAPK) pathways [202].

In addition to wild-type IFNα2 (IFNα2-wt), mutants of IFNα2 presenting various affinities were employed:

- IFNα2-YNS – an IFNα2 comprising mutations H57Y, E58N and Q61S. It has a similar affinity to IFNAR2 and a 60-fold increased affinity towards IFNAR1 as compared with IFNα2-wt [203].
- IFNα2-M148A – binds IFNAR2 with 30 fold lower affinity with respect to IFNα2-wt [204], and with wild-type affinity to IFNAR1.

- IFNα2-M148A-NLYY – an IFNα2-M148A that additional residues 65,80,85 and 89 were mutated. It binds IFNAR2 with similar affinity as compared with IFNα2-M148A and has almost no binding to IFNAR1 [204, 205].
- IFNα2-YNS-α8tail – an IFNα2 in which seven last residues at the C-terminal were exchanged with the C-terminal residues of an IFNα8 resulting in a stronger affinity of 20 fold to IFNAR2 as compared with IFNα2-wt under physiological conditions [206].

1.8 Techniques

1.8.1 Reflectance interference spectroscopy (RIfS)

RIfS is an optical, label-free, time-resolved detection system which enables to monitor binding and interactions of chemical and biological samples in a quantitative manner. The technique is based on interference of a white light beam reflected at a thin silica layer (300-500nm) coated on a glass support (Figure 1-21a). Due to different refractive indices of the multilayer system used (air, glass and silica), an incident light beam is partially reflected at each interface. The reflected beams have different optical path length therefore a phase shift is formed [207].

$$\Delta\phi = 2\frac{nd}{\lambda} + \phi_{refl}$$

Where $\Delta\phi$ is the phase difference, ϕ_{refl} is the phase shift upon reflection, n is the refractive index, d is the thickness of the layer and λ is the wavelength. Superposition of the two reflected light beams leads to interference depending on the phase shift between the beams. At an incidence angle of zero (the illumination is perpendicular to the surface), the intensity is given by [208]

$$I = I_R + I_1 + I_2 + 2\sqrt{I_1 I_2}\cos\left(4\pi\frac{nd}{\lambda}\right)$$

Where I_R is the intensity upon glass reflection and I_1, I_2 are the partially reflected beam intensities. An interference spectrum is generated from the reflected intensity as a function of the wavelength, with maxima and minima for constructive and destructive interference, respectively. The change in optical thickness ($n \cdot d$) is determined from the shift of the interference spectrum at the extremum.

Here, we utilized this technique for a quantitative analysis of protein binding, affinity and kinetic studies. Binding events down to a few pg/mm^2 can be detected [209]. A change in surface loading of 1 pg/mm^2 leads to a shift of the interference minimum by 1.2 pm [210]. The set-up for RIfS detection is schematically depicted in Figure 1-21b.

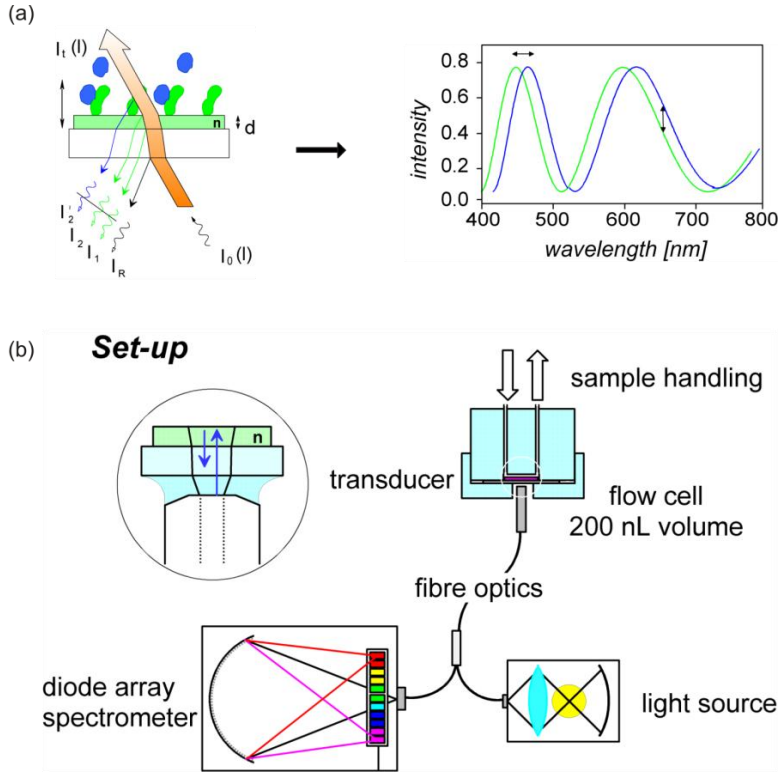

Figure 1-21. Principle of RIfS detection. (a) A glass chip bearing a silica layer is illuminated with a white light beam that is partially reflected at each interface (left). The interference pattern obtained (right). (b) RIfS set-up. The surface is illuminated with a white light source via bifurcated fiber optics. A diode array spectrometer is connected to the second end and is used to detect the reflected light.

1.8.2 Total internal reflection fluorescence spectroscopy in combination with RIF (TIRFS-RIF)

Label-free detection techniques provide a powerful tool for quantifying protein binding and interactions with detection limit as low as a few pg/mm^2 (for RIfS). However these techniques are still limited in sensitivity and are not capable of discriminating different species participating in a binding event. Introducing fluorescence detection increases sensitivity and enables the analysis of different species by means of fluorescent dyes. Thus, the combination of TIRFS and RIF provides high sensitivity for monitoring binding events by a simultaneous label-free and

fluorescence detection [211]. Total internal reflection (TIR) of an incident light occurs between two media with different refractive indices, when the angle of incidence is above the critical angle. The critical angle is subjected to Snell's law, in which the relation between the sine's of the incident angles and the refractive indices is given by

$$\frac{\sin\theta_1}{\sin\theta_2} = \frac{n_2}{n_1}$$

Where θ_1 is the angle of incidence and θ_2 is the refracted angle (Figure 1-22). n_1 and n_2 are the refractive indices. For $n_1>n_2$, $\theta_1<\theta_2$ the critical angle θ_c is reached when the refraction occurs at an angle of 90°. Therefore when $\theta_2=90°$, the critical angle is given by

$$\theta_c = \arcsin\left(\frac{n_2}{n_1}\right)$$

Upon TIR, an electromagnetic field termed 'evanescent wave' penetrates the boundary to the second medium. The intensity of evanescent wave decays exponentially with the distance from the surface boundary as formulated in the following equations:

$$I_z = I_0 e^{(-z/d_p)} \qquad d_p = \frac{\lambda}{4\pi\sqrt{n_1^2\sin^2\theta_1 - n_2^2}}$$

Where I_z is the intensity at a perpendicular distance z from the interface, I_0 is the intensity of the evanescent wave at z=0, d_p is the depth of penetration of the totally reflected light beam and λ is the wavelength of the incident beam in vacuum [212].

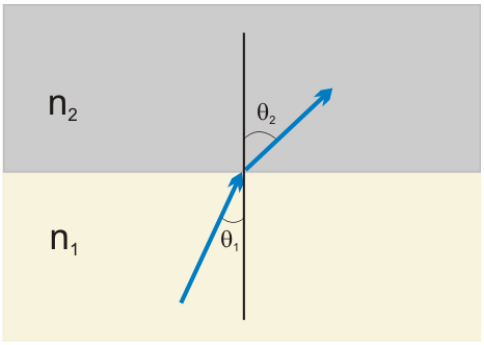

Figure 1-22. Refraction at the boundary of two media with different refractive indices (n1 >n2).

In the experimental system the two detection techniques are spectroscopically separated: the RIF detection is carried out by a single wavelength in the NIR region while the fluorescence detection is in the full visible range [211]. A complete spectral separation avoids cross-talk and ensures two absolute independent detection techniques combined in one set-up which is depicted in Figure 1-23b.

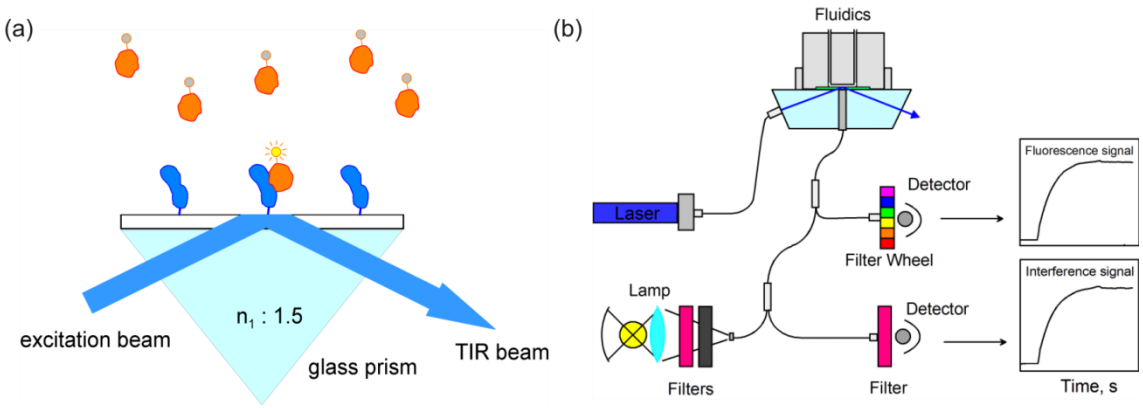

Figure 1-23. Principle of TIRFS-RIF detection. (a) Selective excitation of fluorescence by evanescent wave generated due to TIR. (b) Schematic of the simultaneous TIRFS-RIF set-up.

1.8.3 Confocal laser scanning microscopy (CLSM)

With the utility of antibodies labeled with fluorescent probes, fluorescence microscopes emerged as an indispensable tool for the investigation of biological samples [213]. However, these microscopes were limited to the investigation of only thin and flat specimens. The image of a thick specimen (> 2µm) can be influenced by light from outside the focal plane, which is then reduces the image contrast. In order to address this issue, the confocal microscope was further developed after its invention in 1955 [214]. In a CLSM, as depicted in Figure 1-24, a laser beam passes through a pinhole aperture and is focused onto the specimen by an objective lens. Subsequently, the emitted fluorescence passes back through a beam-splitter and is then collected into a second pinhole aperture to the detector. The pinhole aperture is conjugated to the objective focal plane. Fluorescence that is generated outside the objective focal plane is not

confocal with the pinhole and therefore does not reach the detector (Figure 1-24, dotted line). The scanning process in CLSM is carried out by the illumination of a focused spot that is centered in the focal plane [215]. Therefore, a fluorescence image is formed by scanning the area of interest in a serial fashion and collecting the data from the focal planes to the detector. Hence, in addition to the higher resolution obtained using a CLSM, a 3D image of a complex structure with thickness up to 100 µm can be reconstructed.

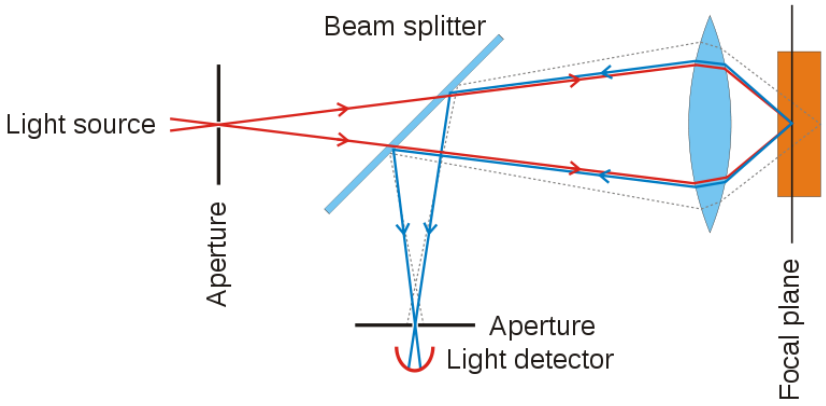

Figure 1-24. Principle of confocal microscopy.[†]

1.8.4 Total internal reflection fluorescence microscopy (TIRFM)

In contrast to confocal microscopy which is based on a pair of pinhole apertures for eliminating background fluorescence outside the focal plane, TIRFM relies upon TIR illumination via high NA objective (as described above). Thus selective excitation of fluorophores in a restricted region of the specimen (~100 nm) is achieved, adjacent to the solid-liquid interface. TIRFM is based on an earlier development of total internal illumination microscopy in which scattered light was detected at the cell/substrate interface [216]. Further extension of this technique to fluorescence was carried out for visualization of cell membranes, for probing cell-substrates contacts and for monitoring ligand-membrane receptor interactions with the reduction of autofluorescence from debris and thick cells [212]. Due to the higher resolution along the z direction and the significant reduction of background fluorescence, diverse applications

[†] Image copied from Wikipedia

including imaging and quantitative analysis of biological samples can be carried out on the single molecule level [217, 218]. In this study we utilized TIRFM for cellular imaging and single-molecule analysis of protein-protein interactions in artificial model systems and in live cells cultured on micropatterns.

1.9 References

1. Christopoulos, A., *Allosteric binding sites on cell-surface receptors: Novel targets for drug discovery.* Nature Reviews Drug Discovery, 2002. **1**(3): p. 198-210.
2. Ullal, A.V., et al., *Nanoparticle-Mediated Measurement of Target-Drug Binding in Cancer Cells.* Acs Nano, 2011. **5**(11): p. 9216-9224.
3. Ng, K.K., J.F. Lovell, and G. Zheng, *Lipoprotein-inspired nanoparticles for cancer theranostics.* Acc Chem Res, 2011. **44**(10): p. 1105-13.
4. Ashley, C.E., et al., *The targeted delivery of multicomponent cargos to cancer cells by nanoporous particle-supported lipid bilayers (vol 10, pg 389, 2011).* Nature Materials, 2011. **10**(6): p. 476-476.
5. Lee, Y.J., et al., *Fabricating Genetically Engineered High-Power Lithium-Ion Batteries Using Multiple Virus Genes.* Science, 2009. **324**(5930): p. 1051-1055.
6. Byun, K.E., et al., *Graphene-Polymer Hybrid Nanostructure-Based Bioenergy Storage Device for Real-Time Control of Biological Motor Activity.* Acs Nano, 2011. **5**(11): p. 8656-8664.
7. Zhou, M. and S.J. Dong, *Bioelectrochemical Interface Engineering: Toward the Fabrication of Electrochemical Biosensors, Biofuel Cells, and Self-Powered Logic Biosensors.* Accounts of Chemical Research, 2011. **44**(11): p. 1232-1243.
8. Benters, R., C.M. Niemeyer, and D. Wohrle, *Dendrimer-activated-solid supports for nucleic acid and protein microarrays.* Chembiochem, 2001. **2**(9): p. 686-694.
9. Yu, T.Y. and C.K. Ober, *Methods for the topographical patterning and patterned surface modification of hydrogels based on hydroxyethyl methacrylate.* Biomacromolecules, 2003. **4**(5): p. 1126-1131.

10. Wylie, R.G., et al., *Spatially controlled simultaneous patterning of multiple growth factors in three-dimensional hydrogels.* Nature Materials, 2011. **10**(10): p. 799-806.
11. Kaminski, W.E., A. Piehler, and G. Schmitz, *Genomic organization of the human cholesterol-responsive ABC transporter ABCA7: Tandem linkage with the minor histocompatibility antigen HA-1 gene.* Biochemical and Biophysical Research Communications, 2000. **278**(3): p. 782-789.
12. Sletten, E.M. and C.R. Bertozzi, *From Mechanism to Mouse: A Tale of Two Bioorthogonal Reactions.* Accounts of Chemical Research, 2011. **44**(9): p. 666-676.
13. Williams, D.F., *On the mechanisms of biocompatibility.* Biomaterials, 2008. **29**(20): p. 2941-2953.
14. Milner, S.T., *Polymer Brushes.* Science, 1991. **251**(4996): p. 905-914.
15. Minko, S., *Responsive polymer brushes.* Polymer Reviews, 2006. **46**(4): p. 397-420.
16. Liu, G.M., et al., *Study of the kinetics of mushroom-to-brush transition of charged polymer chains.* Polymer, 2006. **47**(9): p. 3157-3163.
17. Kjellander, R. and E. Florin, *Water-Structure and Changes in Thermal-Stability of the System Poly(Ethylene Oxide)-Water.* Journal of the Chemical Society-Faraday Transactions I, 1981. **77**: p. 2053-&.
18. Elbert, D.L. and J.A. Hubbell, *Surface treatments of polymers for biocompatibility.* Annual Review of Materials Science, 1996. **26**: p. 365-394.
19. Jeon, S.I., et al., *Protein Surface Interactions in the Presence of Polyethylene Oxide .1. Simplified Theory.* Journal of Colloid and Interface Science, 1991. **142**(1): p. 149-158.
20. Jeon, S.I. and J.D. Andrade, *Protein Surface Interactions in the Presence of Polyethylene Oxide .2. Effect of Protein Size.* Journal of Colloid and Interface Science, 1991. **142**(1): p. 159-166.
21. Steels, B.M., J. Koska, and C.A. Haynes, *Analysis of brush-particle interactions using self-consistent-field theory.* Journal of Chromatography B, 2000. **743**(1-2): p. 41-56.
22. Kolb, H.C., M.G. Finn, and K.B. Sharpless, *Click chemistry: Diverse chemical function from a few good reactions.* Angewandte Chemie-International Edition, 2001. **40**(11): p. 2004-+.

23. Zimmermann, J.L., et al., *Thiol-based, site-specific and covalent immobilization of biomolecules for single-molecule experiments.* Nature Protocols, 2010. **5**(6): p. 975-85.
24. Hoyle, C.E. and C.N. Bowman, *Thiol-Ene Click Chemistry.* Angewandte Chemie-International Edition, 2010. **49**(9): p. 1540-1573.
25. Pauloehrl, T., et al., *Adding Spatial Control to Click Chemistry: Phototriggered Diels-Alder Surface (Bio)functionalization at Ambient Temperature.* Angewandte Chemie-International Edition, 2012. **51**(4): p. 1071-1074.
26. Rusmini, F., Z.Y. Zhong, and J. Feijen, *Protein immobilization strategies for protein biochips.* Biomacromolecules, 2007. **8**(6): p. 1775-1789.
27. Wong, L.S., F. Khan, and J. Micklefield, *Selective covalent protein immobilization: strategies and applications.* Chem Rev, 2009. **109**(9): p. 4025-53.
28. Cha, T., A. Guo, and X.Y. Zhu, *Enzymatic activity on a chip: the critical role of protein orientation.* Proteomics, 2005. **5**(2): p. 416-9.
29. Hodneland, C.D., et al., *Selective immobilization of proteins to self-assembled monolayers presenting active site-directed capture ligands.* Proc Natl Acad Sci U S A, 2002. **99**(8): p. 5048-52.
30. Hodneland, C.D., et al., *Selective immobilization of proteins to self-assembled monolayers presenting active site-directed capture ligands.* Proceedings of the National Academy of Sciences of the United States of America, 2002. **99**(8): p. 5048-5052.
31. Kwon, Y., et al., *Antibody arrays prepared by cutinase-mediated immobilization on self-assembled monolayers.* Analytical Chemistry, 2004. **76**(19): p. 5713-5720.
32. Keppler, A., et al., *A general method for the covalent labeling of fusion proteins with small molecules in vivo.* Nat Biotechnol, 2003. **21**(1): p. 86-9.
33. Tugulu, S., et al., *Protein-functionalized polymer brushes.* Biomacromolecules, 2005. **6**(3): p. 1602-1607.
34. Sielaff, I., et al., *Protein function microarrays based on self-immobilizing and self-labeling fusion proteins.* Chembiochem, 2006. **7**(1): p. 194-202.

35. Hochuli, E., H. Dobeli, and A. Schacher, *New Metal Chelate Adsorbent Selective for Proteins and Peptides Containing Neighboring Histidine-Residues.* Journal of Chromatography, 1987. **411**: p. 177-184.

36. Hochuli, E., et al., *Genetic Approach to Facilitate Purification of Recombinant Proteins with a Novel Metal Chelate Adsorbent.* Bio-Technology, 1988. **6**(11): p. 1321-1325.

37. Gershon, P.D. and S. Khilko, *Stable Chelating Linkage for Reversible Immobilization of Oligohistidine Tagged Proteins in the Biacore Surface-Plasmon Resonance Detector.* Journal of Immunological Methods, 1995. **183**(1): p. 65-76.

38. Schmid, E.L., et al., *Reversible oriented surface immobilization of functional proteins on oxide surfaces.* Analytical Chemistry, 1997. **69**(11): p. 1979-1985.

39. Lata, S. and J. Piehler, *Stable and functional immobilization of histidine-tagged proteins via multivalent chelator headgroups on a molecular poly(ethylene glycol) brush.* Anal Chem, 2005. **77**(4): p. 1096-105.

40. Rakickas, T., et al., *Protein-protein interactions in reversibly assembled nanopatterns.* Nano Letters, 2008. **8**(10): p. 3369-75.

41. Strunk, J.J., et al., *Probing protein conformations by in situ non-covalent fluorescence labeling.* Bioconjug Chem, 2009. **20**(1): p. 41-6.

42. Tang, J., et al., *Detection of metal binding sites on functional S-layer nanoarrays using single molecule force spectroscopy.* J Struct Biol, 2009. **168**(1): p. 217-22.

43. Chaiet, L. and F.J. Wolf, *Properties of Streptavidin Biotin-Binding Protein Produced by Streptomycetes.* Archives of Biochemistry and Biophysics, 1964. **106**(1-3): p. 1-&.

44. Srisa-Art, M., et al., *Monitoring of real-time streptavidin-biotin binding kinetics using droplet microfluidics.* Analytical Chemistry, 2008. **80**(18): p. 7063-7067.

45. Piran, U. and W.J. Riordan, *Dissociation Rate-Constant of the Biotin-Streptavidin Complex.* Journal of Immunological Methods, 1990. **133**(1): p. 141-143.

46. Holmberg, A., et al., *The biotin-streptavidin interaction can be reversibly broken using water at elevated temperatures.* Electrophoresis, 2005. **26**(3): p. 501-10.

47. DeChancie, J. and K.N. Houk, *The origins of femtomolar protein-ligand binding: hydrogen-bond cooperativity and desolvation energetics in the biotin-(strept)avidin binding site.* J Am Chem Soc, 2007. **129**(17): p. 5419-29.

48. Lei, Y., et al., *Theoretical study of cooperativity in biotin.* Journal of Physical Chemistry B, 2007. **111**(51): p. 14370-14377.

49. Izrailev, S., et al., *Molecular dynamics study of unbinding of the avidin-biotin complex.* Biophysical Journal, 1997. **72**(4): p. 1568-1581.

50. Riener, C.K., et al., *Simple test system for single molecule recognition force microscopy.* Analytica Chimica Acta, 2003. **479**(1): p. 59-75.

51. Schwarzenbacher, M., et al., *Micropatterning for quantitative analysis of protein-protein interactions in living cells.* Nat Methods, 2008. **5**(12): p. 1053-60.

52. Howarth, M., et al., *Monovalent, reduced-size quantum dots for imaging receptors on living cells.* Nat Methods, 2008. **5**(5): p. 397-9.

53. Beckett, D., E. Kovaleva, and P.J. Schatz, *A minimal peptide substrate in biotin holoenzyme synthetase-catalyzed biotinylation.* Protein Science, 1999. **8**(4): p. 921-929.

54. Los, G.V., et al., *HaloTag: a novel protein labeling technology for cell imaging and protein analysis.* ACS Chem Biol, 2008. **3**(6): p. 373-82.

55. Zhang, Y., et al., *HaloTag protein-mediated site-specific conjugation of bioluminescent proteins to quantum dots.* Angew Chem Int Ed Engl, 2006. **45**(30): p. 4936-40.

56. Lisse, D., et al., *Selective Targeting of Fluorescent Nanoparticles to Proteins Inside Live Cells.* Angewandte Chemie-International Edition, 2011. **50**(40): p. 9352-9355.

57. Walsh, C.T., et al., *Post-translational modification of polyketide and nonribosomal peptide synthases.* Curr Opin Chem Biol, 1997. **1**(3): p. 309-15.

58. Lambalot, R.H., et al., *A new enzyme superfamily - the phosphopantetheinyl transferases.* Chem Biol, 1996. **3**(11): p. 923-36.

59. Mofid, M.R., et al., *Structure-based mutational analysis of the 4'-phosphopantetheinyl transferases Sfp from Bacillus subtilis: carrier protein recognition and reaction mechanism.* Biochemistry, 2004. **43**(14): p. 4128-36.

60. Quadri, L.E., et al., *Characterization of Sfp, a Bacillus subtilis phosphopantetheinyl transferase for peptidyl carrier protein domains in peptide synthetases.* Biochemistry, 1998. **37**(6): p. 1585-95.

61. Nakano, M.M., et al., *Isolation and Characterization of Sfp - a Gene That Functions in the Production of the Lipopeptide Biosurfactant, Surfactin, in Bacillus-Subtilis.* Molecular & General Genetics, 1992. **232**(2): p. 313-321.

62. George, N., et al., *Specific labeling of cell surface proteins with chemically diverse compounds.* J Am Chem Soc, 2004. **126**(29): p. 8896-7.

63. Yin, J., et al., *Labeling proteins with small molecules by site-specific posttranslational modification.* J Am Chem Soc, 2004. **126**(25): p. 7754-5.

64. Johnsson, N., N. George, and K. Johnsson, *Protein chemistry on the surface of living cells.* Chembiochem, 2005. **6**(1): p. 47-52.

65. Yin, J., et al., *Single-cell FRET imaging of transferrin receptor trafficking dynamics by Sfp-catalyzed, site-specific protein labeling.* Chem Biol, 2005. **12**(9): p. 999-1006.

66. Yin, J., et al., *Genetically encoded short peptide tag for versatile protein labeling by Sfp phosphopantetheinyl transferase.* Proc Natl Acad Sci U S A, 2005. **102**(44): p. 15815-20.

67. Wong, L.S., J. Thirlway, and J. Micklefield, *Direct site-selective covalent protein immobilization catalyzed by a phosphopantetheinyl transferase.* J Am Chem Soc, 2008. **130**(37): p. 12456-64.

68. Zhou, Z., et al., *Genetically encoded short peptide tags for orthogonal protein labeling by Sfp and AcpS phosphopantetheinyl transferases.* ACS Chem Biol, 2007. **2**(5): p. 337-46.

69. Sunbul, M., et al., *Enzyme catalyzed site-specific protein labeling and cell imaging with quantum dots.* Chemical Communications, 2008(45): p. 5927-5929.

70. Coskun, U. and K. Simons, *Cell Membranes: The Lipid Perspective.* Structure, 2011. **19**(11): p. 1543-1548.

71. Singer, S.J. and G.L. Nicolson, *Fluid Mosaic Model of Structure of Cell-Membranes.* Science, 1972. **175**(4023): p. 720-&.

72. Kusumi, A., et al., *Membrane mechanisms for signal transduction: the coupling of the meso-scale raft domains to membrane-skeleton-induced compartments and dynamic protein complexes.* Semin Cell Dev Biol, 2012. **23**(2): p. 126-44.

73. Shevchenko, A. and K. Simons, *Lipidomics: coming to grips with lipid diversity.* Nature Reviews Molecular Cell Biology, 2010. **11**(8): p. 593-598.

74. Sprong, H., P. van der Sluijs, and G. van Meer, *How proteins move lipids and lipids move proteins (vol 2, pg 504, 2001).* Nature Reviews Molecular Cell Biology, 2001. **2**(9): p. 698-698.

75. Bayburt, T.H. and S.G. Sligar, *Membrane protein assembly into Nanodiscs.* Febs Letters, 2010. **584**(9): p. 1721-1727.

76. Hebling, C.M., et al., *Conformational Analysis of Membrane Proteins in Phospholipid Bilayer Nanodiscs by Hydrogen Exchange Mass Spectrometry.* Analytical Chemistry, 2010. **82**(13): p. 5415-5419.

77. Bacia, K., et al., *SNAREs prefer liquid-disordered over "raft" (liquid-ordered) domains when reconstituted into giant unilamellar vesicles.* Journal of Biological Chemistry, 2004. **279**(36): p. 37951-37955.

78. Murray, D.H. and L.K. Tamm, *Clustering of Syntaxin-1A in Model Membranes Is Modulated by Phosphatidylinositol 4,5-Bisphosphate and Cholesterol.* Biochemistry, 2009. **48**(21): p. 4617-4625.

79. Montes, L.R., et al., *Giant unilamellar vesicles electroformed from native membranes and organic lipid mixtures under physiological conditions.* Biophysical Journal, 2007. **93**(10): p. 3548-3554.

80. Pott, T., H. Bouvrais, and P. Meleard, *Giant unilamellar vesicle formation under physiologically relevant conditions.* Chemistry and Physics of Lipids, 2008. **154**(2): p. 115-119.

81. Tamm, L.K. and H.M. Mcconnell, *Supported Phospholipid-Bilayers.* Biophysical Journal, 1985. **47**(1): p. 105-113.

82. Kalb, E., S. Frey, and L.K. Tamm, *Formation of Supported Planar Bilayers by Fusion of Vesicles to Supported Phospholipid Monolayers.* Biochimica Et Biophysica Acta, 1992. **1103**(2): p. 307-316.

83. Boxer, S.G., *Molecular transport and organization in supported lipid membranes.* Current Opinion in Chemical Biology, 2000. **4**(6): p. 704-709.

84. Sapuri, A.R., M.M. Baksh, and J.T. Groves, *Electrostatically targeted intermembrane lipid exchange with micropatterned supported membranes.* Langmuir, 2003. **19**(5): p. 1606-1610.

85. Kam, L. and S.G. Boxer, *Spatially selective manipulation of supported lipid bilayers by laminar flow: Steps toward biomembrane microfluidics.* Langmuir, 2003. **19**(5): p. 1624-1631.

86. Keller, C.A., et al., *Formation of supported membranes from vesicles.* Physical Review Letters, 2000. **84**(23): p. 5443-5446.

87. Keller, C.A. and B. Kasemo, *Surface specific kinetics of lipid vesicle adsorption measured with a quartz crystal microbalance.* Biophysical Journal, 1998. **75**(3): p. 1397-1402.

88. Jackson, B.L. and J.T. Groves, *Scanning probe lithography on fluid lipid membranes.* Journal of the American Chemical Society, 2004. **126**(43): p. 13878-13879.

89. Kung, L.A., et al., *Patterning hybrid surfaces of proteins and supported lipid bilayers.* Langmuir, 2000. **16**(17): p. 6773-6776.

90. Johnson, J.M., et al., *Early steps of supported bilayer formation probed by single vesicle fluorescence assays.* Biophysical Journal, 2002. **83**(6): p. 3371-3379.

91. Richter, R.P., R. Berat, and A.R. Brisson, *Formation of solid-supported lipid bilayers: An integrated view.* Langmuir, 2006. **22**(8): p. 3497-3505.

92. Brian, A.A. and H.M. Mcconnell, *Allogeneic Stimulation of Cyto-Toxic T-Cells by Supported Planar Membranes.* Proceedings of the National Academy of Sciences of the United States of America-Biological Sciences, 1984. **81**(19): p. 6159-6163.

93. Salafsky, J., J.T. Groves, and S.G. Boxer, *Architecture and function of membrane proteins in planar supported bilayers: A study with photosynthetic reaction centers.* Biochemistry, 1996. **35**(47): p. 14773-14781.

94. Raguse, B., et al., *Tethered lipid bilayer membranes: Formation and ionic reservoir characterization.* Langmuir, 1998. **14**(3): p. 648-659.

95. Naumann, R., et al., *Tethered lipid Bilayers on ultraflat gold surfaces.* Langmuir, 2003. **19**(13): p. 5435-5443.

96. Giess, F., et al., *The protein-tethered lipid bilayer: A novel mimic of the biological membrane.* Biophysical Journal, 2004. **87**(5): p. 3213-3220.

97. Taylor, J.D., et al., *Regenerable Tethered Bilayer Lipid Membrane Arrays for Multiplexed Label-Free Analysis of Lipid-Protein Interactions on Poly(dimethylsiloxane) Microchips Using SPR Imaging.* Analytical Chemistry, 2009. **81**(3): p. 1146-1153.

98. Sackmann, E., *Supported membranes: Scientific and practical applications.* Science, 1996. **271**(5245): p. 43-48.

99. Sackmann, E. and M. Tanaka, *Supported membranes on soft polymer cushions: fabrication, characterization and applications.* Trends in Biotechnology, 2000. **18**(2): p. 58-64.

100. Tanaka, M., et al., *Native supported membranes on planar polymer supports and micro-particle supports.* Journal of Structural Biology, 2009. **168**(1): p. 137-142.

101. Heyse, S., et al., *Emerging techniques for investigating molecular interactions at lipid membranes.* Biochimica Et Biophysica Acta-Reviews on Biomembranes, 1998. **1376**(3): p. 319-338.

102. Knoll, W., et al., *Functional tethered lipid bilayers.* J Biotechnol, 2000. **74**(3): p. 137-58.

103. Naumann, C.A., et al., *The polymer-supported phospholipid bilayer: Tethering as a new approach to substrate-membrane stabilization.* Biomacromolecules, 2002. **3**(1): p. 27-35.

104. Wagner, M.L. and L.K. Tamm, *Tethered polymer-supported planar lipid bilayers for reconstitution of integral membrane proteins: Silane-polyethyleneglycol-lipid as a cushion and covalent linker.* Biophysical Journal, 2000. **79**(3): p. 1400-1414.

105. Munro, J.C. and C.W. Frank, *Adsorption of lipid-functionalized poly(ethylene glycol) to gold surfaces as a cushion for polymer-supported lipid bilayers.* Langmuir, 2004. **20**(8): p. 3339-3349.

106. Diaz, A.J., et al., *Double cushions preserve transmembrane protein mobility in supported bilayer systems.* Langmuir, 2008. **24**(13): p. 6820-6826.

107. V, A., et al., *Membrane on a chip: A functional tethered lipid bilayer membrane on silicon oxide surfaces.* Biophysical Journal, 2005. **89**(3): p. 1780-1788.

108. He, L.H., et al., *Tethered bilayer lipid membranes based on monolayers of thiolipids mixed with a complementary dilution molecule. 1. Incorporation of channel peptides.* Langmuir, 2005. **21**(25): p. 11666-11672.

109. Ye, Q., et al., *Liposomes Tethered to Omega-Functional PEG Brushes and Induced Formation of PEG Brush Supported Planar Lipid Bilayers.* Langmuir, 2009. **25**(23): p. 13534-13539.

110. Murray, D.H., L.K. Tamm, and V. Kiessling, *Supported double membranes.* Journal of Structural Biology, 2009. **168**(1): p. 183-189.

111. Roder, F., et al., *Reconstitution of Membrane Proteins into Polymer-Supported Membranes for Probing Diffusion and Interactions by Single Molecule Techniques.* Analytical Chemistry, 2011. **83**(17): p. 6792-6799.

112. Merzlyakov, M., et al., *Surface-supported bilayers with transmembrane proteins: Role of the polymer cushion revisited.* Langmuir, 2006. **22**(24): p. 10145-10151.

113. Besenicar, M., et al., *Surface plasmon resonance in protein-membrane interactions.* Chemistry and Physics of Lipids, 2006. **141**(1-2): p. 169-178.

114. Sigl, H., et al., *Assembly of polymer/lipid composite films on solids based on hairy rod LB-films.* European Biophysics Journal with Biophysics Letters, 1997. **25**(4): p. 249-259.

115. Munro, J.C. and C.W. Frank, *Adsorption of disulfide-modified polyacrylamides to gold and silver surfaces as cushions for polymer-supported lipid bilayers.* Polymer, 2003. **44**(20): p. 6335-6344.

116. El-Khouri, R.J., et al., *pH Responsive Polymer Cushions for Probing Membrane Environment Interactions.* Nano Letters, 2011. **11**(5): p. 2169-2172.

117. Gross, L.C.M., O.K. Castell, and M.I. Wallace, *Dynamic and Reversible Control of 2D Membrane Protein Concentration in a Droplet Interface Bilayer.* Nano Letters, 2011. **11**(8): p. 3324-3328.

118. Cooper, M.A., *Advances in membrane receptor screening and analysis.* J Mol Recognit, 2004. **17**(4): p. 286-315.

119. Boxer, S.G., *Molecular transport and organization in supported lipid membranes.* Curr Opin Chem Biol, 2000. **4**(6): p. 704-9.

120. Ruoslahti, E. and B. Obrink, *Common principles in cell adhesion.* Experimental Cell Research, 1996. **227**(1): p. 1-11.

121. Mrksich, M., *A surface chemistry approach to studying cell adhesion.* Chemical Society Reviews, 2000. **29**(4): p. 267-273.

122. Klee, D., et al., *Surface Modification of a New Flexible Polymer with Improved Cell-Adhesion.* Journal of Materials Science-Materials in Medicine, 1994. **5**(9-10): p. 592-595.

123. Shiu, J.Y., et al., *Observation of enhanced cell adhesion and transfection efficiency on superhydrophobic surfaces.* Lab on a Chip, 2010. **10**(5): p. 556-558.

124. Liu, D., et al., *Cell adhesion on nanopatterned fibronectin substrates.* Soft Matter, 2010. **6**(21): p. 5408-5416.

125. Clemence, J.F., et al., *Photoimmobilization of a Bioactive Laminin Fragment and Pattern-Guided Selective Neuronal Cell Attachment.* Bioconjugate Chemistry, 1995. **6**(4): p. 411-417.

126. Kam, L. and S.G. Boxer, *Cell adhesion to protein-micropatterned-supported lipid bilayer membranes.* Journal of Biomedical Materials Research, 2001. **55**(4): p. 487-495.

127. Groves, J.T. and M.L. Dustin, *Supported planar bilayers in studies on immune cell adhesion and communication.* Journal of Immunological Methods, 2003. **278**(1-2): p. 19-32.

128. Salaita, K., et al., *Restriction of Receptor Movement Alters Cellular Response: Physical Force Sensing by EphA2.* Science, 2010. **327**(5971): p. 1380-1385.

129. Lehnert, D., et al., *Cell behaviour on micropatterned substrata: limits of extracellular matrix geometry for spreading and adhesion.* Journal of Cell Science, 2004. **117**(1): p. 41-52.

130. Sanchez-Cortes, J., K. Bahr, and M. Mrksich, *Cell Adhesion to Unnatural Ligands Mediated by a Bifunctional Protein.* Journal of the American Chemical Society, 2010. **132**(28): p. 9733-9737.

131. Singhvi, R., et al., *Engineering Cell-Shape and Function.* Science, 1994. **264**(5159): p. 696-698.

132. Jiang, X.Y., et al., *Directing cell migration with asymmetric micropatterns.* Proceedings of the National Academy of Sciences of the United States of America, 2005. **102**(4): p. 975-978.

133. Raghavan, S., et al., *Micropaterned Dynamically Adhesive Substrates for Cell Migration.* Langmuir, 2010. **26**(22): p. 17733-17738.

134. Deeg, J.A., et al., *Impact of Local versus Global Ligand Density on Cellular Adhesion.* Nano Letters, 2011. **11**(4): p. 1469-1476.

135. Thelen, K., et al., *Cell adhesion molecule DM-GRASP presented as nanopatterns to neurons regulates attachment and neurite growth.* Soft Matter, 2007. **3**(12): p. 1486-1491.

136. Hersel, U., C. Dahmen, and H. Kessler, *RGD modified polymers: biomaterials for stimulated cell adhesion and beyond.* Biomaterials, 2003. **24**(24): p. 4385-4415.

137. Ruoslahti, E., *RGD and other recognition sequences for integrins.* Annual Review of Cell and Developmental Biology, 1996. **12**: p. 697-715.

138. Artoni, A., et al., *Integrin beta 3 regions controlling binding of murine mAb 7E3: Implications for the mechanism of integrin alpha IIb beta 3 activation.* Proceedings of the National Academy of Sciences of the United States of America, 2004. **101**(36): p. 13114-13120.

139. Beh, W.S., et al., *Formation of patterned microstructures of conducting polymers by soft lithography, and applications in microelectronic device fabrication.* Advanced Materials, 1999. **11**(12): p. 1038-1041.

140. Briseno, A.L., et al., *Patterning organic single-crystal transistor arrays.* Nature, 2006. **444**(7121): p. 913-917.

141. Behl, M., et al., *Towards plastic electronics: Patterning semiconducting polymers by nanoimprint lithography.* Advanced Materials, 2002. **14**(8): p. 588-591.

142. Arnold, M.S., et al., *Direct vapor jet printing of three color segment organic light emitting devices for white light illumination.* Applied Physics Letters, 2008. **92**(5).

143. Strong, V., et al., *Direct Sub-Micrometer Patterning of Nanostructured Conducting Polymer Films via a Low-Energy Infrared Laser.* Nano Letters, 2011. **11**(8): p. 3128-3135.

144. Blawas, A.S. and W.M. Reichert, *Protein patterning.* Biomaterials, 1998. **19**(7-9): p. 595-609.

145. MacBeath, G. and S.L. Schreiber, *Printing proteins as microarrays for high-throughput function determination.* Science, 2000. **289**(5485): p. 1760-3.

146. Zhou, H., et al., *Solution and chip arrays in protein profiling.* Trends Biotechnol, 2001. **19**(10 Suppl): p. S34-9.

147. Zhu, H., et al., *Global analysis of protein activities using proteome chips.* Science, 2001. **293**(5537): p. 2101-2105.

148. Lockhart, D.J. and E.A. Winzeler, *Genomics, gene expression and DNA arrays.* Nature, 2000. **405**(6788): p. 827-836.

149. Zhu, H. and M. Snyder, *Protein chip technology.* Current Opinion in Chemical Biology, 2003. **7**(1): p. 55-63.

150. Lynch, M., et al., *Functional protein nanoarrays for biomarker profiling.* Proteomics, 2004. **4**(6): p. 1695-1702.

151. Mendes, P.M., C.L. Yeung, and J.A. Preece, *Bio-nanopatterning of surfaces.* Nanoscale Research Letters, 2007. **2**(8): p. 373-384.

152. Kane, R.S., et al., *Patterning proteins and cells using soft lithography.* Biomaterials, 1999. **20**(23-24): p. 2363-2376.

153. Tinazli, A., et al., *High-affinity chelator thiols for switchable and oriented immobilization of histidine-tagged proteins: A generic platform for protein chip technologies.* Chemistry-a European Journal, 2005. **11**(18): p. 5249-5259.

154. Valiokas, R., et al., *Differential protein assembly on micropatterned surfaces with tailored molecular and surface multivalency.* Chembiochem, 2006. **7**(9): p. 1325-1329.

155. Li, H.W., et al., *Nanocontact printing: A route to sub-50-nm-scale chemical and biological patterning.* Langmuir, 2003. **19**(6): p. 1963-1965.

156. Coyer, S.R., A.J. Garcia, and E. Delamarche, *Facile preparation of complex protein architectures with sub-100-nm resolution on surfaces.* Angewandte Chemie-International Edition, 2007. **46**(36): p. 6837-6840.

157. Piner, R.D., et al., *"Dip-pen" nanolithography.* Science, 1999. **283**(5402): p. 661-663.

158. Huo, F.W., et al., *Polymer pen lithography.* Science, 2008. **321**(5896): p. 1658-1660.

159. Tinazli, A., et al., *Native protein nanolithography that can write, read and erase.* Nature Nanotechnology, 2007. **2**(4): p. 220-225.

160. Valiokas, R., *Nanobiochips.* Cellular and Molecular Life Sciences, 2012. **69**(3): p. 347-356.

161. Taha, H., et al., *Protein printing with an atomic force sensing nanofountainpen.* Applied Physics Letters, 2003. **83**(5): p. 1041-1043.

162. Senesi, A.J., et al., *Agarose-Assisted Dip-Pen Nanolithography of Oligonucleotides and Proteins.* Acs Nano, 2009. **3**(8): p. 2394-2402.

163. Atkins, P., de Paula, J., *Physical Chemisrty*. 2002: Oxford.

164. Barltrop, J.A., Coyle, J. D., ed. 1975, J. Wiley and Sons, Ltd.

165. Reynolds, N.P., et al., *Site-Specific Immobilization and Micrometer and Nanometer Scale Photopatterning of Yellow Fluorescent Protein on Glass Surfaces.* Journal of the American Chemical Society, 2009. **131**(3): p. 896-+.

166. Christman, K.L., et al., *Positioning Multiple Proteins at the Nanoscale with Electron Beam Cross-Linked Functional Polymers.* Journal of the American Chemical Society, 2009. **131**(2): p. 521-527.

167. Bruckbauer, A., et al., *An addressable antibody nanoarray produced on a nanostructured surface.* Journal of the American Chemical Society, 2004. **126**(21): p. 6508-6509.

168. Alonso, J.M., et al., *Photopatterned surfaces for site-specific and functional immobilization of proteins.* Langmuir, 2008. **24**(2): p. 448-457.

169. Waichman, S., et al., *Functional immobilization and patterning of proteins by an enzymatic transfer reaction.* Anal Chem, 2010. **82**(4): p. 1478-85.

170. Grunwald, C., et al., *In situ assembly of macromolecular complexes triggered by light.* Proceedings of the National Academy of Sciences of the United States of America, 2010. **107**(14): p. 6146-6151.

171. Bhagawati, M., et al., *Native laser lithography of His-tagged proteins by uncaging of multivalent chelators.* J Am Chem Soc, 2010. **132**(17): p. 5932-3.

172. Dillmore, W.S., M.N. Yousaf, and M. Mrksich, *A photochemical method for patterning the immobilization of ligands and cells to self-assembled monolayers.* Langmuir, 2004. **20**(17): p. 7223-7231.

173. Chen, S.Y. and L.M. Smith, *Photopatterned Thiol Surfaces for Biomolecule Immobilization.* Langmuir, 2009. **25**(20): p. 12275-12282.

174. San Miguel, V., et al., *Multiphoton Reactive Surfaces Using Ruthenium(II) Photocleavable Cages.* Langmuir, 2012. **28**(2): p. 1217-21.

175. Manova, R., T.A. van Beek, and H. Zuilhof, *Surface Functionalization by Strain-Promoted Alkyne-Azide Click Reactions.* Angewandte Chemie-International Edition, 2011. **50**(24): p. 5428-5430.

176. Jonkheijm, P., et al., *Photochemical surface patterning by the thiol-ene reaction.* Angewandte Chemie-International Edition, 2008. **47**(23): p. 4421-4424.

177. Weinrich, D., et al., *Oriented immobilization of farnesylated proteins by the thiol-ene reaction.* Angew Chem Int Ed Engl, 2010. **49**(7): p. 1252-7.

178. Bhagawati, M., et al., *Organization of Motor Proteins into Functional Micropatterns Fabricated by a Photoinduced Fenton Reaction.* Angewandte Chemie-International Edition, 2009. **48**(48): p. 9188-9191.

179. Son, K.J., et al., *Graft Copolymer-Templated Mesoporous TiO(2) Films Micropatterned with Poly(ethylene glycol) Hydrogel: Novel Platform for Highly Sensitive Protein Microarrays.* Acs Applied Materials & Interfaces, 2011. **3**(2): p. 573-581.

180. Matsuo, T., *Carbonyl absorption bands in the infrared spectra of some cyclic imides with a five-membered ring.* Bull Chem Soc of Jpn, 1964(37): p. 1844-1848.

181. Nakayama, Y. and G. Smets, *Radical and anionic homopolymerization of maleimide and N-n-butylmaleimide.* J Polym Sci A-1, 1967. **5**: p. 1619-1633.

182. Hoyle, C.E., et al., *Photopolymerization using maleimides as photoinitiators.* Polymer, 1997. **38**(22): p. 5695-5697.

183. Yamada, M., I. Takase, and N. Koutou, *Photopolymerization of Maleimide and Its N-Substituted Derivatives.* Journal of Polymer Science Part B-Polymer Letters, 1968. **6**(12PB): p. 883-&.

184. Aida, H., I. Takase, and T. Nozi, *Uv-Induced Polymerization of Maleimides in Solution.* Makromolekulare Chemie-Macromolecular Chemistry and Physics, 1989. **190**(11): p. 2821-2831.

185. Jonsson, S., et al., *Recent advances in photoinduced donor acceptor copolymerization.* Nuclear Instruments & Methods in Physics Research Section B-Beam Interactions with Materials and Atoms, 1999. **151**(1-4): p. 268-278.

186. Decker, C.M., F.; Jönsson, S.; Clark, S.; Hoyle, C.; , in *Macromolecular Chemistry and Physics*. 1999. p. 1005-1013.

187. Decker, C.B., C.; Morel, F.; Jonsson, S.; Hoyle, C.;, Macromolecular Chemistry and Physics, 2000. **201**: p. 1493-1503.

188. von Sonntag, J., et al., *Electron transfer as the initiation mechanism of photocurable maleimide-vinyl ether based resins.* Radiation Physics and Chemistry, 1999. **55**(5-6): p. 609-613.

189. von Sonntag, J.K., W.;, Journal of Photochemistry and Photobiology A: Chemistry, 2000(136): p. 133-139.

190. Decker, C., *The use of UV irradiation in polymerization.* Polymer International, 1998. **45**(2): p. 133-141.

191. Isaacs, A. and J. Lindenmann, *Virus Interference .1. The Interferon.* Proceedings of the Royal Society of London Series B-Biological Sciences, 1957. **147**(927): p. 258-267.

192. Domanski, P. and O.R. Colamonici, *The type-I interferon receptor. The long and short of it.* Cytokine Growth Factor Rev, 1996. **7**(2): p. 143-51.

193. Lamken, P., et al., *Ligand-induced assembling of the type I interferon receptor on supported lipid bilayers.* Journal of Molecular Biology, 2004. **341**(1): p. 303-318.

194. Piehler, J. and G. Schreiber, *Biophysical analysis of the interaction of human ifnar2 expressed in E-coli with IFN alpha 2.* Journal of Molecular Biology, 1999. **289**(1): p. 57-67.

195. Piehler, J. and G. Schreiber, *Fast transient cytokine-receptor interactions monitored in real time by reflectometric interference spectroscopy.* Analytical Biochemistry, 2001. **289**(2): p. 173-186.

196. Cutrone, E.C. and J.A. Langer, *Contributions of cloned type I interferon receptor subunits to differential ligand binding.* Febs Letters, 1997. **404**(2-3): p. 197-202.

197. Novick, D., B. Cohen, and M. Rubinstein, *The Human Interferon-Alpha/Beta Receptor - Characterization and Molecular-Cloning.* Cell, 1994. **77**(3): p. 391-400.

198. Colamonici, O.R., et al., *P135(Tyk2), an Interferon-Alpha-Activated Tyrosine Kinase, Is Physically Associated with an Interferon-Alpha Receptor.* Journal of Biological Chemistry, 1994. **269**(5): p. 3518-3522.

199. Li, X.X., et al., *Functional subdomains of STAT2 required for preassociation with the alpha interferon receptor and for signaling.* Molecular and Cellular Biology, 1997. **17**(4): p. 2048-2056.

200. Stark, G.R., et al., *How cells respond to interferons.* Annual Review of Biochemistry, 1998. **67**: p. 227-264.

201. Schindler, C., et al., *Interferon-Dependent Tyrosine Phosphorylation of a Latent Cytoplasmic Transcription Factor.* Science, 1992. **257**(5071): p. 809-813.

202. Platanias, L.C., *Mechanisms of type-I- and type-II-interferon-mediated signalling.* Nature Reviews Immunology, 2005. **5**(5): p. 375-86.

203. Kalie, E., et al., *An interferon alpha2 mutant optimized by phage display for IFNAR1 binding confers specifically enhanced antitumor activities.* J Biol Chem, 2007. **282**(15): p. 11602-11.

204. Turgut, Z., et al., *Microstructural and magnetic observations of compacted FeCoV nanoparticles.* Ieee Transactions on Magnetics, 2000. **36**(5): p. 3024-3025.

205. Kalie, E., et al., *The Stability of the Ternary Interferon-Receptor Complex Rather than the Affinity to the Individual Subunits Dictates Differential Biological Activities.* Journal of Biological Chemistry, 2008. **283**(47): p. 32925-32936.

206. Slutzki, M., et al., *Variations in the unstructured C-terminal tail of interferons contribute to differential receptor binding and biological activity.* Journal of Molecular Biology, 2006. **360**(5): p. 1019-1030.

207. Piehler, J., et al., *Assessment of affinity constants by rapid solid phase detection of equilibrium binding in a flow system.* Journal of Immunological Methods, 1997. **201**(2): p. 189-206.

208. Gauglitz, G., et al., *Chemical and Biochemical Sensors Based on Interferometry at Thin (Multi-)Layers.* Sensors and Actuators B-Chemical, 1993. **11**(1-3): p. 21-27.

209. Piehler, J., et al., *Specific binding of low molecular weight ligands with direct optical detection.* Biosensors & Bioelectronics, 1997. **12**(6): p. 531-538.

210. Waichman, S., et al., *Functional Immobilization and Patterning of Proteins by an Enzymatic Transfer Reaction.* Analytical Chemistry, 2010. **82**(4): p. 1478-1485.

211. Gavutis, M., S. Lata, and J. Piehler, *Probing 2-dimensional protein-protein interactions on model membranes.* Nature Protocols, 2006. **1**(4): p. 2091-2103.

212. Axelrod, D., *Cell-Substrate Contacts Illuminated by Total Internal-Reflection Fluorescence.* Journal of Cell Biology, 1981. **89**(1): p. 141-145.

213. Amos, W.B. and J.G. White, *How the Confocal Laser Scanning Microscope entered Biological Research.* Biology of the Cell, 2003. **95**(6): p. 335-342.

214. Minsky, M., *Memoir on Inventing the Confocal Scanning Microscope.* Scanning, 1988. **10**(4): p. 128-138.

215. Nathan S. Claxton, T.J.F., and Michael W. Davidson, *Laser scanning confocal microscopy*, Laser scanning confocal microscopy; Olympus.

216. Ambrose, E.J., *Surface Contact Microscope for the Study of Cell Movements.* Nature, 1956. **178**(4543): p. 1194-1194.

217. Axelrod, D., *Total internal reflection fluorescence microscopy in cell biology.* Traffic, 2001. **2**(11): p. 764-774.

218. Appelhans, T., et al., *Nanoscale Organization of Mitochondrial Microcompartments Revealed by Combining Tracking and Localization Microscopy.* Nano Letters, 2012. **12**(2): p. 610-616.

2 Functional Immobilization of Proteins by an Enzymatic Transfer Reaction

2.1 Introduction

Protein immobilization on solid supports is rapidly gaining importance in diverse applications that require targeting of proteins to surfaces, while preserving their functional integrity to the highest possible level. Functional attachment of proteins to solid supports is a key challenge because of the fragile nature of proteins and their wide-ranging physicochemical properties. For this purpose, protein capturing techniques are required, which site-specifically tether proteins to biocompatible polymer layers through protein or peptide tags fused to the protein of interest. However, selective recognition pairs with high binding stability are required for successful applications in surface engineering. Several approaches based on either the interaction between biotin and streptavidin or related proteins [1-4], or on the complexation of immobilized transition metal ions by oligohistidine-tags [5-8] have been reported. In addition to protein capturing through affinity handles, covalent approaches such as chemical ligation [9], Staudinger ligation [10], thiol-ene reaction [3] or “click” chemistry utilizing azide alkyne Huisgen cycloaddition [11], were applied. Recently, enzymatic reactions have found increasing attention for posttranslational labeling and immobilization of proteins [12, 13]. Surface chemistries based on enzymes, which specifically react with substrate analogues [14], have been developed [15, 16]. Another prominent approach is based on enzymatic phosphopantetheinyl transfer (PPT) as discussed in detail in 1.2.4.

Here, we have explored PPT-based functional immobilization of proteins fused to the short peptides ybbR and S6 onto glass type surfaces in a flow through format. To this end, CoA was coupled to a dense poly(ethylene glycol) (PEG) polymer brush and protein immobilization was monitored in real time by label-free detection using reflectance interference spectroscopy (RIfS). Immobilization of the extracellular domains of the type I interferon receptor subunits IFNAR1 and IFNAR2 (IFNAR1-EC and IFNAR2-EC, respectively) fused to ybbR- and S6-tags mediated by the PPTase Sfp was investigated. The functionality of the immobilized protein was

probed quantitatively by monitoring binding of the protein ligand interferon-α2 (IFNα2). We explored immobilization at different termini, as well as immobilization of ybbR-tagged IFNα2.

2.2 Experimental

2.2.1 Materials

Homo-bifunctional diamino-polyethylene glycol (DAPEG) with an average molecular mass of 2000 g/mol was purchased from Rapp Polymere, Tübingen/Germany. 2-mercaptoethanol (2-ME), manganese(II)-chloride tetrahydrat, HEPES and Sodium chloride were purchased from Carl Roth, Karlsruhe/Germany. Oregon Green 488 maleimide was purchased from Invitrogen. Streptavidin labeled with ATTO 565 (AT565SAv) was purchased from ATTO-TEC GmbH, Siegen/Germany. CoA-488 and phosphopantetheinyl transferase Sfp was purchased from New England Biolabs GmbH (Frankfurt am Main, Germany). All other chemicals were purchased from Sigma Aldrich.

2.2.2 Protein production, purification and labeling

IFNα2, IFNα2-YNS and IFNAR2-EC carrying an N-terminal ybbR-tag (ybbR-IFNα2, ybbR-IFNα2-YNS and ybbR-IFNAR2) were cloned by insertion of an oligonucleotide linker coding for the ybbR peptide (DSLEFIASKLA) into the *Nde*I restriction site upstream of the corresponding genes in the plasmids pT72Cα2 and pT72CR2, respectively [17]. The proteins were expressed and purified by the same protocols established for wild-type IFNα2 and wild-type IFNAR2-EC [18]. IFNAR2 with C-terminal ybbR- and S6-tags (IFNAR2-ybbR and IFNAR2-S6) were cloned by inserting the corresponding oligonucleotide linker coding for the corresponding peptides sequences (GDSLSWLLRLLN in case of S6) into a *Sal*I restriction site, which was generated at the C-terminus of IFNAR2-EC in pT72CR2 by removing the stop codon by site-directed mutagenesis. These proteins were expressed in *E. coli*, refolded from inclusion bodies and purified as described previously [17, 19]. IFNAR2-ybbR and ybbR-IFNα2 were labeled by PPT using CoA-488 and Sfp according to published protocols [20]. His-tagged IFNAR1-EC and its mutant N23C were expressed in insect cells and purified by IMAC as described previously [21]. IFNAR1-EC N23C

was site-specifically labeled with Oregon Green 488 (^{OG488}IFNAR1-EC) as described recently [22]. His-tagged IFNAR1-EC was fused to a C-terminal ybbR-tag by insertion of an oligonucleotide linker coding for the ybbR peptide and was expressed and purified the same way as IFNAR1-EC.

2.2.3 Surface chemistry

Surface chemistry was carried out on transducer slides for RIfS detection (a thin silica layer on a glass substrate). Surface coating with a thin PEG polymer brush and further functionalization with maleimide groups was carried out as described in detail previously [23]: After surface cleaning in fresh Piranha solution (one part 30% H_2O_2 and two parts concentrated H_2SO_4), the surface was activated by reaction with pure (3-glycidyloxypropyl)trimethoxysilane for 1 h at 75 °C. Subsequently, the surface was reacted with molten DAPEG for 4 h at 75 °C. For functionalization with maleimide groups, the amine-functionalized surfaces were incubated under a saturated solution of 3-(maleimido)propionic acid N-Hydroxy-succinimide ester (MPA-NHS) in dry DMF for 30 min at room-temperature. All further steps were carried out *in situ* under aqueous conditions in a flow-through format (see below).

2.2.4 Binding assays

Protein immobilization and protein interactions were monitored by RIfS and by total internal reflection fluorescence spectroscopy (TIRFS). Label-free detection by RIfS is based on probing changes in optical thickness of a thin silica layer by white light interference [24] as mentioned at the general introduction. The measurements were performed under continuous flow-through conditions using home-built set-ups as described in detail earlier [25-27]. Maleimide-functionalized RIfS transducer slides (prepared as described above) were equilibrated in HBS (20 mM HEPES pH 7.5, 150 mM sodium-chloride and 0.01% Triton X-100) and then reacted with 1 mM CoA in HBS. Prior to protein immobilization, the remaining maleimide groups were blocked by injection of 10 mM 2-mercaptoethanol in HBS. Subsequently, 1 µM of the extracellular domain of the type I interferon subunit IFNAR2 (IFNAR2-EC) which was fused to a ybbR tag at the N-terminus (ybbR-IFNAR2) in HBS was immobilized in the presence of 1 µM Sfp and 10 mM Mn^{2+} ions. Surface-bound metal ions were removed by an injection of 25 mM EDTA. Then, the activity of the immobilized protein was probed by injecting a suitable binding partner:

ybbR-IFNAR2, IFNAR2-ybbR and IFNAR2-S6 were probed by injection of the ligand interferon-α2 (IFNα2). YbbR-IFNα2 and ybbR-IFNα2-YNS were probed by injection of the interferon receptor subunits IFNAR2-EC and IFNAR1-EC, respectively.

Association and dissociation curves were fitted using the BIAevaluation 3.1 software (GE Healthcare). Standard kinetic models assuming a 1:1 Langmuir interaction as provided by the software were applied. For binding kinetics at relatively high protein surface concentrations employed in RIfS experiments, simultaneous fitting of the association and dissociation curves by a model considering mass transport effects was applied. At low protein surface concentrations used in TIRFS experiments, association and dissociation curves were fitted separately with single exponential functions assuming an unbiased 1:1 Langmuir interaction.

2.3 Results and discussion

2.3.1 Protein immobilization

Immobilization of proteins on solid supports was carried out by employing a bottom-up chemical strategy based on a PEG polymer brush as a biocompatible scaffold [23] for preventing non-specific adsorption of proteins onto surfaces. The chemical strategy was described in 1.2.4. Surfaces presenting maleimide functionalities were employed for attachment of CoA via its thiol group as depicted in Figure 2-1. Subsequently, the immobilization of the protein of interest fused to ybbR tag was carried out through PPT mediated by Sfp and Mn^{2+}. CoA functionalization and protein immobilization were probed directly, in real time using RIfS.

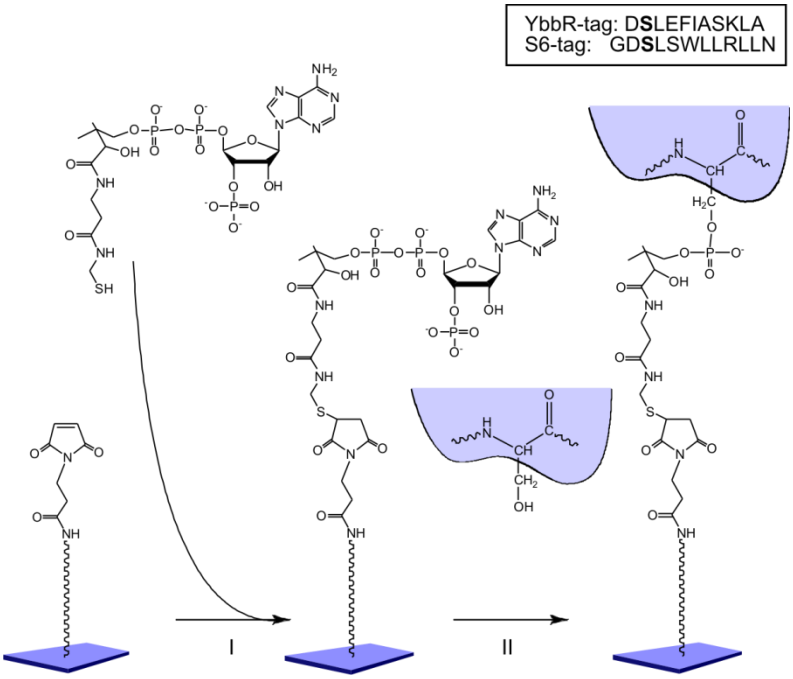

Figure 2-1. Surface chemistry based on maleimide functionalities for the immobilization of ybbR-tagged proteins onto solid supports. Attachment of CoA molecules (I) followed by ybbR-tagged protein immobilization in the presence of Sfp and Mn^{2+}(II).

The immobilization procedure is depicted in Figure 2-2a and the binding experiment is shown in Figure 2-2b. After CoA moieties were reacted with surface maleimides, free maleimide groups were quenched by reaction with 2-mercaptoethanol (2-ME). YbbR-IFNAR2 immobilization was carried out in the presence of Sfp and Mn^{2+}. Subsequent injection of the ligand IFNα2-wt confirmed functional immobilization of ybbR-IFNAR2. In this method, CoA functions as a substrate for protein immobilization by PPT as verified via an experiment which was carried out in the absence of CoA (Figure 2-2b). An insignificant amount of protein binding was observed, confirming the very low level of nonspecific binding to the PEG polymer brush.

Figure 2-2c is the magnified binding signal of IFNα2-wt interaction with the immobilized ybbR-IFNAR2 as obtained from the binding assay presented in Figure 2-2b. The interaction analysis was carried out using a pseudo-first order association and dissociation kinetic model, which takes into account mass transfer effects. Association rate constant of $1\times10^{6}\,M^{-1}s^{-1}$ was determined, while the dissociation yielded a rate constant of 0.02 s. Both kinetic parameters obtained, fit perfectly with previous analysis reported using different immobilization methods [22, 25, 28].

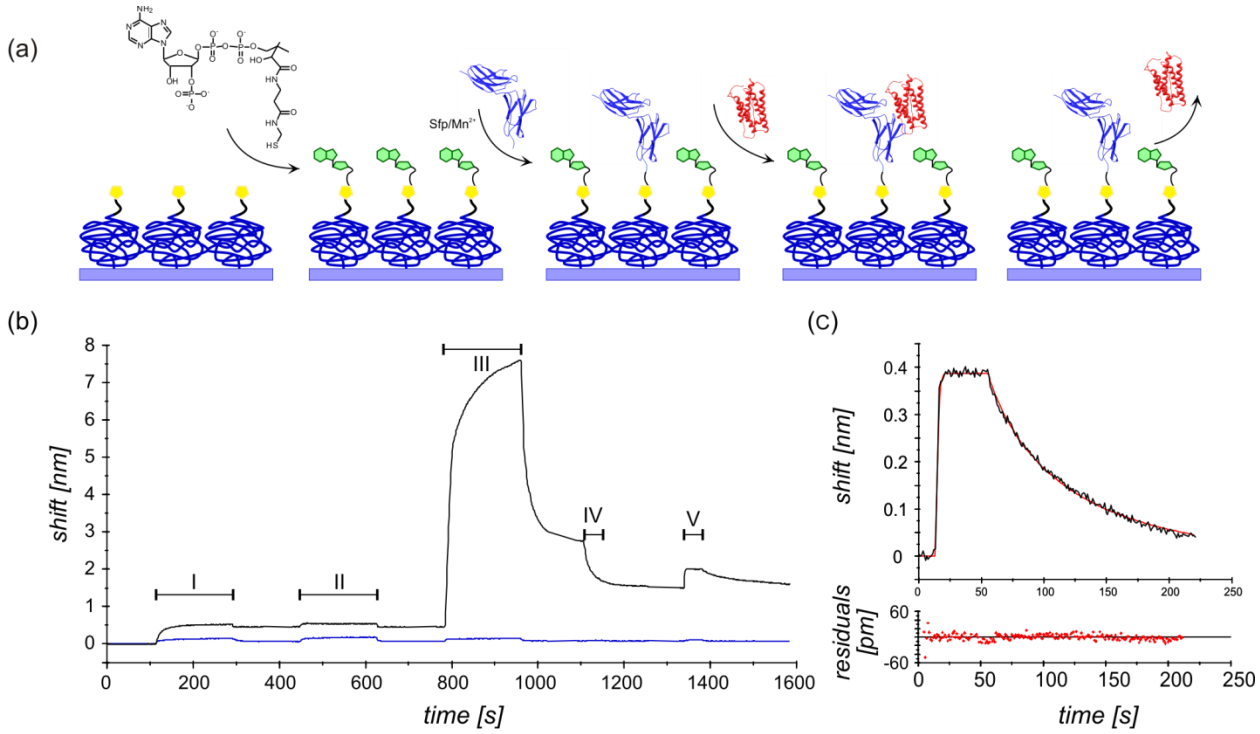

Figure 2-2. Site-specific immobilization of ybbR-IFNAR2 as detected using RIfS. (a) Schematic representation of the sequential steps of the immobilization procedure. (b) Binding signal of the immobilization process (black). Injection of CoA (I) followed by 2-ME (II). Next, a mixture of 1 µM ybbR-IFNAR2 ,1 µM Sfp and Mn^{2+} was introduced into the flow system for specific covalent coupling of the protein to the surface (III). Subsequent EDTA injection was carried out for removal of Mn^{2+} metal ions from the surface (IV). At the final step the interaction of the ligand IFNα2-wt with the immobilized receptor was detected (V). A measurement in which 2-ME was injected to the system instead of CoA (step I, blue) was carried out as a control for the binding assay. The next steps (II-V) were performed exactly as indicated for the black curve. (c) Enlarged view of step V from the black curve showing the interaction of IFNα2-wt with its surface immobilized receptor. The curve could be very well fitted using a pseudo-first order kinetic model considering mass transfer effects.

In addition, the specificity of the immobilization method was examined. For this purpose, experiments on CoA functionalized surfaces with and without subsequent 2-ME treatment were carried out. Sfp signals obtained on these surfaces are shown in Figure 2-3a. The significant binding signal of Sfp, which was observed on a non-treated surface, emphasizes the need for 2-ME blocking step in order to prevent non-specific attachment of proteins that contain free cysteine residues, as Sfp in our case. Furthermore, the specificity of the tag was investigated (Figure 2-3b). Upon injection of Sfp and IFNAR2-EC without an ybbR-tag, a low amount of protein was bound to the surface. Moreover, a binding signal of IFNα2-wt could not be detected (Figure 2-3c). The same observed for a binding experiment performed in the absence of CoA (Figure 2-3c), confirming the high specificity of the PPT-mediated

immobilization. In addition, a binding inhibition assay was carried out as demonstrated in Figure 2-3d. Binding of IFNα2-wt could not be observed in presence of soluble IFNAR2-EC, corroborating the specificity of the interaction. Hence, the data presented above confirms the selectivity of immobilization of proteins by PPT, in which the functional properties of the immobilized protein are retained to a high degree.

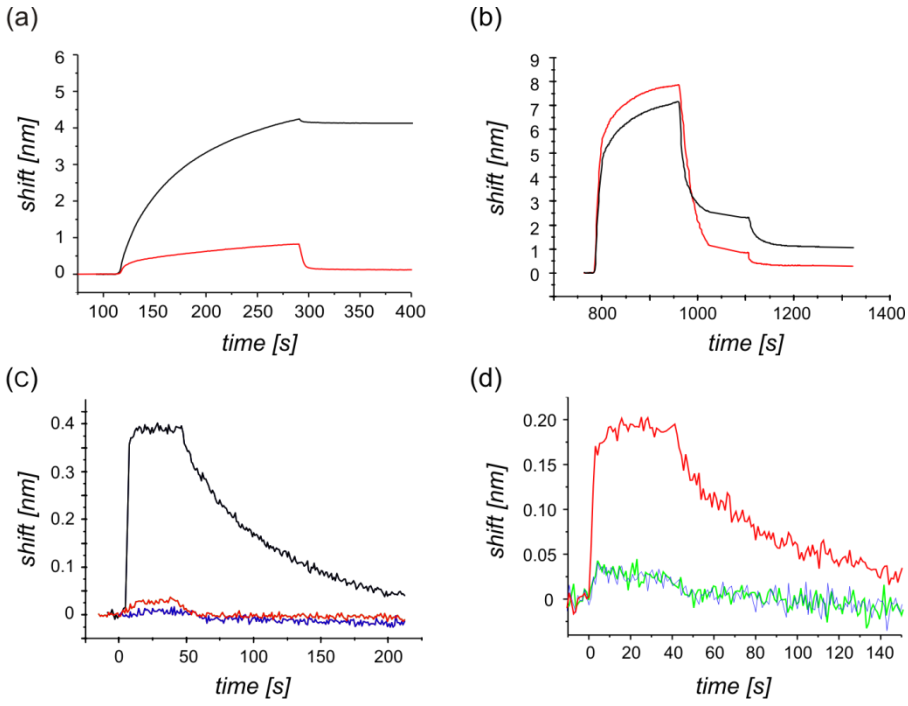

Figure 2-3. Binding specificity (a) Binding signals of Sfp obtained on CoA surface treated with (red) and without (black) 2-ME prior to Sfp injection. (b) Injection of the protein binding mixture which in addition to Sfp and Mn^{2+}contains ybbR-tagged IFNAR2 (black) or tagless-IFNAR2-EC (red). (c) IFNα2-wt binding signal observed after ybbR-IFNAR2 immobilization in presence (black) and in absence (red) of CoA on the surface. IFNα2-wt signal obtained using tagless-IFNAR2-EC at the reaction mixture (blue). (d) Binding inhibition carried out in presence (blue) and in absence (red) of IFNAR2-EC. Green curve represents injection of the IFNAR2-EC as a control.

2.3.2 Generic application of PPT-based immobilization

PPT-based immobilization was further applied to different proteins. Immobilization of IFNα2-wt carrying an N-terminal ybbR-tag was employed (ybbR-IFNα2), yielding a typical binding curve of IFNAR2-EC (Figure 2-4a). Moreover, the immobilized ybbR-IFNα2 retained a high degree of functionality over time as verified by the IFNAR2-EC binding signals obtained (Figure 2-4b). The immobilization procedure was also applied using the IFNα2 mutant YNS. YbbR-IFNα2-YNS was

immobilized on a CoA surface exactly in the same manner as previously discussed and its functionality was probed by the interaction with IFNAR2-EC (Figure 2-4c) and IFNAR1-EC (Figure 2-4d). Kinetic measurements of ybbR-IFNα2-YNS produced similar binding affinities towards IFNAR2-EC as for ybbR-IFNα2, but higher affinities towards IFNAR1-EC [29]. The immobilization data obtained using different ybbR-tagged proteins and the reversibility of the interaction with the binding partner corroborates, in addition to specificity, the applicability of this method on different types of proteins.

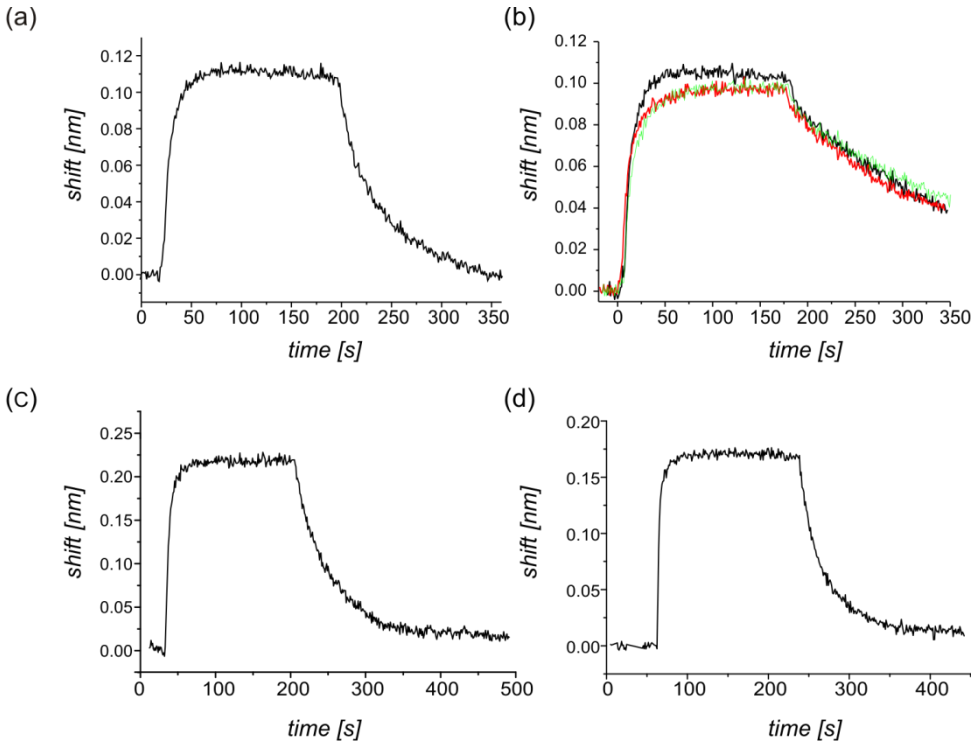

Figure 2-4. Interaction signals of soluble IFNAR subunits with various ybbR-tagged proteins. The interaction signal of IFNAR2-EC with the immobilized ybbR-IFNα2-wt (a). Binding signal of IFNAR2-EC observed (black) after 1 h (red) and after 24 h (green) (b). The interaction signals of IFNAR2-EC (c) and IFNAR1-EC (d) with immobilized ybbR-IFNα2-YNS.

2.3.3 Protein immobilization via N- or C- termini ybbR-tag fusion

Next, we probed the impact of the location of the tag on the immobilization efficiency. To this end, ybbR-tags were fused at the C-termini of IFNAR2-EC (IFNAR2-ybbR) and IFNAR1-EC (IFNAR1-ybbR). Upon immobilization of these proteins *in situ* as discussed previously, very low amounts of proteins were stably bound on the surface. Moreover, interaction of the injected IFNα2-wt with the immobilized IFNAR2-ybbR could not be observed (Figure 2-5a). A comparison

between immobilized ybbR-IFNAR2 and IFNAR2-ybbR is demonstrated in Figure 2-5a. In order to further explore whether immobilization of proteins tagged via their C-termini was possible, we employed a highly sensitive approach that combines label-free detection together with solid-phase fluorescence detection TIRFS-RIF. For these measurements, IFNα2 and its mutant IFNα2-YNS were labeled with the fluorescent dye ATTO488. After IFNAR2-ybbR immobilization and upon injection of ^{AT488}IFNα2, the interaction of the labeled ligand with the immobilized receptor could be detected (Figure 2-5b). The same approach was carried out using surface-immobilized IFNAR1-ybbR in which ^{AT488}IFNα2-YNS binding signal was monitored (Figure 2-5c). These results confirm a selective immobilization of proteins tagged through their C-terminus, although at a very low efficiency as compared with the N-terminus fusion. This can be due to a constraint in the enzyme recognition of the tag, accessibility obstacles or the impact of the amino-acids conjugated to the tag at the C-terminus.

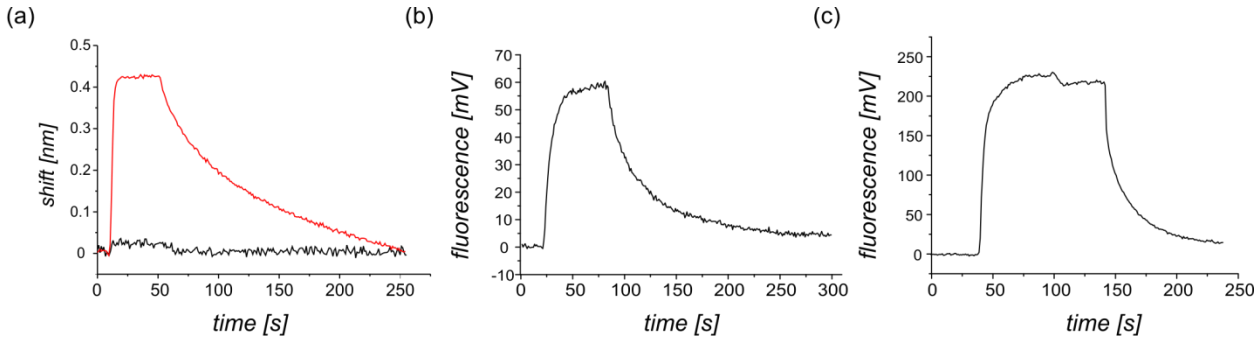

Figure 2-5. The effect of C-terminus ybbR-tag on the immobilization efficiency. (a) IFNα2-wt RIfS signals detected by the interaction with immobilized ybbR-IFNAR2 (red) and IFNAR2-ybbR (black). (b) ^{AT488}IFNα2 fluorescence signal detected by the interaction with surface immobilized IFNAR2-ybbR. (c) ^{AT488}IFNα2-YNS fluorescence signal detected by the interaction with surface immobilized IFNAR1-ybbR.

2.3.4 Protein immobilization via a short peptide tag - S6

The S6 tag is a short peptide chain comprising 12 amino acids, which was developed for orthogonal protein labeling by Sfp and ACPS as discussed in 1.2.4. This tag was proved to be highly efficient for protein labeling when fused to the protein of interest at the N- as well as at the C-terminus. Moreover, the catalytic efficiency (K_{cat}/K_M) of S6-tag is twice as high as for the ybbR tag [30]. The tag was genetically fused to IFNAR2-EC in its C-terminus and the efficiency of the immobilization was tested. A comparison of the immobilization efficiencies of IFNAR2-ybbR

and IFNAR2-S6 was performed by analyzing the interaction with IFNα2 as demonstrated in Figure 2-6. A significant difference in the amplitude signals suggests that the efficiency using S6 tag at the C-terminus of the protein is higher than that using the ybbR tag. Both tags share the same conserved sequence DSL (cf. Figure 2-1) which has been proved to be essential for enzymatic recognition. However, it is not clear whether the glycine residue at the N-terminus of the S6 is responsible for better catalysis or if the different residues at the C terminus of the tags make the difference. The binding curve of IFNα2-wt to immobilized IFNAR2-S6 was fitted using a simultaneous fitting model for association and dissociation based on first order kinetics considering mass transfer effects. Association rate constant of $2\times10^{6}\,M^{-1}s^{-1}$ and dissociation rate constant of 0.014 s were obtained. This is in a good agreement with the results discussed above and with the results previously reported [22, 25, 28].

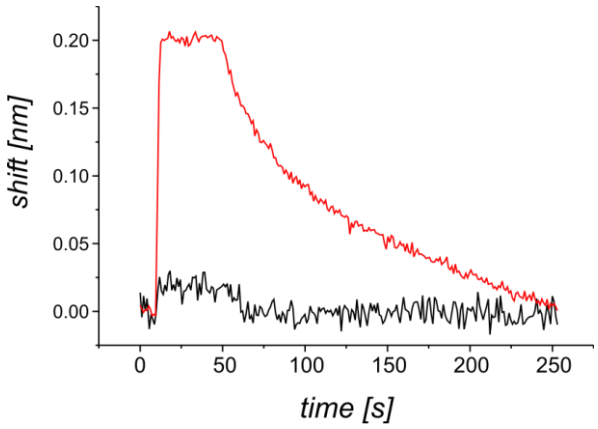

Figure 2-6. A comparison of enzymatic catalysis efficiency between IFNAR2-EC immobilized via C-terminal S6 (red) and C-terminal ybbR tag (black) detected by injection of 1 µM IFNα2-wt.

2.4 Summary and conclusions

We have implemented here a protein immobilization method which relies upon enzymatic catalysis by PPT. Using this method, a site-specific, covalent linkage between the protein of interest and its substrate was obtained while the biological activity of the immobilized proteins was preserved to a high degree. The method is based on a PEG polymer brush as a biocompatible platform, which inhibits non-specific proteins-substrate interactions. Surface binding of proteins was measured using RIfS or a simultaneous label-free and fluorescence

detection based on total internal reflection (TIRFS-RIF) in a flow through format. Rapid immobilization (150 s in RIfS and 180 s in TIRFS-RIF) using ybbR-tagged proteins at a low micromolar concentration range (1 µM) was possible. Subsequent analysis allowed determining kinetics and affinities of the protein complexes, therefore resulting in a direct quantitative confirmation of the protein activity after immobilization. Albeit immobilization of ybbR-tagged proteins through their C-termini was shown to have low efficiency as compared with N-termini, utilizing S6 tag fused at the C-terminus of the protein of interest was emerged to be an appropriate alternative.

We envisage that this immobilization method will open exciting prospects for applications in combination with fluorescence imaging techniques. Therefore, this method will be a valuable tool for covalent functional protein immobilization for bioanalytical and biophysical applications such as label- free biosensor detection, single molecule force spectroscopy and fluorescence imaging techniques.

2.5 References

1. Christman, K.L., et al., *Submicron streptavidin patterns for protein assembly.* Langmuir, 2006. **22**(17): p. 7444-50.
2. Hyun, J., et al., *Microstamping on an activated polymer surface: Patterning biotin and streptavidin onto common polymeric biomaterials.* Langmuir, 2001. **17**(20): p. 6358-6367.
3. Jonkheijm, P., et al., *Photochemical surface patterning by the thiol-ene reaction.* Angew Chem Int Ed Engl, 2008. **47**(23): p. 4421-4.
4. Alonso, J.M., et al., *Photopatterned Surfaces for Site-Specific and Functional Immobilization of Proteins.* Langmuir, 2008. **24**(2): p. 448-457.
5. Lata, S. and J. Piehler, *Stable and functional immobilization of histidine-tagged proteins via multivalent chelator headgroups on a molecular poly(ethylene glycol) brush.* Anal Chem, 2005. **77**(4): p. 1096-105.

6. Strunk, J.J., et al., *Probing Protein Conformations by in Situ Non-Covalent Fluorescence Labeling.* Bioconjugate Chemistry, 2009. **20**(1): p. 41-46.
7. Rakickas, T., et al., *Protein-protein interactions in reversibly assembled nanopatterns.* Nano Letters, 2008. **8**(10): p. 3369-75.
8. Bhagawati, M., et al., *Organization of Motor Proteins into Functional Micropatterns Fabricated by a Photoinduced Fenton Reaction.* Angewandte Chemie-International Edition, 2009. **48**(48): p. 9188-9191.
9. Camarero, J.A., Y. Kwon, and M.A. Coleman, *Chemoselective attachment of biologically active proteins to surfaces by expressed protein ligation and its application for "protein chip" fabrication.* J Am Chem Soc, 2004. **126**(45): p. 14730-1.
10. Kalia, J., N.L. Abbott, and R.T. Raines, *General method for site-specific protein immobilization by Staudinger ligation.* Bioconjug Chem, 2007. **18**(4): p. 1064-9.
11. Jean-François Lutz, *1,3-Dipolar Cycloadditions of Azides and Alkynes: A Universal Ligation Tool in Polymer and Materials Science.* Angewandte Chemie International Edition, 2007. **46**(7): p. 1018-1025.
12. Johnsson, N. and K. Johnsson, *Chemical tools for biomolecular imaging.* ACS Chem Biol, 2007. **2**(1): p. 31-8.
13. Johnsson, N., N. George, and K. Johnsson, *Protein chemistry on the surface of living cells.* Chembiochem, 2005. **6**(1): p. 47-52.
14. Juillerat, A., et al., *Directed evolution of O6-alkylguanine-DNA alkyltransferase for efficient labeling of fusion proteins with small molecules in vivo.* Chem Biol, 2003. **10**(4): p. 313-7.
15. Sielaff, I., et al., *Protein function microarrays based on self-immobilizing and self-labeling fusion proteins.* Chembiochem, 2006. **7**(1): p. 194-202.
16. Tugulu, S., et al., *Protein-functionalized polymer brushes.* Biomacromolecules, 2005. **6**(3): p. 1602-1607.
17. Piehler, J. and G. Schreiber, *Biophysical analysis of the interaction of human ifnar2 expressed in E-coli with IFN alpha 2.* J Mol Biol, 1999. **289**(1): p. 57-67.

18. Piehler, J., L.C. Roisman, and G. Schreiber, *New structural and functional aspects of the type I interferon- receptor interaction revealed by comprehensive mutational analysis of the binding interface.* Journal of Biological Chemistry, 2000. **275**(51): p. 40425-40433.

19. Piehler, J. and G. Schreiber, *Mutational and structural analysis of the binding interface between type I interferons and their receptor ifnar2.* J Mol Biol, 1999. **294**(1): p. 223-237.

20. Yin, J., et al., *Site-specific protein labeling by Sfp phosphopantetheinyl transferase.* Nat Protoc, 2006. **1**(1): p. 280-5.

21. Lamken, P., et al., *Ligand-induced assembling of the type I interferon receptor on supported lipid bilayers.* J Mol Biol, 2004. **341**(1): p. 303-18.

22. Strunk, J.J., et al., *Ligand binding induces a conformational change in ifnar1 that is propagated to its membrane-proximal domain.* J Mol Biol, 2008. **377**(3): p. 725-39.

23. Kaminski, W.E., A. Piehler, and G. Schmitz, *Genomic organization of the human cholesterol-responsive ABC transporter ABCA7: Tandem linkage with the minor histocompatibility antigen HA-1 gene.* Biochemical and Biophysical Research Communications, 2000. **278**(3): p. 782-789.

24. Brecht, A., G. Gauglitz, and J. Polster, *Interferometric immunoassay in a FIA-system: a sensitive and rapid approach in label-free immunosensing.* Biosens Bioelectron, 1993. **8**: p. 387-392.

25. Piehler, J. and G. Schreiber, *Fast transient cytokine-receptor interactions monitored in real time by reflectometric interference spectroscopy.* Anal Biochem, 2001. **289**(2): p. 173-86.

26. Gavutis, M., S. Lata, and J. Piehler, *Probing 2-dimensional protein-protein interactions on model membranes.* Nature Protocols, 2006. **1**(4): p. 2091-2103.

27. Gavutis, M., et al., *Lateral ligand-receptor interactions on membranes probed by simultaneous fluorescence-interference detection.* Biophys J, 2005. **88**(6): p. 4289-302.

28. Lamken, P., et al., *Functional cartography of the ectodomain of the type I interferon receptor subunit ifnar1.* J Mol Biol, 2005. **350**(3): p. 476-88.

29. Kalie, E., et al., *An interferon alpha2 mutant optimized by phage display for IFNAR1 binding confers specifically enhanced antitumor activities.* J Biol Chem, 2007. **282**(15): p. 11602-11.

30. Zhou, Z., et al., *Genetically encoded short peptide tags for orthogonal protein labeling by Sfp and AcpS phosphopantetheinyl transferases.* ACS Chem Biol, 2007. **2**(5): p. 337-46.

3 Maleimide photolithography for single molecule protein-protein interaction analysis in micropatterns

3.1 Introduction

Lateral organization of proteins into functional microstructures has a major impact not only in fundamental research but also in analytical and biomedical applications [1-3]. Biophysical and biotechnological applications, however, require protein micropatterning under native conditions in order to maintain the functional integrity of the immobilized protein. This is, in particular, important for probing protein function on the single molecule level, which requires homogeneous functionality and minimum background binding. Moreover, simple and generic surface fabrication techniques are required for broad applications. For this purpose, photolithographic surface patterning is ideally suited because it is based on relatively simple equipment and procedures as discussed in detail in 1.5. Protein capturing to surfaces rendered biocompatible using a thin, protein-repellent polymer coating has proven to be very suitable for functional protein micropatterning. For site-specific capturing of target proteins, spatially resolved functionalization of these layers with suitable capturing groups is required [4]. Optimal strategy has to be bioorthogonal to enable direct capturing of proteins from crude cell lysates into micropatterns, in order to avoid purification of the target proteins.

Here, we aimed to meet these requirements by implementing a highly generic approach for functional surface patterning, which is amenable with different methods for protein capturing. Our chemical strategy follows the bottom-up surface approach presented in 1.2. For surface patterning, the terminal amine groups of the PEG polymer brush were reacted with a hetero-bifunctional cross-linker to obtain maleimide functionalities. As a patterning strategy, we explored photodestruction of surface maleimides upon UV irradiation through a photomask. Thus, subsequent surface modification with thiol-functionalized molecules is only possible in non-irradiated areas. Surface functionalization was carried out with biotin for characterization of the process. In addition, we have adapted this method for generic, site-specific immobilization of recombinant proteins: (i) covalent immobilization by enzymatic phosphopantetheinyl transfer (PPT) as discussed in the previous chapter; (ii) affinity-based

immobilization utilizing the interaction of the oligohistidine tag of recombinant proteins with tris-(nitrilotriacetic acid)-OEG_7-thiol (tris-NTA) modified surfaces.

3.2 Experimental

3.2.1 Materials

Biotin-OEG_3-undecanethiol (BT-thiol) was purchased from ProChimia, Sopot/Poland. Streptavidin (SAv) was purchased from SERVA Electrophoresis GmbH, Heidelberg/Germany. tris-NTA was synthesized as described previously [5]. Imidazole, ethylenediaminetetraacetic acid (EDTA) and absolute ethanol were purchased from Carl Roth, Karlsruhe/Germany. Streptavidin labeled with ATTO 655 (^{AT655}SAv) and ATTO 655 maleimide was purchased from ATTO-TEC GmbH, Siegen/Germany. Microstructured masks for photo-patterning (chrome on quartz) were obtained from NB Technologies, Bremen/Germany. CoA conjugated with Dy547 (CoA547) were purchased from New England Biolabs GmbH (Frankfurt am Main, Germany). CoA conjugates with ATTO 655 and Alexa Fluor 568 (Invitrogen) were synthesized and purified according to published protocols *[6]*. Other chemicals are listed in 2.2.1. The rest were purchased from Sigma Aldrich.

3.2.2 Protein production and labeling

Enhanced Green Fluorescent Protein carrying an N-terminal hexahistidine tag (H6-EGFP) cloned in the plasmid pET21a was expressed in *E. coli* and purified by immobilized metal ion chromatography and size exclusion chromatography by standard protocols. For binding experiments with crude cell lysates, cells were sonicated in HEPES buffered saline (20 mM HEPES, 150 mM sodium chloride, pH 7.5, HBS) containing protease inhibitor, DNAse and 1 mM EDTA followed by centrifugation at 200,000 g. The H6-EGFP concentration in the supernatant was determined from its absorption at 480 nm and for surface binding experiments it was further diluted into HBS buffer. IFNα2 carrying an N-terminal ybbR-tag (ybbR-IFNα2) for posttranslational labeling using PPT from CoA derivatives [7] was expressed and purified like wildtype IFNα2. YbbR-IFNα2 was labeled with Dy-547 (^{Dy547}IFNα2), AlexaFluor 568 (^{AF568}IFNα2) or ATTO 655 (^{AT655}IFNα2) conjugated to CoA by means of the PPTase Sfp according to the

protocol from the manufacturer (Covalys Biosciences). After the labeling reaction, labeled IFNα2 was further purified by size exclusion chromatography. The ectodomain domain of type I interferon receptor subunit IFNAR2 fused to ybbR-tag (ybbR-IFNAR2) and the ecodomain of IFNAR2 fused to a C-terminal decahistidine tag (IFNAR2-H10) were expressed in *E. coli*, refolded from inclusion bodies and purified as described before [8, 9]. The ectodomain of the type I interferon receptor subunit IFNAR1 fused to a C-terminal decahistidine tag (IFNAR1-H10) was expressed in insect cells and purified as described before [8].

3.2.3 Surface chemistry and patterning

Surface chemistry was carried out as described in chapter 2. This was performed on transducer slides for reflectance interference spectroscopy (RIfS) detection (a thin silica layer on a glass substrate) [10] as well as standard glass cover slides for fluorescence microscopy. After surfaces were reacted with DAPEG, incubation of 1 M mercaptoethanol in DMF for 10 min at room temperature was carried out in order to block thiol-reactive sites. For functionalization with maleimide groups, the amine-functionalized surfaces were incubated under a saturated solution of 3-(maleimido)propionic acid N-hydroxy-succinimide ester (MPA-NHS) in dry DMF for 30 min at room-temperature. If not stated otherwise, photolithographic patterning was performed by irradiation for 5 minutes through a photomask using a 75 W Xenon lamp equipped with a 280-400 nm dichroic mirror (Newport Spectra-Physics). Thereafter, the chemically modified slides were washed with absolute ethanol. Further functionalization was performed by incubation with 500 µM Biotin-thiol or tris-NTA thiol in HBS for 30 min at room-temperature. Functionalization with CoA was carried out by incubation 100 mM CoA for 10 min at room-temperature.

3.2.4 Binding assays by solid phase detection

Protein binding to surfaces functionalized before and after photodestruction of maleimides was monitored in real time by RIfS as described in 2.2.4. Photoirradiated maleimide-functionalized RIfS transducer slides (prepared as described above) were equilibrated in HBS containing 0.01% Triton X-100 and then reacted with 1 µM BT-thiol in HBS. The presence of biotin groups was confirmed by a subsequent injection of 100 nM SAv.

3.2.5 Fluorescence imaging of protein micropatterns

Ensemble fluorescence imaging of protein micropatterns was performed in a confocal laser-scanning microscope (CLSM, FluoView 1000, Olympus) equipped with an Argon ion laser (488 nm line for excitation of EGFP), a 559 nm diode laser (excitation of AlexaFluor 568) and a 635 nm diode laser (excitation of ATTO 655). Proteins were diluted in HBS containing 1% (w/v) Bovine Serum Albumin (BSA). All binding assays were carried out in a flow-through format. Protein samples were injected through a 500 µl sample loop using an injection valve and incubated at continous flow for 2-5 min. Before imaging immobilized ^{AT655}SAv and H6-EGFP, the flow cell was thoroughly rinsed with HBS. Binding of IFNα2 to immobilized extracellular domain of IFNAR2 (IFNAR2-EC) was probed by injecting 50-100 nM fluorescence-labeled IFNα2 and images were acquired without rinsing. The dissociation kinetics of fluorescence-labeled IFNα2 were probed by subsequently injecting unlabeled 1 µM IFNα2 and time-lapse imaging in presence of unlabeled IFNα2. All images were acquired without flow.

3.2.6 Single molecule imaging of protein-protein interactions

Single molecule fluorescence imaging was carried out with an inverted microscope (Olympus IX71) equipped with a single-line TIR-illumination condenser (Olympus) and a back-illuminated electron multiplied (EM) CCD camera (iXon DU897D, 512×512 pixel from Andor Technology). An argon krypton laser (C70 Spectrum, Coherent) was coupled into the microscope through a polarization maintaining monomode fiber (KineFlex, Pointsource). The 647 nm laser line was selected by means of an acousto-optical tunable filter (AOTF, AAoptics). A 60X objective with a numerical aperture of 1.45 (PLAPON 60X/1.45 TIRFM, Olympus) was used for TIR excitation. The excitation beam was reflected into the objective by a quad-line dichroic beamsplitter for reflection at 405 nm, 488 nm, 568 nm and 647 nm (Di R405/488/561/647, Semrock), and the fluorescence was detected through a quadruple bandpass filter (FF01 446/523/600/677-25, Semrock). Fluorescence imaging was performed by excitation at 647 nm with a typical power output of 5 mW at the objective. The camera was operated at -80°C with a typical EM gain of 300 and a frame rate of 1-10 Hz, depending on the kinetics of the interaction. The laser was pulsed synchronized to the camera read-out using the AOTF. All binding experiments were

carried out at room temperature in HBS containing 0.01% Triton X-100 and 50µM EDTA complemented with oxygen scavenger [0.5 mg/ml glucose oxidase (Sigma), 40 mg/ml catalase (Roche AppliedScience), 5% (w/v) glucose and 1mM Trolox] to minimize photobleaching.

Localization and residence times of individual IFNα2 molecules were determined from trajectories obtained by the multiple target tracker [11]. Trajectories of less than three frames were not considered in the evaluation of residence times. Histograms of the frequency of different residence times were fitted by a monoexponential decay function.

3.3 Results and Discussion

3.3.1 Surface modification and patterning

The functionalization of glass-type surfaces with maleimide groups was carried out using a dense PEG polymer brush, which was covalently coupled to the surface through of silanization. Subsequently, surfaces were reacted with 3-(maleimido)propionic acid N-hydroxy-succinimide ester (MPA-NHS), followed by functional groups containing thiols for a specific interaction with surface maleimides (Figure 3-1).

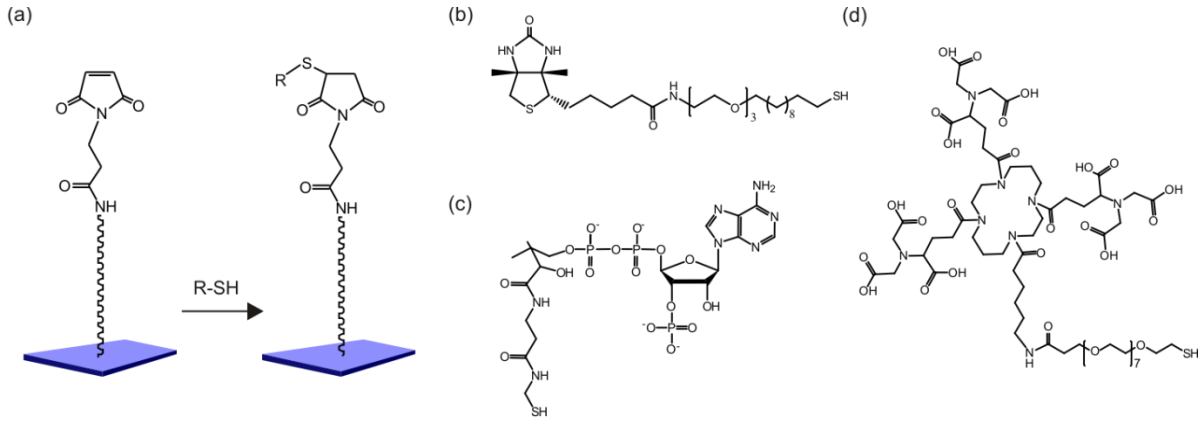

Figure 3-1. Surface modification and functionalization. (a) Bottom-up surface chemistry. After coupling of a dense PEG layer to a silanized glass-type surface, a reaction with MPA-NHS for subsequent coupling of thiol-functionalized capturing groups was carried out. (b-d) chemical structures of the functional groups for capturing proteins: (b) biotin-OEG_3-undecanethiol; (c) Coenzyme A (d) tris-(nitrilotriacetic acid)-OEG_7-thiol.

An efficient surface functionalization with maleimide groups was confirmed by monitoring the reaction with CoA by RIfS as presented in Figure 3-2a, yielding a final surface concentration of 0.4 pmole/mm² (0.24 molecules/nm²). Moreover rapid kinetics of the reaction was observed

with a rate constant of 80 $M^{-1}s^{-1}$ (Figure 3-2b). Thus, saturated binding can be obtained within a few minutes of incubation of a thiol-functionalized compound at millimolar concentration.

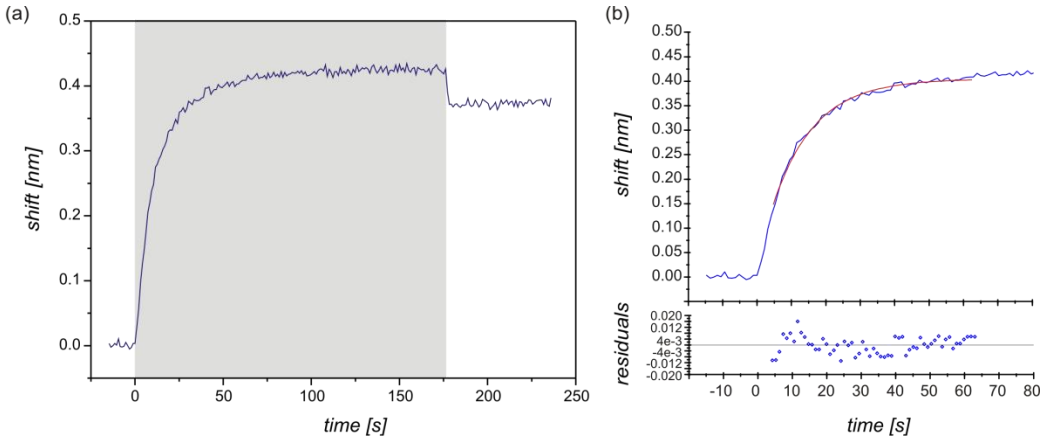

Figure 3-2. In situ coupling of 1 mM CoA to maleimide-functionalized surfaces monitored by RIfS. (a) Full binding curve, yielding a final binding amplitude of 0.36 nm corresponding to 0.3 ng/mm² CoA, was observed. Taking the molecular mass of CoA into account (767.5g/mol), a molar surface concentration of 0.4 pmole/mm². The injection of CoA is indicated by the grey bar. (b) Fitting the association kinetics by a pseudo-first order reaction model yielded a reaction rate constant of ~80 $M^{-1}s^{-1}$.

3.3.2 Biotin patterning by photodestruction (proof-of-concept)

In the first step, optimum conditions for maleimide-based protein micropatterning were established using the immobilization of BT-thiol for a functional read-out (Figure 3-3a). After reaction of maleimide-functionalized surfaces with BT-thiol, strong, highly specific binding of streptavidin was detected by using RIfS (Figure 3-3b). Upon UV irradiation of maleimide-functionalized surfaces prior to the reaction with BT-thiol, substantially reduced binding of streptavidin was detected. Rapid photodestruction of surface maleimides with a half life of 13 seconds was observed (Figure 3-3c). This photodestruction can occur due to photoinduced radical polymerization of maleimide groups on the surface [12] as discussed in 1.6. This effect was readily employed for micropatterning of biotin on surfaces, as confirmed by fluorescence imaging using streptavidin labeled with ATTO655 (^{AT655}SAv, Figure 3-3d). Strong binding of ^{AT655}SAv to non-illuminated surface areas was observed, while no significant fluorescence was detectable in areas where the maleimide groups were destroyed by UV irradiation. Besides demonstrating the proof-of-principle of maleimide-based protein micropatterning, such architectures can be readily employed for capturing biotinylated proteins.

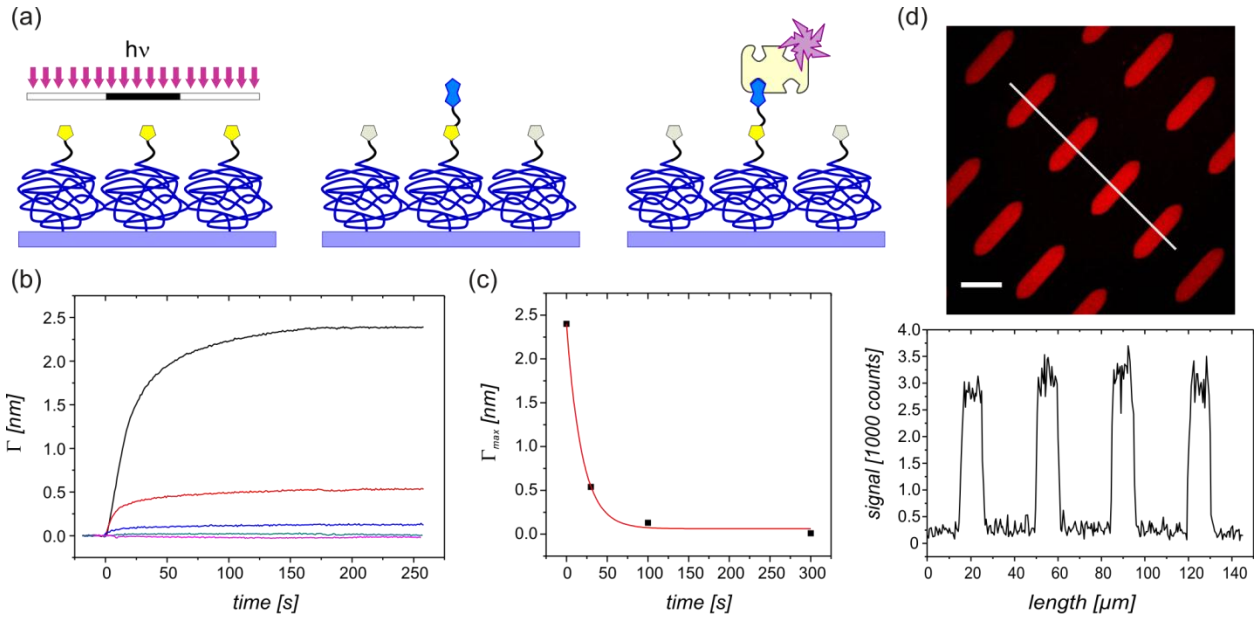

Figure 3-3. Biotin patterning by photodestruction of surface maleimides. (a) Schematic of the patterning process: after UV-irradiation of surface maleimides through a photomask, BT-thiol only reacts with non-irradiated surface areas. (b) Binding of SAv to surfaces reacted with BT-thiol before (black) and after UV irradiation of maleimide-functionalized surfaces for time periods of 30 s (red), 100 s (blue) and 300 s (cyan). A negative control without BT-thiol is shown in magenta. SAv binding was monitored in real by label-free detection using RIfS. (c) Saturation signal for SAv after different times of UV-irradiation of surface maleimides. The red curve is a monoexponential fit of the experimental data. (d) Binding of ^{ATTO655}SAv to micropatterned biotin-functionalized surfaces imaged by CLSM (left) and intensity profile along the indicated line (right). Scale bar 25 µm.

3.3.3 Generic application of maleimide-based patterning

Efficient and selective protein capturing into micropatterns even from complex sample matrices is an important prerequisite for biological applications, where small amounts of proteins are available and purification results in loss of function and material. We therefore aimed to establish selective protein capturing into micropatterns from crude cell lysates. To this end, we employed stable, yet reversible immobilization of His-tagged proteins by surface functionalization with tris-NTA [13]. For micropatterning tris-NTA through maleimide photolithography, we employed a thiol-functionalized tris-NTA derivative (cf. Figure 3-1), which was generated by reduction of the corresponding disulfide [5]. This compound was incubated on surfaces subjected to maleimide patterning by UV-illumination through a photomask (Figure 3-4a). After loading the NTA moieties with Ni(II) ions, selective binding of H6-EGFP to tris-NTA-functionalized regions was observed with a contrast of > 50:1 compared to non-functionalized areas (Figure 3-4b).

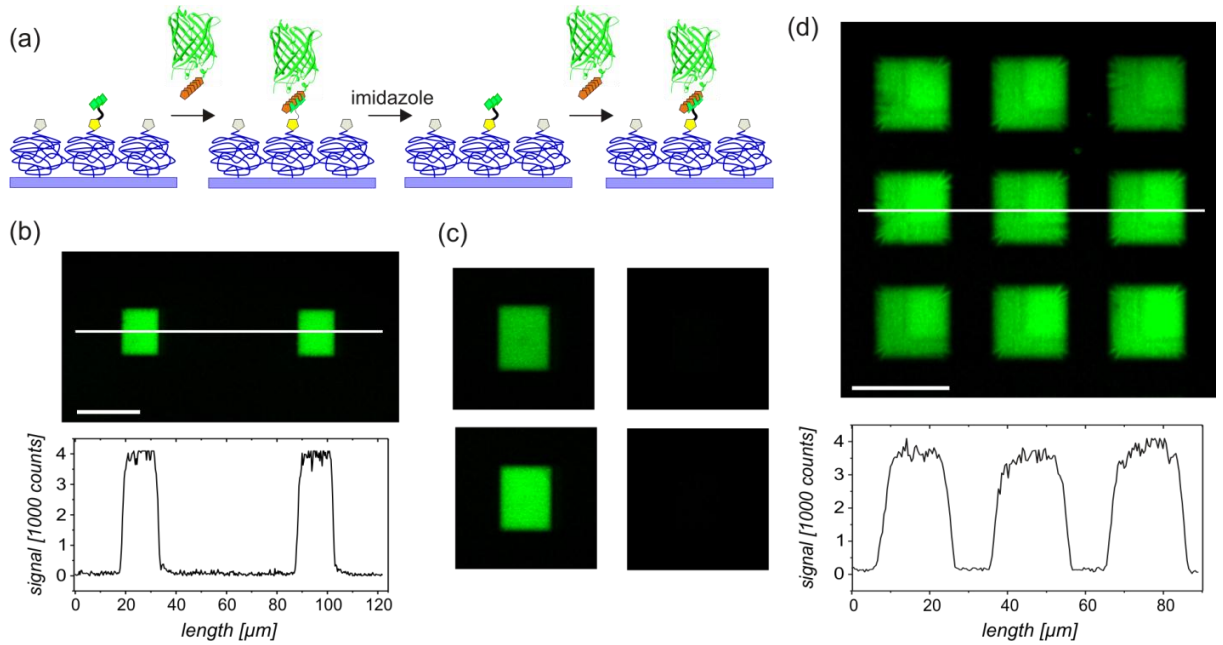

Figure 3-4. Reversible capturing of H6-EGFP to micropatterned tris-NTA surfaces. (a) Immobilization scheme. (b) Binding of H6-EGFP to micropatterned tris-NTA surfaces (top). Intensity profile along the indicated line (bottom). Scale bar 25 µm. (c) Reversibility and specificity of H6-EGFP binding. Top: EGFP signal before (left) and after (right) addition of imidazole. Bottom: EGFP signal after re-loading the surface with EGFP in presence (left) and in absence (right) of Ni(II) ions. (d) Capturing of H6-EGFP from crude *E. coli* lysates to micropatterned tris-NTA (top) and the intensity profile across the indicated line (bottom). Scale bar 25 µm.

While very stable binding of H6-EGFP during rinsing over extended time periods was observed, rapid, quantitative elution was observed upon injection of imidazole, which competes with the His-tag (Figure 3-4c). After washing with imidazole, the surface could be repeatedly reloaded with H6-EGFP without requiring incubation of Ni(II) ions (Figure 3-4c). However, after removal of complexed Ni(II) ions from the surface, binding of H6-EGFP was completely abolished (Figure 3-4c), confirming specific protein capturing to the surface. In order to demonstrate the high specificity of protein capturing into micropatterns, we incubated a crude cell lysate, which was prepared from *E. coli* cells expressing H6-EGFP, on micropatterned tris-NTA surfaces. The lysate was diluted into HBS to a final concentration of 1 µM H6-EGFP as determined by the absorption at 480 nm. Strikingly, selective and very efficient targeting of H6-EGFP into micropatterns was achieved (Figure 3-4d) even in this very complex sample matrix containing all soluble *E. coli* proteins. Again, specific binding of H6-EGFP was confirmed by elution with imidazole, and repetitive loading was possible.

For site-specific covalent immobilization of recombinant proteins, we employed enzymatic PPT-transfer from CoA, which was coupled to maleimide-functionalized surfaces through its thiol

group (cf. Figure 3-1). Micropatterned CoA-functionalized surfaces were obtained by coupling CoA after photodestruction of surface maleimdes through a photomask. As a target amino acid sequence for enzymatic PPT, we chose the peptide-tag ybbR as described in chapter 2. This tag was fused to the N-terminus of the ectodomain of the type I interferon receptor subunit IFNAR2 (ybbR-IFNAR2) as a model protein for probing protein-protein interactions. Functional immobilization of ybbR-IFNAR2 into micropatterns was detected by probing the interaction with fluorescence-labeled IFNα2 (Figure 3-5a).

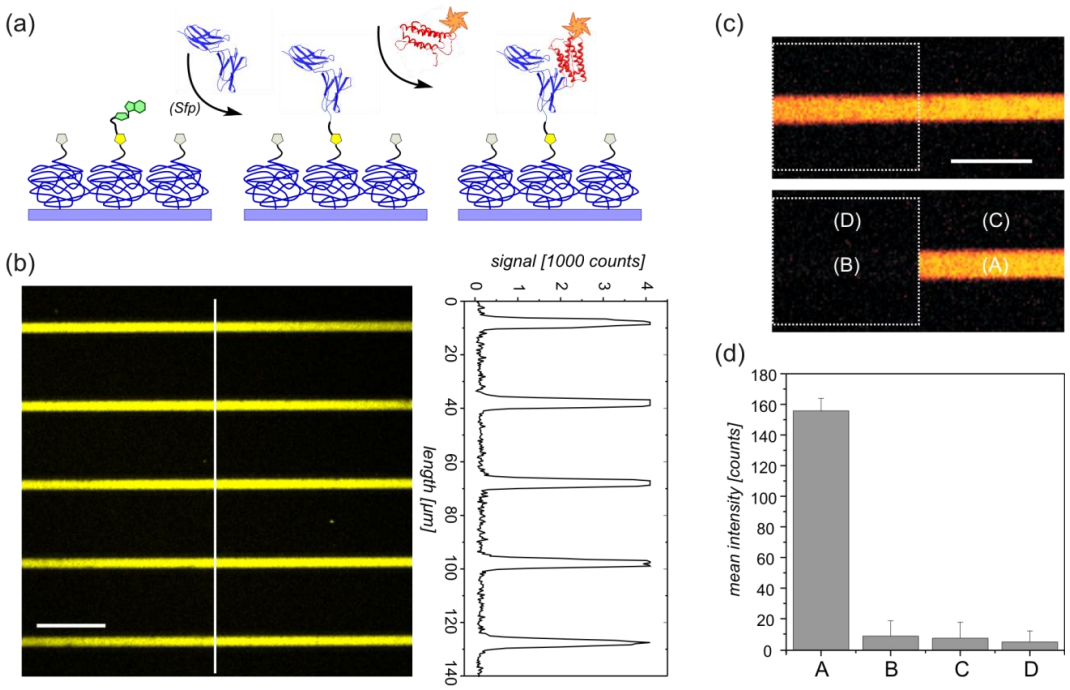

Figure 3-5. Protein-protein interactions in micropatterns. (a) Schematic of the assay: site-specific immobilization of ybbr-IFNAR2 to micropatterned CoA in presence of the PPTase Sfp followed by binding of ^{AF568}IFNα2. (b) Patterning of ybbR-IFNAR2 as detected by its interaction with ^{Dy547}IFNα2 (scale bar 25 µm). The intensity profile across the indicated line is shown on the right. (c) Determination of the contrast: after binding of ^{AF568}IFNα2 to micropatterned ybbR-IFNAR2, a selected area (indicated by the white rectangle) was photobleached. Subsequently, the fluorescence in functionalized and non-functionalized areas was determined (scale bar 20 µm). (d) Comparison of the fluorescence intensities in bleached and non-bleached areas. The different areas are indicated in panel c.

Upon incubation of IFNα2 labeled with Dy-547 (^{Dy547}IFNα2), selective binding to non-illuminated surface areas was detected (Figure 3-5b). In a similar experiment carried out with IFNα2 labeled with AlexaFluor 568 (^{AF568}IFNα2), we quantitatively assessed the contrast between functionalized and non-functionalized regions. For this purpose, part of the structure was photobleached by the confocal laser beam (Figure 3-5c) and fluorescence intensity in the

photobleached areas was compared with the fluorescence intensity in the non-bleached areas. A very low difference between the background fluorescence signals observed in the photobleached area compared to the non-bleached area was observed (Figure 3-5d). From these signals, a contrast of > 60:1 was estimated, confirming the very efficient photodestruction of surface maleimides and the highly selective coupling of thiol-modified compounds to non-illuminated areas.

In order to probe reversible interaction between IFNα2 labeled with ATTO 655 (^{AT655}IFNα2) and immobilized ybbR-IFNAR2, we monitored the fluorescence intensity within functionalized microstructures upon chasing with 1 µM unlabeled IFNα2 (Figure 3-6). The dissociation curve obtained from the fluorescence intensity within the microstructures was well fitted by a monoexponential decay function (Figure 3-6c).

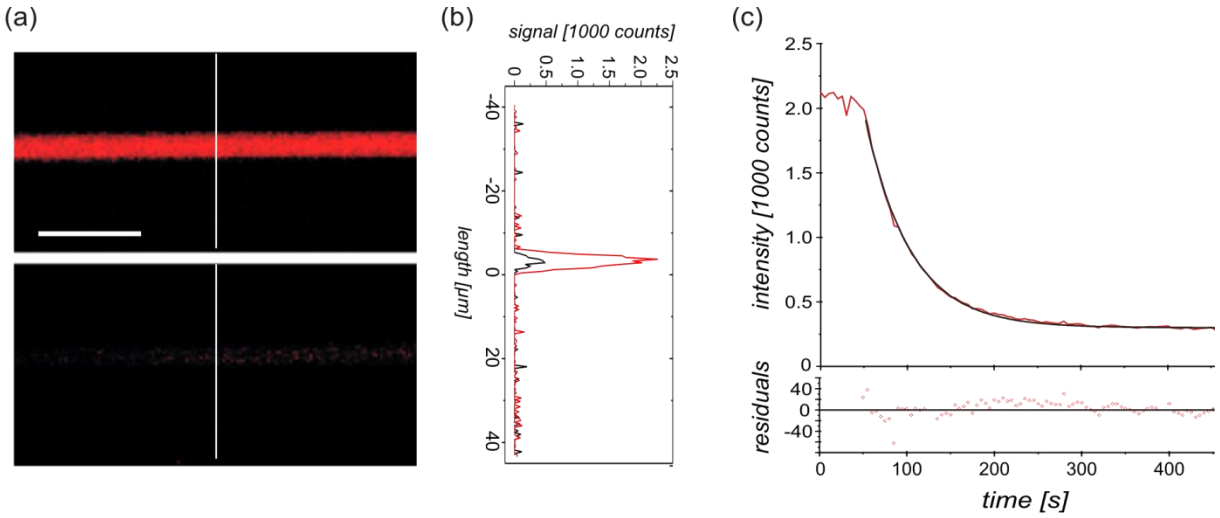

Figure 3-6. Reversible protein-protein interactions in micropatterns. (a) Signal for ^{AT655}IFNα2 before (top) and after (bottom) chasing with 1 µM unlabeled IFNα2 for 450s (scale bar 20 µm). (b) Intensity profile across the line indicated in panel (a) before (red) and after (black) chasing with 1 µM unlabeled IFNα2. (c) Dissociation curve during chasing with 1 µM unlabeled IFNα2 obtained from time resolved fluorescence imaging (red) and fit by an exponential decay function (black).

A dissociation rate constant of 0.02 s^{-1} was obtained from the fit, which is in perfect agreement with the dissociation rate constant previously obtained for this interaction [14]. These reversible protein-protein interaction assays confirmed functional immobilization of a highly fragile protein into micropatterns. The measurements demonstrated the possibility to quantitatively probe protein-protein interactions in these micropatterns.

3.3.4 Single-molecule detection of protein-protein interactions in patterns

Even more challenging than ensemble binding assays is to immobilize proteins for interaction studies on the single molecule level. In order to evaluate the suitability of our micropatterning technique with single molecule analysis methods, we aimed to monitor the interactions of individual ^{AT655}IFNα2 molecules with micropatterned IFNAR2-EC. For this purpose, IFNAR2-H10 was immobilized on micropatterned tris-NTA. Specific and reversible binding of ^{AT655}IFNα2 was confirmed by ensemble measurements (Figure 3-7a,b). For single molecule experiments, we employed the IFNα2 mutant M148A, which binds to IFNAR2 with an approximately 30-fold decreased binding affinity [15], which is based on a 30-times higher dissociation rate constant (~0.6 s^{-1}). IFNα2-M148A labeled with AT655 (^{AT655}IFNα2-M148A) was incubated on tris-NTA micropatterns loaded with IFNAR2-H10. Transient binding of ^{AT655}IFNα2-M148A was observed preferentially to surface areas covered with IFNAR2-H10. A maximum intensity overlay of consecutive 1000 frames confirmed the high contrast observed for ensemble experiments (Figure 3-7c). From localizing individual binding events in each frame, a contrast of >100:1 was determined for ^{AT655}IFNα2-M148A, which is in good agreement with the ensemble measurements. A histogram of the residence times of individual ^{AT655}IFNα2 M148A (Figure 3-7d) could be fitted by a monoexponential decay function yielding a rate constant of 0.8 s^{-1}, in good agreement with the dissociation rate constant determined for this mutant.

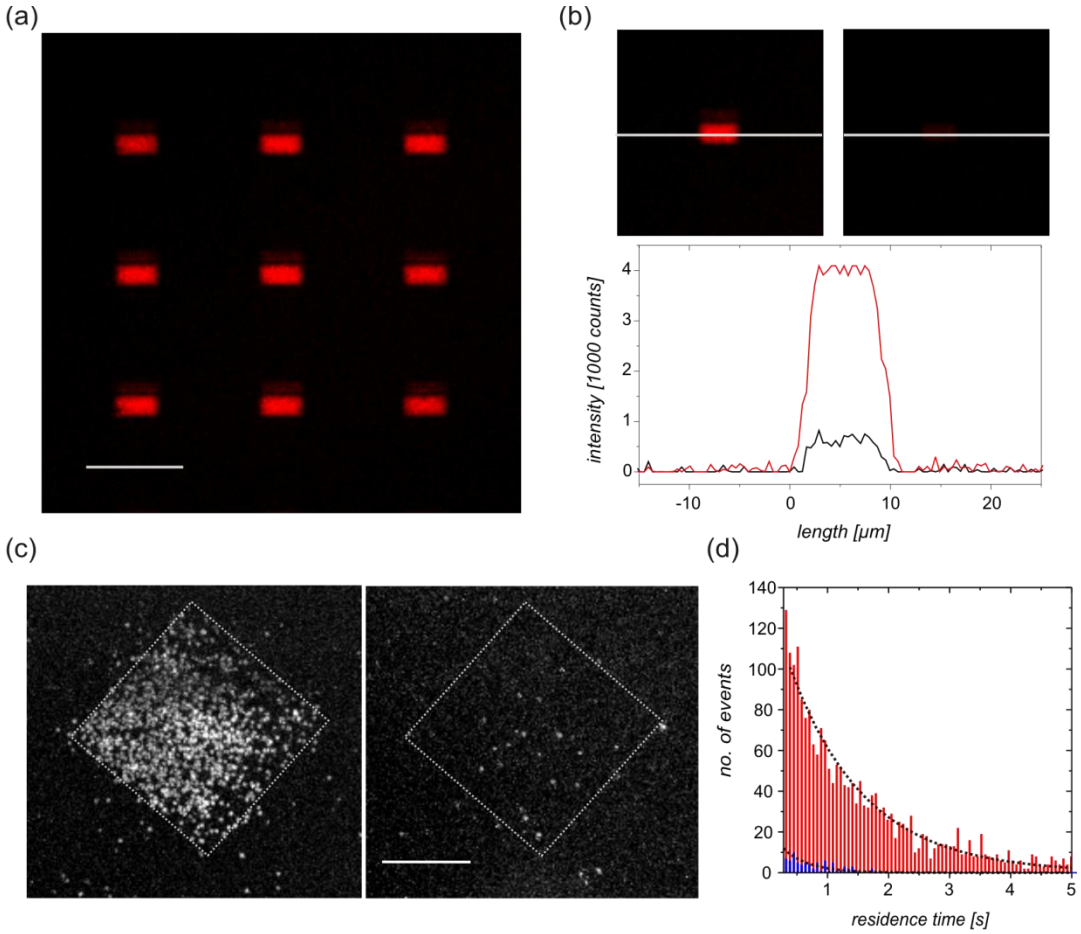

Figure 3-7. Single molecule detection of transient protein-protein interactions in micropatterns. (a) Binding of ^{AT655}IFNα2 to IFNAR2-H10 immobilized on micropatterned tris-NTA (scale bar 20 µm). (b) Chasing of ^{AT655}IFNα2 bound to IFNAR2-H10 with unlabeled IFNα2. (c) Maximum intensity overlay image of 1000 consecutive frames acquired during incubation of 5 nM ^{AT655}IFNα2-M148A in absence (left) and in presence (right) of 5 µM unlabeled IFNα2 (scale bar 10 µm). The white squares indicate the patterned tris-NTA regions. (d) Histogram of residence times for individual ^{AT655}IFNα2-M148A binding to micropatterns loaded with IFNAR2-H10 (red) and MBP-H10 (blue) measured over 1000 frames. Black lines are the best fits by an exponential decay function.

These results demonstrate that the micropatterns generated by maleimide photolithography are suitable for detecting protein-protein interactions on the single molecule level with very high specificity.

3.4 Summary and conclusions

We have employed maleimide photodestruction for micropatterned surface functionalization with a very high contrast, which in our hands was substantially higher than those observed for other photopatterning techniques such as uncaging of functional groups [16, 17] or photodestruction of NTA moieties [18]. While uncaging offers the possibility for binary functional patterning, photodestruction of maleimides is ideal for generating microstructures with a single functionality. Based on this approach, we have implemented two complementary methods for capturing proteins into micropatterns under physiological conditions. Very efficient non-covalent targeting of His-tagged proteins into microstructures functionalized with tris-NTA thiol was achieved yielding micropatterns with very high contrast. We demonstrated micropatterning of His-tagged proteins directly from crude cell extracts. Thus, small quantities of highly fragile proteins and protein complexes in complex sample matrices can be assembled into functional microstructures. Proteins immobilized into tris-NTA micropatterns were efficiently eluted with imidazole and repetitive loading into the microstructures was possible. Thus, patterned substrates can be used for sequentially targeting different His-tagged proteins or for binding experiments with different protein densities. Since most recombinant proteins are fused to a His-tag for affinity purification by immobilized metal ions [19], this generic approach is highly applicable for *in situ* protein micropatterning. As an alternative approach, we implemented site-specific, covalent protein immobilization by PPT into microstructures functionalized with CoA. For this approach as well, functional protein micropatterns with a very high contrast were obtained. This method is advantageous for applications which require very robust, irreversible protein immobilization. Maleimide photopatterning is simple, compatible with many substrates and surface architectures and it can be used with many other thiol-functionalized compounds, e.g. for direct coupling of peptides or proteins with free cysteine residues into micropatterns or for micropatterning of thiol-functionalized oligonucleotides. In addition to the versatile application of maleimide-based immobilization, excellent functionality of micropatterned proteins was demonstrated. Owing to the high patterning contrast and the excellent protein repelling properties of the surface, transient protein-protein interactions could be detected and quantitatively analysed on the single molecule level. While

micropatterned surfaces have previously been applied for probing protein interactions on the cell surface [20], as well as for real-time protein-protein interaction analysis [21, 22], quantitative analysis of interactions between isolated proteins in micropatterns on the single molecule level has not yet been reported to our knowledge. The key challenge in such experiments is the presence of labeled protein in the bulk, so that even weak non-specific binding to the surface will result in substantial background signals. The very good signal-to-background observed in our study suggests that interactions of protein complexes with affinities of up to 10 µM can be readily measured. Thus, the kinetics of protein-protein interactions with such low binding affinities can be reliably quantified on the single molecule level.

Acknowledgement

I thank Oliver Beutel for single-molecule measurements and analysis.

3.5 References

1. Zhou, H., et al., *Solution and chip arrays in protein profiling.* Trends Biotechnol, 2001. **19**(10 Suppl): p. S34-9.
2. Cooper, M.A., *Optical biosensors in drug discovery.* Nat Rev Drug Discov, 2002. **1**(7): p. 515-28.
3. van den Heuvel, M.G. and C. Dekker, *Motor proteins at work for nanotechnology.* Science, 2007. **317**(5836): p. 333-6.
4. You, C., et al., *Affinity capturing for targeting proteins into micro and nanostructures.* Anal Bioanal Chem, 2009. **393**(6-7): p. 1563-70.
5. You, C., et al., *Self-controlled monofunctionalization of quantum dots for multiplexed protein tracking in live cells.* Angew Chem Int Ed Engl, 2010. **49**(24): p. 4108-12.
6. Yin, J., et al., *Site-specific protein labeling by Sfp phosphopantetheinyl transferase.* Nat Protoc, 2006. **1**(1): p. 280-5.

7. Yin, J., et al., *Genetically encoded short peptide tag for versatile protein labeling by Sfp phosphopantetheinyl transferase.* Proc Natl Acad Sci U S A, 2005. **102**(44): p. 15815-20.
8. Lamken, P., et al., *Ligand-induced assembling of the type I interferon receptor on supported lipid bilayers.* Journal of Molecular Biology, 2004. **341**(1): p. 303-318.
9. Piehler, J. and G. Schreiber, *Biophysical analysis of the interaction of human ifnar2 expressed in E-coli with IFN alpha 2.* Journal of Molecular Biology, 1999. **289**(1): p. 57-67.
10. Schmitt, H.M., et al., *An integrated system for optical biomolecular interaction analysis.* Biosensors & Bioelectronics, 1997. **12**(8): p. 809-816.
11. Serge, A., et al., *Dynamic multiple-target tracing to probe spatiotemporal cartography of cell membranes.* Nat Methods, 2008. **5**(8): p. 687-94.
12. Yamada, M., I. Takase, and N. Koutou, *Photopolymerization of Maleimide and Its N-Substituted Derivatives.* Journal of Polymer Science Part B-Polymer Letters, 1968. **6**(12PB): p. 883-&.
13. Lata, S. and J. Piehler, *Stable and functional immobilization of histidine-tagged proteins via multivalent chelator head-groups on a molecular poly(ethylene glycol) brush.* Anal Chem, 2005. **77**(4): p. 1096 -1105.
14. Gavutis, M., et al., *Lateral ligand-receptor interactions on membranes probed by simultaneous fluorescence-interference detection.* Biophys J, 2005. **88**(6): p. 4289-302.
15. Piehler, J., L.C. Roisman, and G. Schreiber, *New structural and functional aspects of the type I interferon- receptor interaction revealed by comprehensive mutational analysis of the binding interface.* Journal of Biological Chemistry, 2000. **275**(51): p. 40425-40433.
16. Alonso, J.M., et al., *Photopatterned Surfaces for Site-Specific and Functional Immobilization of Proteins.* Langmuir, 2008. **24**(2): p. 448-457.
17. Waichman, S., et al., *Functional Immobilization and Patterning of Proteins by an Enzymatic Transfer Reaction.* Anal Chem, 2010.
18. Bhagawati, M., et al., *Organization of motor proteins into functional micropatterns fabricated by a photo-induced Fenton reaction.* Angew Chem Int Ed Engl, 2009. **48**(48): p. 9188-91.

19. Ueda, E.K., P.W. Gout, and L. Morganti, *Current and prospective applications of metal ion-protein binding.* J Chromatogr A, 2003. **988**(1): p. 1-23.

20. Schwarzenbacher, M., et al., *Micropatterning for quantitative analysis of protein-protein interactions in living cells.* Nat Methods, 2008. **5**(12): p. 1053-60.

21. Klenkar, G., et al., *Addressable adsorption of lipid vesicles and subsequent protein interaction studies.* Biointerphases, 2008. **3**(2): p. 29-37.

22. Klenkar, G., et al., *Piezo Dispensed Microarray of Multivalent Chelating Thiols for Dissecting Complex Protein-Protein Interactions.* Anal Chem, 2006. **78**: p. 3643-3650.

4 Diffusion and interactions of individual membrane proteins confined in micropatterned polymer-supported membranes

4.1 Introduction

The mechanistic complexity of transport and communication across membranes still poses a fundamental challenge for a biophysical understanding of these processes. Often, the subtle interplay of diffusion, interactions and conformational changes involved in membrane protein function critically depend on the lipid environment [1-4]. A more detailed understanding of transmembrane protein functions in the context of biological membranes therefore requires *in vitro* reconstitution into membranes with a defined lipid composition. Solid-supported membranes provide elegant means for this purpose as they are compatible with microfluidic sample handling as well as a broad spectrum of spectroscopic and microscopic techniques [5-9]. In particular single molecule fluorescence imaging of lipids and proteins in solid supported membranes [7, 10, 11] has promising prospects for simultaneously monitoring diffusion, interactions and conformational changes. Functional reconstitution of transmembrane proteins, however, requires polymer cushions between the membrane and the substrate surface in order to maintain the structural integrity of reconstituted proteins and their uncompromised mobility in the membrane [12-14], as discussed previously in 1.3. Such polymer-supported membranes (PSMs) have already proven suitable for functional studies of reconstituted transmembrane proteins by fluorescence imaging techniques[15-17] down to the level of individual protein complexes [18]. However, owing to the high mobility of proteins in such PSM, individual proteins and protein complexes can be assigned only for the time they can be tracked. Efficient long-term tracking not only requires a low density of labeled molecules, but also a rapid image acquisition. Spatially confined PSM could allow for capturing and monitoring individual membrane proteins in fluid membranes over extended time periods. While simple methods for generating micropatterned solid-supported membranes have been reported [19, 20], functional reconstitution of transmembrane proteins into spatially confined membranes remains highly challenging and only few, specialized approaches have been

pioneered so far [21, 22]. Imaging diffusion and interactions of individual transmembrane proteins confined in micropatterned PSM with a defined lipid environment has to our knowledge not yet been achieved.

Here, we have implemented a rugged approach for rapid functional transmembrane protein reconstitution in micropatterned PSM. To this end, a PEG polymer brush on a glass substrate [23] was functionalized with maleimide groups [24] as discussed in chapter 3. Maleimide groups were then photoactivated in presence of hexadecyl vinyl ether (HDVE). Thus, hexadecyl moieties were covalenty coupled to the surface for capturing proteoliposomes. After fluid bilayer formation, we probed transmembrane protein diffusion, functionality and interactions using ensemble and single-molecule techniques.

4.2 Experimental

4.2.1 Materials

1-Stearoyl-2-oleoyl-*sn*-glycero-3-phosphocholine (SOPC) was purchased from Avanti Polar Lipids. Oregon Green® 488-labeled 1,2-dihexadecanoyl-*sn*-glycero-3-phosphoethanolamine (^{OG488}DHPE) was purchased from Invitrogen Darmstadt/Germany. DY-649 maleimide was purchased from Dyomics, Jena/Germany. CoA-647 was purchased from New England Biolabs GmbH (Frankfurt am Main, Germany. The baculovirus expression vector system BaculoGold was purchased from BD Biosciences. A 75 W Xenon lamp equipped with a 280 – 400 nm dichroic mirror was purchased from Newport Spectra-Physics and microstructured masks for photo-patterning (chrome on quartz) were obtained from NB Technologies, Bremen/Germany. Other chemicals are listed in 2.2.1 and 3.2.1. All the rest were purchased from Sigma Aldrich.

4.2.2 Protein production, purification and labeling

Transmembrane domains were fused to maltose-binding protein (MBP) by insertion of the corresponding oligonucleotide linker into the MCS of pMALc2x via restriction with *BamH*I and *Hind*III. The following transmembrane (TM) domains were used:
(i) GSGNTSK**IWLIVGISIALFALPFVIYAA**KVFLRCSR (MBP-TM1) from the type I interferon receptor subunit IFNAR1 and (ii) GSK**ALAALAALAALAALAALAALA**KSSR (MBP-ALA_7) as a model TMD. For

efficient purification, an N-terminal His_{10}-tag was inserted via the *Nde*I site. These proteins were expressed in *E. coli* TG-1 cells at 37 °C according to standard protocols. After cell lysis, the membrane fraction was solubilized with buffer containing 20 mM Triton X-100 and the proteins were purified by immobilized metal ion affinity chromatography (5 ml HiTrap Chelating, GE Healthcare). Subsequently, MBP-TM1 was reacted with a 3-fold molar concentration of DY-649-maleimide (^{DY649}MBP-TM1) for 1 h at room temperature. Finally, ^{DY649}MBP-TM1 and MBP-ALA_7 were further purified by size exclusion chromatography in 20 mM Hepes, 150 mM NaCl (HBS) containing 0.6 mM Triton X-100 (Superdex 200 10/300, GE Healthcare).

The IFNAR2 truncated after its transmembrane helix (after Cys245) (IFNAR2-TM) was expressed in Sf9 insect cells using a baculovirus expression system. For this purpose, IFNAR2-TM was cloned into the expression vector pAcGP67-B fusing it to the secretion sequence of the baculoviral protein gp67. Virus generation and protein expression was carried out according to the manufacturer's protocol. IFNAR2-TM was purified from the membrane fraction and labeled with DY-547-maleimide (^{DY547}IFNAR2-TM) as described for MBP-TM1.

IFNα2 and IFNα2-M148A carrying an N-terminal ybbR-tag (ybbR-IFNα2) for posttranslational labeling using phosphopantetheinyl transfer (PPT) from CoA derivatives [25] were expressed and purified as described for wildtype IFNα2 [26]. YbbR-IFNα2 and IFNα2-M148A were site-specifically labeled with DY-647 (^{DY647}IFNα2) by means of the PPTase Sfp and CoA647 and further purified by size exclusion chromatography as described previously [27].

4.2.3 Surface chemistry and micropatterning

Surface chemistry was carried out as described in chapter 2 and 3. This was performed on transducer slides for reflectance interference spectroscopy (RIfS) detection (a thin silica layer on a glass substrate) [28] as well as standard glass cover slides for fluorescence microscopy. Photolithographic patterning was performed in the presence of hexadecyl vinyl ether *in* acetonitrile (1:1, v/v) by irradiation for 60 seconds through a photomask using a 75 W Xenon lamp. Thereafter, the chemically modified slides were carefully washed with acetonitrile, chloroform and absolute ethanol.

4.2.4 Preparation of liposomes and proteoliposomes

Liposomes and proteoliposomes were prepared from detergent solution by addition of cyclodextrin which was described previously [29]. A thin lipid film was prepared from a solution of SOPC in chloroform, which was removed using a rotary evaporator. This lipid film was solubilized in HBS supplemented with Triton X-100 resulting in a lipid-detergent stock solution of 1 mM SOPC and 4 mM Triton X-100 for liposome preparation and 5 mM SOPC and 20 mM Triton X-100 for proteoliposomes. Liposomes were prepared from a 20-fold dilution of the stock solution in HBS by addition of cyclodextrin to a concentration of 2 mM followed by thorough mixing. Incorporation of the fluorescent lipids ^{OG488}DHPE into the vesicles was achieved by preparation of the lipid-detergent stock solution with fluorescent lipid in a molar ratios of 1:10^2 (^{OG488}DHPE:SOPC) for ensemble measurements. Reconstitution of transmembrane proteins was achieved by incubation of the lipid-detergent stock solution with the proteins for 5 min, followed by a 20-fold dilution in HBS containing 50 mM EDTA (HBSE) and subsequent detergent removal by cyclodextrin. The fluorescently labeled transmembrane proteins were added in molar ratios of 1:10^3 (labeled protein:SOPC) for ensemble measurements. Ratios of 1:10^4 and 1:10^7 (labeled protein:SOPC) were used for single molecule measurements of diffusion and interactions respectively. The protein reconstitution samples for single molecule studies contained additional unlabeled MBP-ALA_7 at a ratio of 1:10^3 (protein:SOPC) in order to minimize unspecific interactions of labeled protein with the surface.

4.2.5 Solid phase binding assays

Vesicle binding to photochemically functionalized surfaces was monitored in real time by RIfS. After conditioning of the surface by injection of 0.1% Triton X-100 for 150 s, SUV (250 µM SOPC) were injected for 400 s. Subsequently, the surface was regenerated by injecting 0.1% Triton X-100 in HBS for 150 s. Reconstitution of IFNAR2-TM into PSM and the interaction with ^{DY647}IFNα2 was probed in real time by simultaneous detection by total internal reflection fluorescence spectroscopy (TIRFS) and by reflectance interference (RIF) in a flow-through system using a home-built set-up [30, 31]. Proteoliposomes containing IFNAR2-TM were captured to the surface and fused by injection of 10 % (w/v) PEG solution for 285 s. Before injection of

^{DY647}IFNα2, excessive lipid was washed off and the surface blocked with 50 mg/ml BSA solution to minimize unspecific binding. The IFNα2 binding curve was fitted using the BIAevaluation 3.0 software (BIACORE) by applying a 1:1 Langmuir model accounting for mass transport limitation.

4.2.6 Confocal imaging and FRAP experiments

Confocal imaging and FRAP experiments were carried out in a confocal laser-scanning microscope which was described in 3.2.5. ^{OG488}DHPE was excited with the 488 nm laser line and fluorescence emission was filtered by a spectral grating and collected between 500-600 nm while ^{DY649}MBP-TM1 was excited with the 635 nm laser line and fluorescence emission was collected between 650-750 nm. For PSM preparation the functionalized surfaces were incubated with VSUV containing ^{OG488}DHPE in a molar ratio of 1:10^2 or the labeled transmembrane protein ^{DY649}MBP-TM1 in a molar ratio of 1:10^3 (fluorescent probe:lipid) for 10 minutes. Unbound vesicles were washed off and fusion was induced by incubation under 10 % (w/v) PEG solution for 10-20 minutes. Excessive material was washed off the bilayer by intensive pipetting of HBSE. For probing ^{OG488}DHPE diffusion by FRAP, a pre-bleach image was recorded before a circular region of interest (ROI) with a radius of $\omega = 20$ µm was scanned by the 405 nm and the 488 nm lasers at 148 and 300 µW, respectively, within a 0.6 – 2.6 s. Fluorescence recovery F_{ROI} of ^{OG488}DHPE was monitored for 1-1.5 min with a time resolution of 1 s. FRAP experiments with ^{DY649}MBP-TM1 were done in the same way using the 405 nm and the 635 nm laser at 148 and 300 µW, respectively, for photobleaching. The recovery of ^{DY649}MBP-TM1 was monitored for 10-15 min at a time resolution of 30 s. ^{OG488}DHPE was excited at 488 nm (3 µW) and ^{DY649}MBP-TM1 was excited at 635 nm (25 µW). A background signal BG (obtained from the center of the bleached ROI) was subtracted from the ROI intensity signal and it was normalized by division of the ROI intensity prior to bleaching. A reference ROI outside the bleached area was processed in the same way. To correct for photobleaching during the measurement the normalized ROI intensity was divided by the normalized intensity of the reference region:

$$f = \frac{F_{ROI} - BG}{F_{ROI}(prebleach) - BG} \Big/ \frac{F_{REF} - BG}{F_{REF}(prebleach) - BG}$$

The corrected fluorescence recovery curves f were fitted by Eqn. 1 according to the analysis of Soumpasis [32] but allowing less than 100 % of the maximum recovery possible (I_0 and I_1 are modified Bessel functions). For curve fitting the nonlinear regression function *nlinfit* in the Matlab software (The Mathworks, Inc.) was employed.

$$f(t) = F_{\max} \cdot e^{\left(\frac{-2\cdot\tau_D}{t}\right)} \cdot \left[I_0\left(\frac{2\cdot\tau_D}{t}\right) + I_1\left(\frac{2\cdot\tau_D}{t}\right) \right] \qquad \text{Eqn. 1}$$

Diffusion constants were determined by the slope of the linear relation of the square radius ω^2 of the circular ROI to the diffusion time τ_D (Eqn. 2).

$$\tau_D = \frac{1}{4D}\omega^2 + c \qquad \text{Eqn. 2}$$

4.2.7 Atomic force microscope (AFM) imaging

Imaging of captured vesicles and PSM was performed in tapping mode with a NanoWizard 2 (JPK Instruments) mounted on an inverted microscope (Olympus IX71) placed on an anti-vibration stage. Prior to use, the AFM probes were cleaned in fresh piranha solution for 15 minutes to get rid of oil contaminations. The acquired images were further processed using the Data Processing software (JPK Instruments).

4.2.8 Single molecule tracking

Single molecule tracking experiments were carried out by TIRF microscopy with an inverted microscope (Olympus IX71) equipped with a triple-line total internal reflection illumination condenser (Olympus) and a back-illuminated electron multiplied (EM) CCD camera (iXon DU897D, 512×512 pixel from Andor Technology). A 150× magnification objective with a

numerical aperture of 1.45 (UAPO 150×/1.45 TIRFM, Olympus) was employed for TIR illumination of the sample. For single molecule binding assays, IFNAR2-TM was reconstituted under the same conditions as described for MBP-TM1. After blocking the surface with 10 mg/ml BSA, ^{DY647}IFNα2 was added to a final concentration of 1 nM and incubated for 10 minutes. TIRF imaging was carried out in presence of 1 nM ^{DY647}IFNα2, using a 642 nm laser diode (50 mW, CrystaLaser) for excitation, operated at an output power of ~0.5 mW at the objective. Fluorescence was detected using a 690/70 band pass filter (Chroma). Images were acquired with a time resolution of 22-45 ms/frame. All experiments were carried out using media complemented with oxygen scavenger and a redox-active photoprotectant [0.5 mg/ml glucose oxidase (Sigma), 0.04 mg/ml catalase (Roche AppliedScience), 5% w/v glucose, 1 µM ascorbic acid and 1µM methyl viologene] to minimize photobleaching.

Individual fluorescent molecules were localized and tracked using the multi-target tracing (MTT) algorithm [33]. Evaluation of the trajectories obtained from single-molecule images was carried out by a statistical step-distance analysis [34]. Confinement in one dimension, assuming two barriers of a distance L_X that reflect diffusing particles, leads to a saturation curve of the MSD with time and can be evaluated by the method introduced by Kuzumi *et.al* [34].Diffusion constants of single trajectories were determined by linear regression of the mean square displacement (MSD) vs. different lag times as described previously [35-38]. For the determination of local diffusion constants, the MSD analysis was carried out within a window of 0.68 s (31 frames).

4.3 Results and discussion

4.3.1 Surface modification and patterning

Our strategy for surface functionaliztion is based on PEG polymer coated glass substrates for biocompatibility[23] and maleimide moieties as chemical functionalities for photopatterning as shown in chapter 3 [24] Maleimide and its derivatives can function as monomers and photocatalysts in a polymerization reaction induced by UV light [39]. These unique properties were utilized for the cross-linking of chemical moieties that are rich in electrons and function as

electron donors in this process [40]. Exploiting these features, an efficient lipid membrane patterning approach has been obtained for probing diffusion and interactions of the reconstituted transmembrane proteins in a confined manner. In this regard, maleimide functionalized surfaces were reacted with hexadecyl vinyl ether moieties (HDVE) upon UV irradiation in the presence of a photomask as depicted in Figure 4-1a,b. Subsequently, lipid vesicles containing reconstituted transmembrane proteins were selectively captured onto the irradiated areas to which hexadecyl chains were coupled as illustrated in Figure 4-1c.

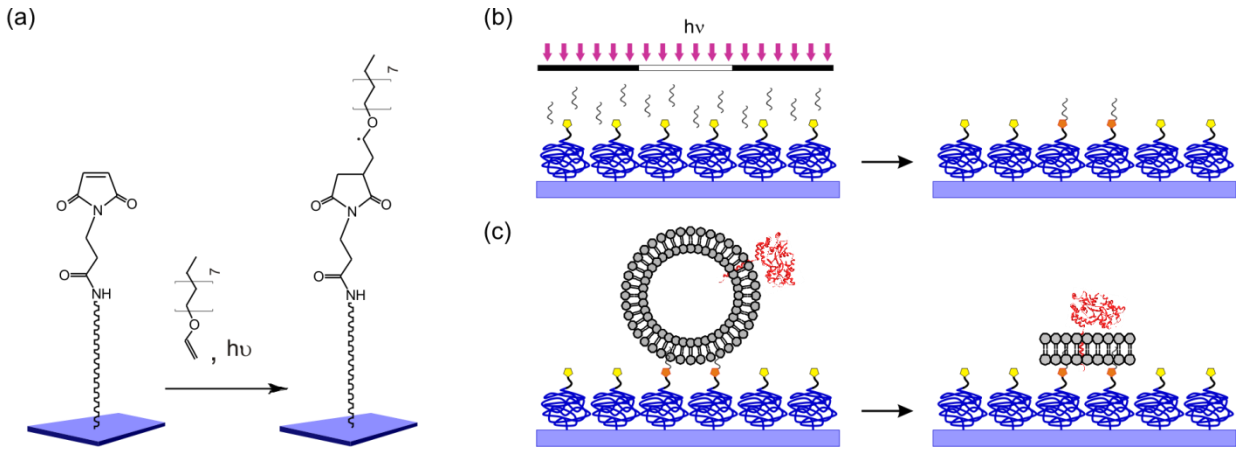

Figure 4-1. Strategy for membrane protein reconstitution into patterned polymer-supported membranes. (a) Surface chemistry based on photochemical polymerization of surface maleimides in presence of HDVE. (b, c) Membrane micropatterning: by illumination through a photomask, HDVE moieties for vesicle tethering are selectively coupled in the illuminated area (b). (Proteo)liposomes are captured by the HDVE groups and subsequently fused into PSM by addition of PEG (c).

4.3.2 Capturing, fusion and diffusion

At first we quantified lipid vesicle binding onto biocompatible, maleimide functionalized surfaces after UV treatment in the presence of HDVE moieties. We employed very small unilamellar vesicles (VSUV) having diameter of ~ 25 nm [18], which were generated by detergent depletion with cyclodextrin [29, 41]. Utilizing reflectance interference spectroscopy (RIfS), a label-free, solid-phase detection technique, the amount of VSUV captured on such surfaces was reliably determined. In order to assure that binding of lipid vesicles is sufficient to obtain a bilayer, different UV irradiation times were tested (Figure 4-2a). Here, VSUV were captured on maleimide surfaces reacted with HDVE for different irradiation times. Strong and specific binding of VSUV was observed after irradiation for 60 s, allowing VSUV to go beyond

the threshold necessary for a bilayer formation. Surfaces that were irradiated for 100 s and 300 s present similar behavior as for the 60 s or at least provide a sufficient amount of VSUV after UV exposure. However, surfaces that were irradiated for 60 s emerged to be more reproducible and therefore, unless stated otherwise, we applied UV irradiation for time duration of 60s. Surface regeneration was carried out using a detergent solution.

In order to confirm the formation of a lipid bilayer and quantify its lateral fluidity we performed fluorescence recovery after photobleaching (FRAP) measurements using confocal laser scanning microscope (CLSM). For this purpose Oregon Green® 488 1,2-dihexadecanoyl-*sn*-glycero-3-phosphoethanolamine (^{OG488}DHPE) were incorporated to the lipids in a ratio of 1:10^2 (fluorescent probes: lipids) to obtain fluorescently labeled vesicles. After vesicle capturing, fusion was triggered by incubation with 10 % poly(ethylene glycol) (PEG) solution with average molecular weight of 8000 g/mol. The mechanism through which PEG promotes fusion is not yet clear, however it was observed that its excluded volume has a significant role in fusion. In the presence of PEG, osmotic force is generated and causes inter-membranes to be in contact [42].

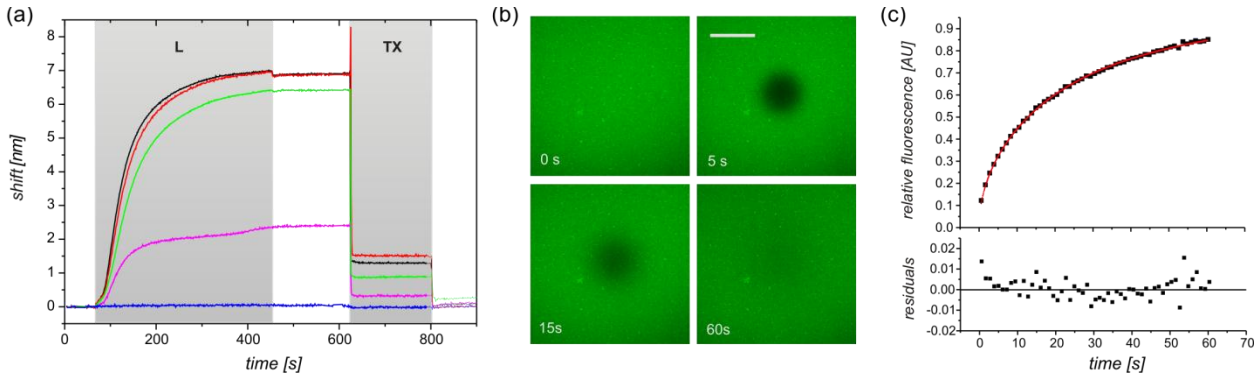

Figure 4-2. Vesicle capturing and fusion on a HDVE-functionalized PEG polymer brush. (a) Binding of VSUV (L) to surfaces reacted with HDVE for irradiation time periods of 10 s (magenta), 60 s (black), 100 s (red) and 300 s (green) as detected by RIfS. The blue curve represents VSUV injection on an untreated maleimide surface .After binding, surfaces were regenerated with detergent solution (TX). The injection periods are marked by a grey background. (b) Lipid diffusion in PSM after fusing vesicles captured by a HDVE-functionalized PEG polymer brush as probed by FRAP (scale bar 30 µm). (c) Recovery of the fluorescence in the bleached spot over time, and fit of a diffusion model.

After vesicle fusion, fluorescence imaging indicated uniform and rather homogeneous surface as demonstrated in Figure 4-2b, before bleaching. From the FRAP experiment, in which a circular area of 20 µm in diameter was bleached, a rapid fluorescence recovery confirmed a highly fluid membrane. Figure 4-2c represents the fitted recovery curve from which a diffusion

coefficient of 2.4 $\mu m^2/s$ was determined and is in good agreement with previous analyses performed on PSMs [18]. Thus at the following step, we applied this approach for probing diffusion of transmembrane protein reconstituted in liposomes. For this purpose maltose binding protein fused to the transmembrane helix of the type I interferon (IFN) receptor subunit IFNAR1 labeled with DY-649 (^{DY649}MBP-TM1) was reconstituted in VSUV. From the FRAP experiment (Figure 4-3a) performed and the fitted recovery (curve Figure 4-3b) a high degree of transmembrane protein mobility about 60% was obtained. A small fraction of immobile proteins can be assigned to opposite orientation of the reconstituted proteins and its permanent interaction with the hexadecyl hydrophobic domains [18].

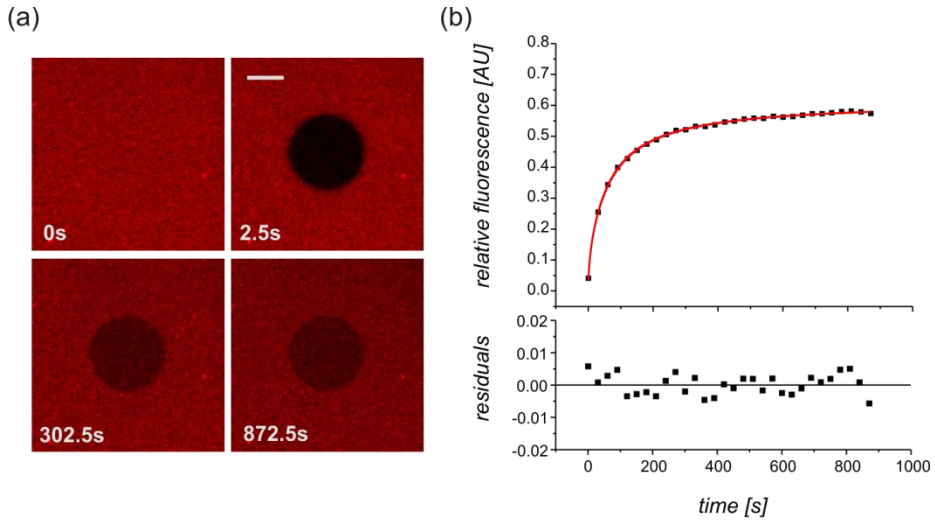

Figure 4-3. Diffusion of ^{DY649}MBP-TM1 reconstituted into PSM. (a) Typical FRAP experiment (scale bar 10 µm). (b) Recovery of the fluorescence in the bleached spot over time, and fit of a diffusion model.

A diffusion coefficient of 0.5 $\mu m^2/s$ was obtained which is in perfect accord with previous published data observed in PSMs [18]. Thus the surfaces devised, provide a suitable environment for the investigation of transmembrane proteins.

4.3.3 Liposomes capturing, fusion and diffusion in micropatterns

Here, our patterning approach was implemented for capturing lipid vesicles into micro-sized architectures. Fluorescently labeled VSUV were captured onto HDVE patterns as shown in Figure 4-4 with the intensity profile along the indicated line. Thus, a high contrast vesicle patterns were observed.

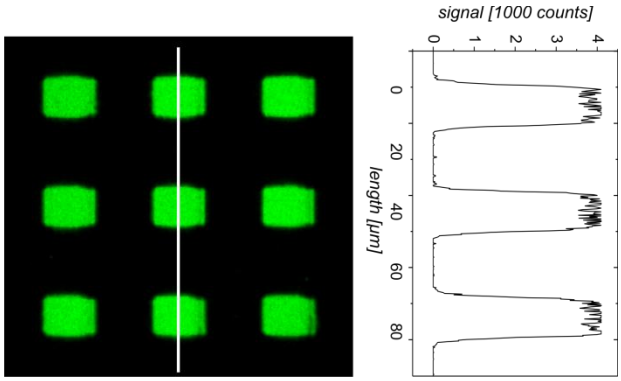

Figure 4-4. VSUVs capturing into micropatterns probed by fluorescence microscopy. Fluorescence image after capturing VSUV doped with ^{OG488}DHPE to micropatterned HDVE and the intensity profile along the white line.

Surface characterization was carried out using atomic force microscope (AFM) in tapping mode before and after fusion. Before fusion, surfaces were seemingly presenting homogeneous patterns of lipid vesicles as demonstrated in Figure 4-5a, left image. However, magnifying the patterned vesicle areas unveiled a non-uniform grainy structure (Figure 4-5a central and right images) that can be attributed to intact liposomes that underwent a certain degree of spontaneous fusion. After PEG addition and a subsequent fusion, homogeneous surfaces were obtained as can be clearly seen in Figure 4-5b. The thickness of the membrane obtained was ~6 nm, which is in good agreement with AFM data of membranes obtained on planar substrates [43-45].

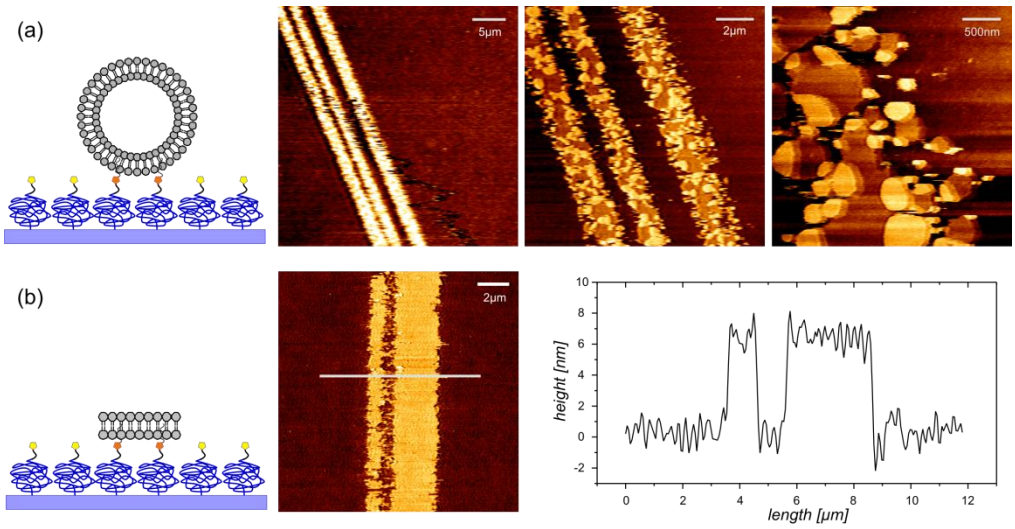

Figure 4-5. Vesicle capturing and fusion probed by AFM. (a) Tapping mode images after vesicle capturing into micropatterns shown at different magnifications. (b) AFM image of a micropatterned PSM after vesicle fusion and a height profile across the white line.

In addition to topography, further characterization was carried out for probing the diffusion of lipids in the patterns. For this purpose we performed FRAP experiments that yielded a high degree of lipid recovery > 80% in micropatterens within less than 1.5 min (Figure 4-6a). Rapid recovery could be observed from the recovery curve presented in Figure 4-6b. Therefore, in the following step we utilized these highly fluid patterned membranes for studying the behavior of transmembrane proteins reconstituted into lipid membranes.

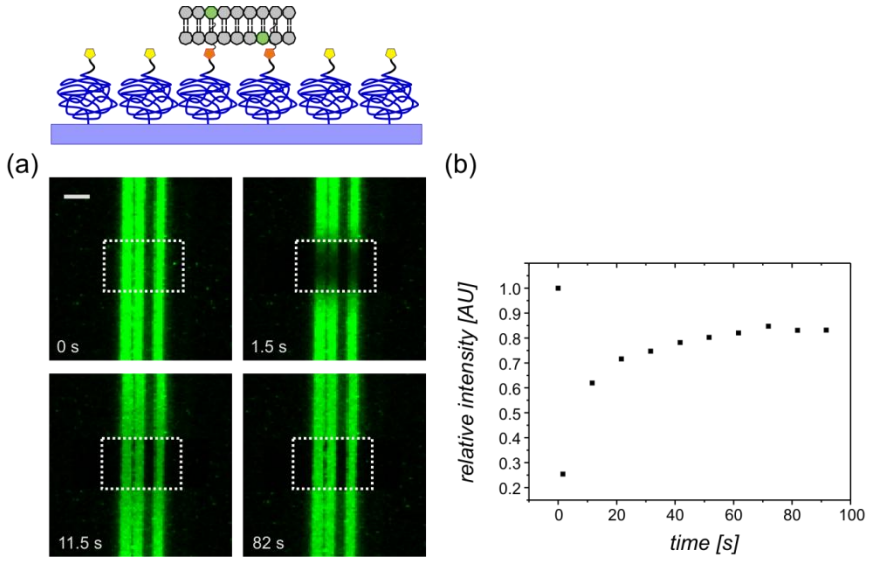

Figure 4-6. Lipid diffusion in micropatterned PSM probed by FRAP. (a) FRAP experiment with micropatterned PSM doped with fluorescent lipids (scale bar 5 µm). (b) Recovery curve observed.

4.3.4 Diffusion of transmembrane proteins in micropatterns

Subsequently our patterning approach was applied for probing transmembrane protein diffusion in a confined fashion (Figure 4-7). ^{DY649}MBP-TM1 was reconstituted in VSUV at the same manner as previously discussed in ratio of 1:10^3 (proteins:lipids) and lateral diffusion was monitored by FRAP. Fluorescence recovery of > 70% was observed (Figure 4-7b) and corroborated the high mobility of the proteins in the patterns. This provides an evidence for the suitability of our patterning method for probing transmembrane proteins reconstituted in artificial model membranes in a collective manner. In addition to an ensemble analysis of the diffusion properties, probing diffusion of individual transmembrane proteins reconstituted in our model patterned membrane system was possible using single molecule techniques.

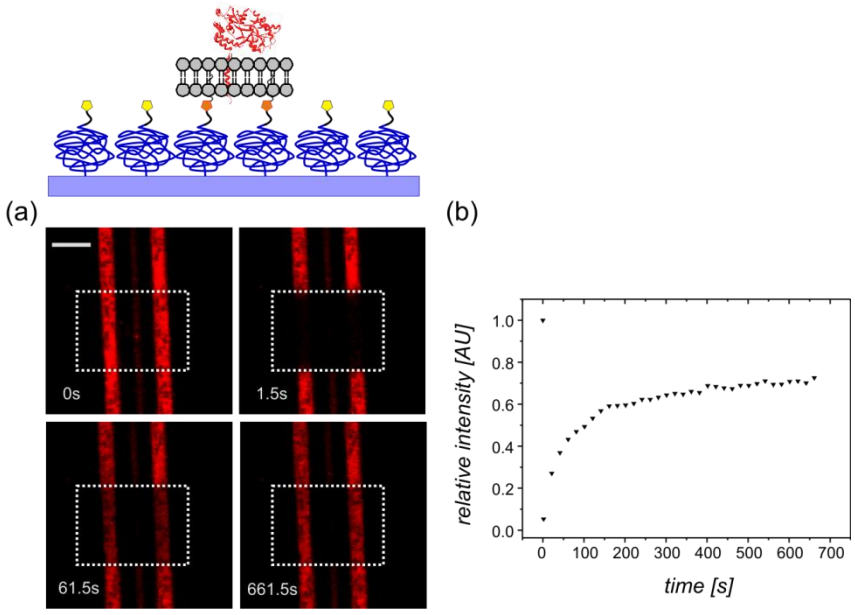

Figure 4-7. Transmembrane protein diffusion in micropatterned PSM probed by FRAP. (a) FRAP experiment with fluorescently labeled ^{DY649}MBP-TM1 reconstituted into micropatterned PSM. (b) Recovery curve observed.

^{DY649}MBP-TM1 was reconstituted in lipid vesicles in a ratio of 1:10^4 (proteins:lipids) together with MBP-ALA_7 in a ratio of 1:10^3 (proteins:lipids) for reducing nonspecific binding. Subsequently, these proteoliposomes were captured and fused onto a micropatterned surface and individual proteins were visualized by single molecule imaging as presented in Figure 4-8. Maximum fluorescence intensity image of the proteins, which diffuse in the pattern, obtained from 3,000 frames and is shown in Figure 4-8a. In addition to rapid diffusion of the proteins, a number of immobile species could be observed not only outside, but also inside the pattern. The immobile species observed outside the patterns can be assigned to non-specific adsorption of proteoliposomes, while immobile species in the pattern can be attributed to surface defects at the nanometer scale. For this reason, images were rendered by removal of immobile species in order to optimize tracking fidelity (Figure 4-8a). Homogeneous distribution of the diffusing ^{DY649}MBP-TM1 is shown in the magnified region (Figure 4-8a).

In order to quantify protein diffusion in micropatterns, single molecule tracking (SMT) experiments were carried out. From 1,000 trajectories detected for > 50 steps (Figure 4-8a), the mobility of the reconstituted ^{DY649}MBP-TM1 in lateral dimensions was then quantified in a patterned (Figure 4-8b, left) and non-patterned (Figure 4-8b, right) PSM. A two component analysis based on free diffusion in 1D (Figure 4-8b, black curve) and a restricted diffusion model

[46] (Figure 4-8b, green curve) was performed. Homogeneous diffusion along the pattern with diffusion constant of 1.55 $\mu m^2/s$ was determined. Considering protein diffusion in a restricted area (vertical to the line direction), a diffusion constant of 1.6 $\mu m^2/s$ was determined which is in perfect agreement with the value obtained along the pattern direction. Free diffusion with the same diffusion constant in the non-patterned PSM was obtained for both components (Figure 4-8b, right). The values obtained are about three times higher compared with the FRAP experiments performed (as demonstrated above) which can be ascribed to the different length scales probed by these methods. This corroborates that the protein diffusion properties in the restricted area were not affected by the confinement. Hence, the presented micropatterning technique is shown to be highly suitable for the investigation of diffusion properties of reconstituted transmembrane proteins by utilizing single molecule techniques.

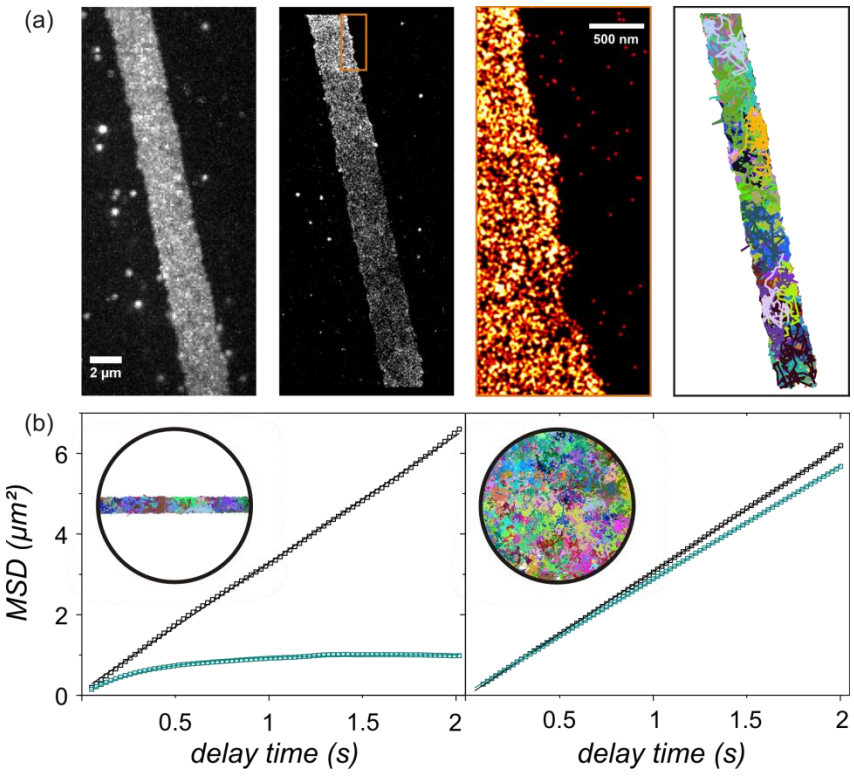

Figure 4-8. Diffusion of individual transmembrane proteins reconstituted into micropatterned PSM. (a) Images from typical single molecule tracking experiments. From left: I. maximum intensity image from a single molecule experiment; II: super-resolution tracking and localization microscopy (TALM) image rendered from individual molecules localized within 3,000 frames. Immobile molecules were removed by a spatio-temporal cluster analysis; III: zoom into the boundary of the PSM as indicated in II. IV: overlay of single molecule trajectories obtained from this data set. (b) Mean square displacement (MSD) analysis of the motion along (black) and vertical (green) to the line direction for line width of 2.4 µm (left). For comparison the same analysis on a non-patterned PSM is shown (right).

4.3.5 Ligand-receptor interactions

Next, the functionality of the proteins embedded in the membrane was probed. Here, the type I interferon receptor subunit IFNAR2, truncated after its transmembrane helix (IFNAR2-TM), was reconstituted in VSUV. Proteoliposomes were then captured and fused on surface functionalized HDVE, followed by the interaction of the reconstituted proteins with their ligand interferon-α2 (IFNα2) (Figure 4-9a). The binding assay was monitored using simultaneous TIRFS-RIF detection system as demonstrated in Figure 4-9b.

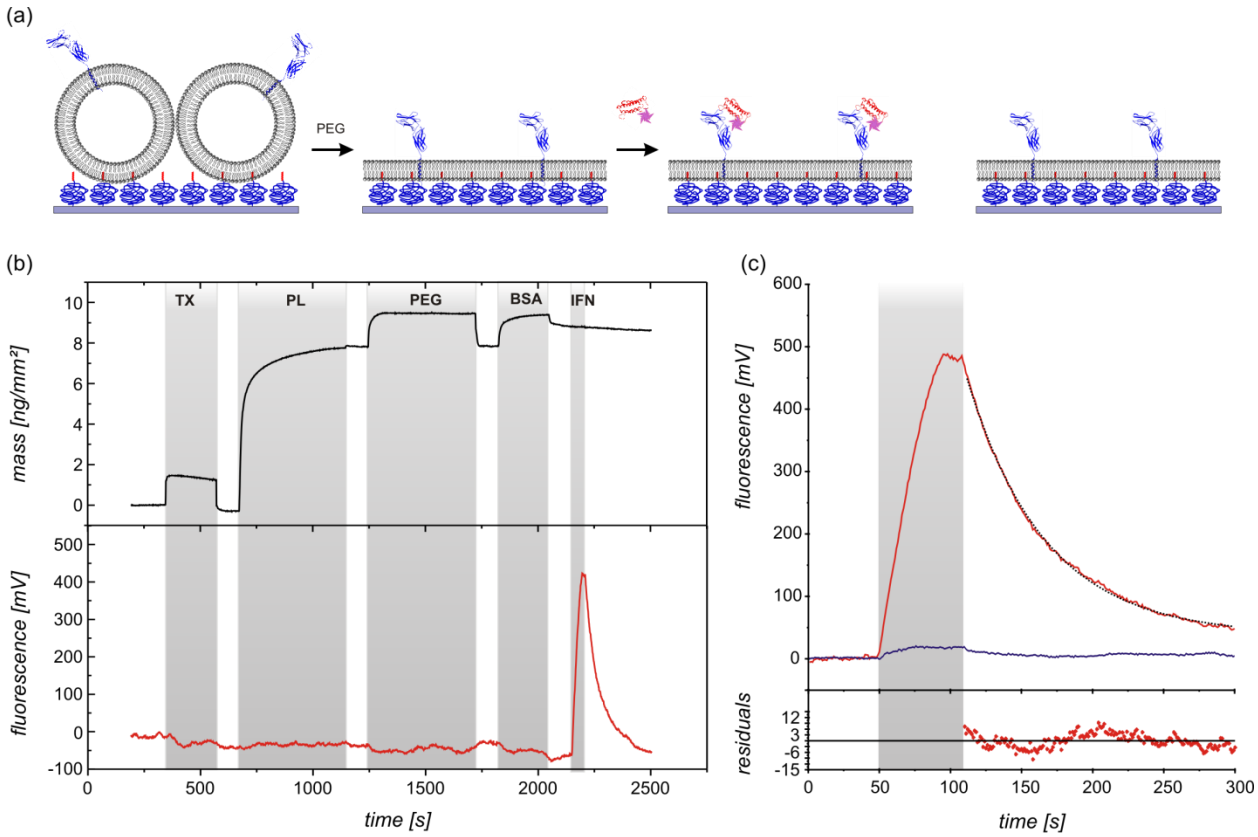

Figure 4-9. Specific ligand binding of IFNAR2-TM reconstituted into PSM. (a) Cartoon of the experiment: VSUV with reconstituted IFNAR2-TM (blue) were captured on the surface and fused by addition of PEG, followed by binding of IFNα2 (red). (b) Reconstitution of IFNAR2-TM into PSM and binding of ^{DY647}IFNα2 as detected by simultaneous TIRFS-RIF detection. Top: RIF channel; bottom: fluorescence channel (^{DY647}IFNα2). After surface conditioning with Triton X-100 (TX), IFNAR2-TM reconstituted into proteoliposomes (PL) was injected, followed by fusion with PEG solution (PEG). A BSA solution was injected to block unspecific binding (BSA). Subsequently, ^{DY647}IFNα2 was injected (IFN). Injection periods are marked by a grey bar. (c) Binding of ^{DY647}IFNα2 to IFNAR2-TM reconstituted in PSM as detected by TIRFS (red curve) and fit of the dissociation kinetics (black curve). For comparison, binding of ^{DY647}IFNα2 to PSM without IFNAR2-TM is shown (blue curve).

Rapid proteoliposome capturing to the HDVE moieties was observed, followed by a subsequent fusion to a bilayer. Injection of fluorescently labeled IFNα2 (^{DY647}IFNα2) confirmed that the functionality of the reconstituted IFNAR2-TM was preserved. Figure 4-9c represents the binding

of ^{DY647}IFNα2 to reconstituted IFNAR2-TM, which yielded a dissociation rate constant of 0.018 s^{-1} by applying monoexponential decay function. The value obtained perfectly correlates with former published interaction analysis data [27, 47]. A control experiment was performed without IFNAR2-TM in VSUV. As can be clearly seen, binding of ^{DY647}IFNα2 could not be observed, which therefore corroborates the specificity of the interaction to the reconstituted IFNAR2-TM. Hence, this artificial model system we devised is highly suitable for interaction analysis.

At the following step we tested the suitability of this system for a quantitative analysis of individual binding events in micropatterns. To this end, IFNAR2-TM was reconstituted in SOPC VSUV at the same procedure as for the ^{DY649}MBP-TM1. The ratio of proteins/lipids was $1:10^7$ together with MBP-ALA_7 in a ratio of $1:10^3$. Binding of labeled IFNα2 to the reconstituted IFNAR2-TM was probed by single molecule TIRF imaging. Figure 4-10a represents a super-resolution image of individual IFNα2 mutant M148A (^{DY647}M148A) molecules that were detected in the pattern. The image was constructed of 10,000 consecutive frames and was rendered by removal of immobile species from the pattern and the outside surroundings.

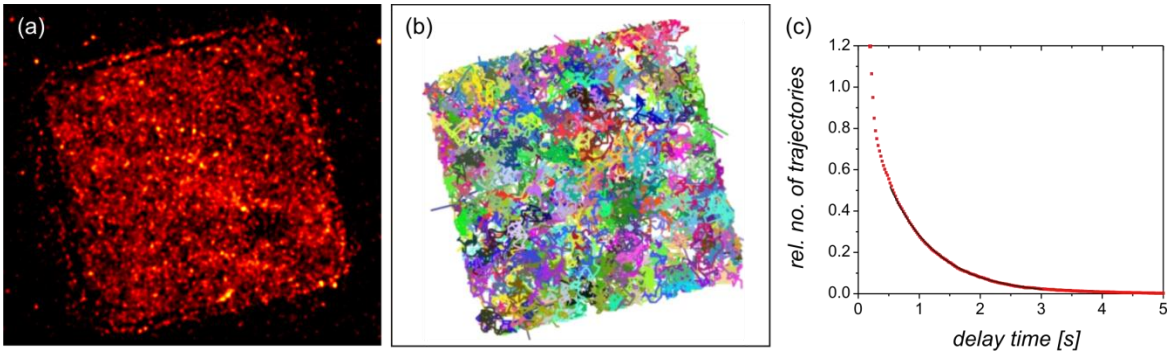

Figure 4-10. Single molecule protein-protein interaction analysis in micropatterned PSM. (a) A super-resoltion image obtained from ^{DY647}M148A binding to IFNAR2-TM reconstituted into micropatterned PSM after removing immobile particles (square 5 µm). (b) Overlay of trajectories of individual IFNα2 from the same experiment as shown in panel a. (c) Stability of individual protein complexes determined from the trajectory length of ^{DY647}M148A. The monoexponential fit is shown in black.

Figure 4-10b demonstrates the trajectories of individual ^{DY647}M148A molecules obtained. Based on a quantitative analysis of ~ 15,000 trajectories for > 20 steps, a dissociation rate constant of 0.8 s^{-1} was determined using a monoexponential decay function as shown in Figure 4-10c. After a correction for bleaching effects a final value of 0.85 s^{-1} was obtained, which is in a good agreement with previous single molecule studies [24].

A diffusion constant of $1.1 \pm 0.08\,\mu m^2/s$ was determined from the trajectories of the ^{DY647}M148A/IFNAR2 complex. However, a quantitative kinetic study of ^{DY647}IFNα2/IFNAR2-TM interactions was limited by bleaching, which was determined to be 2.5 s. Nevertheless, it was still possible to determine the diffusion of the ligand-receptor complex. From the trajectories of ^{DY647}IFNα2 confined in a square-shaped pattern, a diffusion constant of $1.14 \pm 0.01\ \mu m^2/s$ was obtained, which fits with the value obtained for ^{DY647}M148A. Moreover, diffusion analysis of ^{DY647}IFNα/IFNAR2 complex was carried out on the level of individual trajectories (Figure 4-11). From a diffusion analysis over 20 s, a diffusion constant of $1.1\ \mu m^2/s$ was determined (Figure 4-11b). This is in accord with the values obtained from the ensemble analysis. Thus, long-term observation of individual membrane protein complexes was successfully achieved.

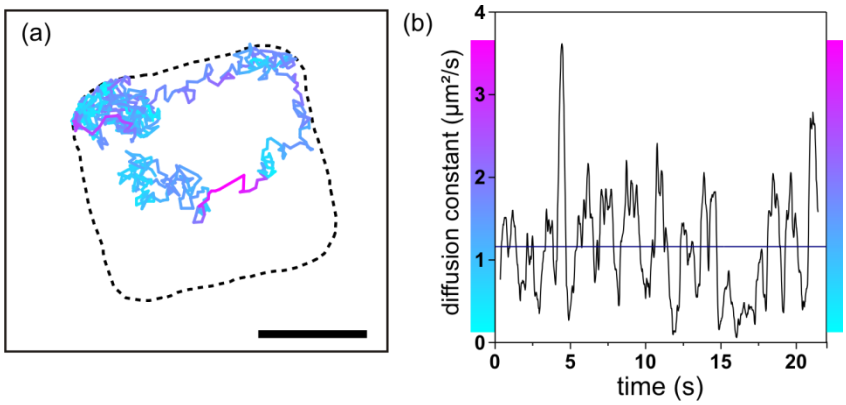

Figure 4-11. Single trajectory analysis. (a) Individual trajectory obtained for ^{DY647}IFNα2 bound to IFNAR2-TM reconstituted into a micropatterned PSM. (b) Local diffusion constant obtained by MSD analysis within a time window of 0.68 s (scale bar: 5 μm). The color-coding of the trajectory presented in panel indicates the local diffusion constant. The average diffusion constant is indicated by the blue line.

4.4 Summary and conclusions

We have here presented a simple and rugged method for spatial organization of PSM on solid supports in micrometer dimensions. Our micropatterning approach was carried out via a photochemical reaction of surface-immobilized maleimide moieties in presence of hexadecyl vinyl ether chains that function as anchors for capturing proteoliposomes and in order to obtain PSM. We demonstrated functional reconstitution of transmembrane proteins in these PSM, which freely diffuse within the spatially confined lipid bilayers. In these proof-of-concept experiments, individual protein-protein complexes could be followed over a few seconds, which

was mainly limited by photobleaching and the trajectory reconnection fidelity. While this is already sufficient for quantitative studies of many processes, further improvement of the tracking fidelity is possible by confinement into smaller structures. PSMs covering an area of 1-4 µm² can be readily achieved by this technique, which will allow tracking complexes with even higher fidelity at lower acquisition rate.

We envisage this method to play an important role for quantitatively probing the subtle interplay of protein-protein and protein-lipid interactions as well as conformational changes in a defined lipid environment, which is the basis for unraveling the molecular mechanisms of transport and communication across biological membranes.

Acknowledgement

I thank Friedrich Roder for single-molecule measurements and analysis and Oliver Birkholz for AFM measurements.

4.5 References

1. Coskun, U. and K. Simons, *Cell Membranes: The Lipid Perspective.* Structure, 2011. **19**(11): p. 1543-1548.
2. Sprong, H., P. van der Sluijs, and G. van Meer, *How proteins move lipids and lipids move proteins.* Nat Rev Mol Cell Biol, 2001. **2**(7): p. 504-13.
3. Phillips, R., et al., *Emerging roles for lipids in shaping membrane-protein function.* Nature, 2009. **459**(7245): p. 379-85.
4. Marsh, D., *Protein modulation of lipids, and vice-versa, in membranes.* Biochim Biophys Acta, 2008. **1778**(7-8): p. 1545-75.
5. Heyse, S., et al., *Emerging techniques for investigating molecular interactions at lipid membranes.* Biochimica and Biophysica Acta-Reviews on Biomembranes, 1998. **1376**(3): p. 319-338.
6. Janshoff, A. and C. Steinem, *Scanning force microscopy of artificial membranes.* Chembiochem, 2001. **2**(11): p. 798-808.

7. Kiessling, V., J.M. Crane, and L.K. Tamm, *Transbilayer effects of raft-like lipid domains in asymmetric planar bilayers measured by single molecule tracking.* Biophys J, 2006. **91**(9): p. 3313-26.
8. Fox, C.B., et al., *Single-molecule fluorescence imaging of peptide binding to supported lipid bilayers.* Anal Chem, 2009. **81**(13): p. 5130-8.
9. Thompson, N.L., X. Wang, and P. Navaratnarajah, *Total internal reflection with fluorescence correlation spectroscopy: Applications to substrate-supported planar membranes.* J Struct Biol, 2009. **168**(1): p. 95-106.
10. Sharonov, A., et al., *Lipid diffusion from single molecules of a labeled protein undergoing dynamic association with giant unilamellar vesicles and supported bilayers.* Langmuir, 2008. **24**(3): p. 844-50.
11. Deverall, M.A., et al., *Membrane lateral mobility obstructed by polymer-tethered lipids studied at the single molecule level.* Biophys J, 2005. **88**(3): p. 1875-86.
12. Tanaka, M. and E. Sackmann, *Polymer-supported membranes as models of the cell surface.* Nature, 2005. **437**(7059): p. 656-663.
13. Sackmann, E. and M. Tanaka, *Supported membranes on soft polymer cushions: fabrication, characterization and applications.* Trends Biotechnol, 2000. **18**(2): p. 58-64.
14. Tanaka, M., et al., *Native supported membranes on planar polymer supports and micro-particle supports.* J Struct Biol, 2009. **168**(1): p. 137-42.
15. Kiessling, V., M.K. Domanska, and L.K. Tamm, *Single SNARE-mediated vesicle fusion observed in vitro by polarized TIRFM.* Biophys J, 2010. **99**(12): p. 4047-55.
16. Wagner, M.L. and L.K. Tamm, *Reconstituted syntaxin1A/SNAP25 interacts with negatively charged lipids as measured by lateral diffusion in planar supported bilayers.* Biophys J, 2001. **81**(1): p. 266-275.
17. Diaz, A.J., et al., *Double cushions preserve transmembrane protein mobility in supported bilayer systems.* Langmuir, 2008. **24**(13): p. 6820-6826.
18. Roder, F., et al., *Reconstitution of membrane proteins into polymer-supported membranes for probing diffusion and interactions by single molecule techniques.* Anal Chem, 2011. **83**(17): p. 6792-9.

19. Groves, J.T. and S.G. Boxer, *Micropattern formation in supported lipid membranes.* Acc Chem Res, 2002. **35**(3): p. 149-57.

20. Bally, M., et al., *Liposome and lipid bilayer arrays towards biosensing applications.* Small, 2010. **6**(22): p. 2481-97.

21. Bieri, C., et al., *Micropatterned immobilization of a G protein-coupled receptor and direct detection of G protein activation.* Nat Biotechnol, 1999. **17**(11): p. 1105-8.

22. Tanaka, M., et al., *Selective deposition of native cell membranes on biocompatible micropatterns.* J Am Chem Soc, 2004. **126**(10): p. 3257-60.

23. Kaminski, W.E., A. Piehler, and G. Schmitz, *Genomic organization of the human cholesterol-responsive ABC transporter ABCA7: Tandem linkage with the minor histocompatibility antigen HA-1 gene.* Biochemical and Biophysical Research Communications, 2000. **278**(3): p. 782-789.

24. Waichman, S., et al., *Maleimide photolithography for single-molecule protein-protein interaction analysis in micropatterns.* Anal Chem, 2011. **83**(2): p. 501-8.

25. Yin, J., et al., *Genetically encoded short peptide tag for versatile protein labeling by Sfp phosphopantetheinyl transferase.* Proc Natl Acad Sci U S A, 2005. **102**(44): p. 15815-20.

26. Turgut, Z., et al., *Microstructural and magnetic observations of compacted FeCoV nanoparticles.* Ieee Transactions on Magnetics, 2000. **36**(5): p. 3024-3025.

27. Waichman, S., et al., *Functional immobilization and patterning of proteins by an enzymatic transfer reaction.* Anal Chem, 2010. **82**(4): p. 1478-85.

28. Schmitt, H.M., et al., *An integrated system for optical biomolecular interaction analysis.* Biosensors & Bioelectronics, 1997. **12**(8): p. 809-816.

29. Degrip, W.J., J. Vanoostrum, and P.H. Bovee-Geurts, *Selective detergent-extraction from mixed detergent/lipid/protein micelles, using cyclodextrin inclusion compounds: a novel generic approach for the preparation of proteoliposomes.* Biochem J, 1998. **330 (Pt 2)**: p. 667-74.

30. Gavutis, M., et al., *Lateral ligand-receptor interactions on membranes probed by simultaneous fluorescence-interference detection.* Biophys J, 2005. **88**(6): p. 4289-302.

31. Gavutis, M., S. Lata, and J. Piehler, *Probing 2-dimensional protein-protein interactions on model membranes.* Nature Protocols, 2006. **1**(4): p. 2091-2103.

32. Soumpasis, D.M., *Theoretical analysis of fluorescence photobleaching recovery experiments.* Biophys J, 1983. **41**(1): p. 95-7.

33. Serge, A., et al., *Dynamic multiple-target tracing to probe spatiotemporal cartography of cell membranes.* Nat Methods, 2008. **5**(8): p. 687-94.

34. Kusumi, A., Y. Sako, and M. Yamamoto, *Confined lateral diffusion of membrane receptors as studied by single particle tracking (nanovid microscopy). Effects of calcium-induced differentiation in cultured epithelial cells.* Biophys J, 1993. **65**(5): p. 2021-40.

35. You, C., et al., *Self-controlled monofunctionalization of quantum dots for multiplexed protein tracking in live cells.* Angew Chem Int Ed Engl, 2010. **49**(24): p. 4108-12.

36. Hess, S.T., et al., *Dynamic clustered distribution of hemagglutinin resolved at 40 nm in living cell membranes discriminates between raft theories.* Proc Natl Acad Sci U S A, 2007. **104**(44): p. 17370-5.

37. Manley, S., et al., *High-density mapping of single-molecule trajectories with photoactivated localization microscopy.* Nat Methods, 2008. **5**(2): p. 155-7.

38. Schutz, G.J., H. Schindler, and T. Schmidt, *Single-molecule microscopy on model membranes reveals anomalous diffusion.* Biophys J, 1997. **73**(2): p. 1073-80.

39. Yamada, M., I. Takase, and N. Koutou, *Photopolymerization of Maleimide and Its N-Substituted Derivatives.* Journal of Polymer Science Part B-Polymer Letters, 1968. **6**(12PB): p. 883-&.

40. Jonsson, S., et al., *Photo-induced alternating copolymerization of N-substituted maleimides and electron donor olefins.* Nuclear Instruments & Methods in Physics Research Section B-Beam Interactions with Materials and Atoms, 1997. **131**(1-4): p. 276-290.

41. Signorell, G.A., et al., *Controlled 2D crystallization of membrane proteins using methyl-beta-cyclodextrin.* J Struct Biol, 2007. **157**(2): p. 321-8.

42. Lentz, B.R., *PEG as a tool to gain insight into membrane fusion.* European Biophysics Journal with Biophysics Letters, 2007. **36**(4-5): p. 315-326.

43. Grandbois, M., H. Clausen-Schaumann, and H. Gaub, *Atomic force microscope imaging of phospholipid bilayer degradation by phospholipase A(2).* Biophysical Journal, 1998. **74**(5): p. 2398-2404.

44. Indrieri, M., et al., *Quantitative investigation by atomic force microscopy of supported phospholipid layers and nanostructures on cholesterol-functionalized glass surfaces.* Langmuir, 2008. **24**(15): p. 7830-7841.

45. Okazaki, T., et al., *Polymerized Lipid Bilayers on a Solid Substrate: Morphologies and Obstruction of Lateral Diffusion.* Langmuir, 2009. **25**(1): p. 345-351.

46. Kusumi, A., Y. Sako, and M. Yamamoto, *Confined Lateral Diffusion of Membrane-Receptors as Studied by Single-Particle Tracking (Nanovid Microscopy) - Effects of Calcium-Induced Differentiation in Cultured Epithelial-Cells.* Biophysical Journal, 1993. **65**(5): p. 2021-2040.

47. Piehler, J. and G. Schreiber, *Fast transient cytokine-receptor interactions monitored in real time by reflectometric interference spectroscopy.* Analytical Biochemistry, 2001. **289**(2): p. 173-186.

5 Lateral organization of cell surface receptors for probing cellular events

5.1 Introduction

Selective recognition of extracellular molecules by specific cell surface receptors activates communication from outside to inside the cell. This is carried out by signal propagation through protein interactions, conformational changes and chemical responses. Signal transduction has a significant role for gene transcription and cell metabolism, while disorder in signaling causes diseases. The importance of this cellular function can be judged from the fact that at least 60% of the current drugs target cell surface receptors. For these reasons, understanding the intracellular processes that occur during signal transduction has a great impact on various fields such as pharmacology and therapeutics. Spatial organization of proteins on solid supports is nowadays commonly utilized for probing protein functionalities and interactions in artificial model systems as discussed previously. Such *in vitro* systems, however, still lack the degree of complexity which exists in cells. Hence, investigation of proteins in their native surroundings is of a great importance for understanding the origin of their behavior in a complex mixture of biological molecules and their impact on diverse cellular events. For this reason, approaches that enable the investigation of cellular processes in live cells are highly required. However, studying protein functions, intracellular interactions and responses is a highly challenging task which requires methods that allow the simultaneous investigation of diverse interaction species in live cells. By controlling the lateral organization of cell surface receptors in artificial surface architectures we can discriminate different interaction species that are specifically bound to the designated regions. The key challenge is to preserve the biological activity of the proteins while they are selectively anchored to solid supports. However, methods for selective capturing of cell surface receptors directly from live cells are still scarce. Few methods for capturing or restricting cell-surface receptors into patterns from live cells were reported recently [1-3]. Using these methods protein interaction and regulation analyses were carried out for better understanding of signaling processes. However, such methods rely upon special surface design using time consuming and expensive technology or non-specific attachment of cells to the

support. Thus, generic and simple yet reliable methods for patterning of cell surface receptors are required.

Here, we have developed a patterning approach for covalent immobilization of cell surface receptors directly from live cells, based on the photochemistry of maleimide moieties. The patterning strategy was carried out on glass substrates exploiting a poly(ethylene glycol) (PEG) layer as a biocompatible scaffold. By the combination of RGD peptides together with HaloTag ligands (HTLs) we implemented selective cell attachment and cell-surface receptors capturing into micropatterns. HTL is a chloroalkane that reacts specifically to the 34 kDa HaloTag protein (HTP) upon dehalogenation [4] as described in 1.2.4. Thus, cell-surface receptors which were genetically fused to HTP and expressed in cells could be spatially confined into regions bearing HTLs for probing extra- and intracellular processes. We utilized this method in order to identify interactions involved in Janus-activated kinase (JAK) – Signal Transducer and Activator of Transcription (STAT) signaling pathways [5, 6]. We employed HeLa cells transiently transfected with type I interferon receptor subunits IFNAR1 and IFNAR2 and cytoplasmic effector proteins for recognition and characterization of protein interactions in live cells upon IFNα2 stimulation. Using this method we could successfully detect ligand binding, ternary complex formation and recruitment of effector proteins.

5.2 Experimental

5.2.1 Materials

Adhesive peptide Ac-CGRGDS-COOH was purchased from Coring System Diagnostix, Gernsheim /Germany. A 75 W Xenon lamp fitted with a 280 – 400 nm dichroic mirror was purchased from Newport Spectra-Physics and microstructured masks for photo-patterning (chrome on quartz) were obtained from NB Technologies, Bremen/Germany. Other chemicals are listed in 2.2.1 and 3.2.1. All the rest were purchased from Sigma Aldrich.

5.2.2 Synthesis of maleimide-functionalized RGD peptide

Maleimide-RGD (MI-RGD) sysnthesis was carried-out using 1-4-bis(maleimido)butane linker and a short peptide sequence Ac-CGRGDS-COOH as demonstrated in Scheme 1. 6.5 mg Ac-CGRGDS-COOH (Mw 635) in 0.5 ml 1 M HEPES buffer pH 8.0 was mixed with 10 mg 1,4-

bis(maleimido)butane (Mw 248) in 1 ml DMSO for 1 h at room-temperature. The mixture was diluted in water and loaded on a C_{18} reverse phase HPLC column for purification using a 0-70 % acetonitrile gradient in 0.1% TFA/water. Purified maleimide-RGD was lyophilized to obtain a white powder. MS-ESI: *m/z* 883.1; Calc. $[M]^+$: 883.

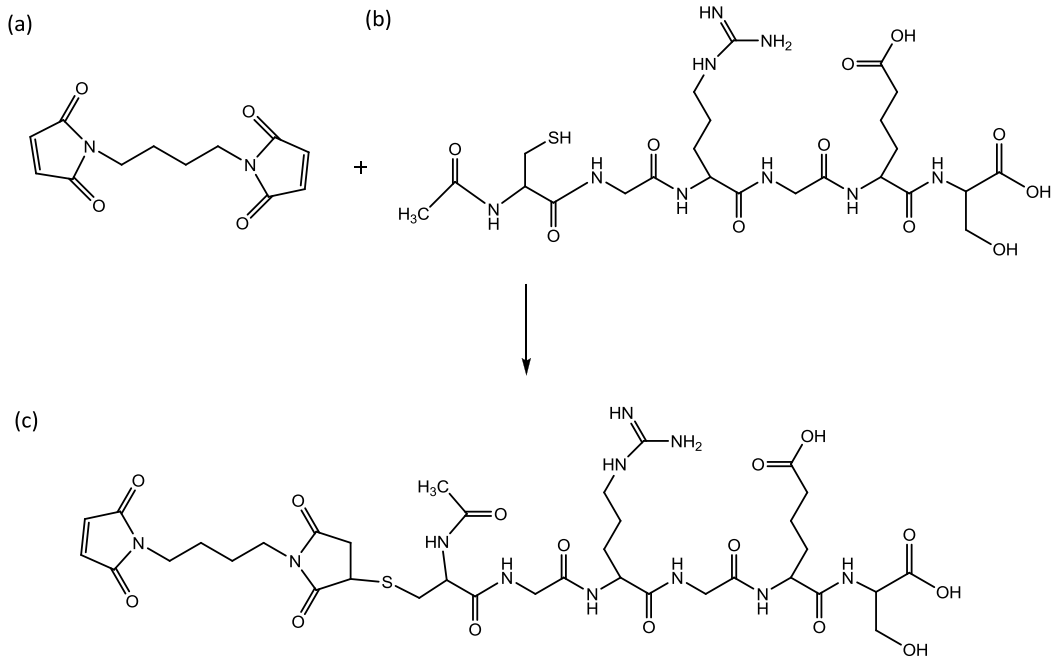

Scheme 1. MI-RGD synthesis. (a) 1-4-bis(maleimido)butane, (b) Ac-CGRGDS-COOH adhesive peptide and (c) the product MI-RGD.

5.2.3 Surface chemistry

Surface chemistry was carried out as described in chapter 2 and 3. This was performed on transducer slides for reflectance interference spectroscopy (RIfS) detection (a thin silica layer on a glass substrate) [7] as well as standard glass cover slides for fluorescence microscopy. If not stated otherwise, photolithographic patterning was performed in the presence of 10-20 mM MI-RGD in DMSO by irradiation for 5 minutes through a photomask using a 75 W Xenon lamp equipped with a 280-400 nm dichroic mirror (Newport Spectra-Physics). Thereafter, the chemically modified slides were washed with DMSO following by absolute ethanol. Further functionalization with 500 µM HTL was performed for 1 h at room-temperature.

5.2.4 Cell culture and transfection

HeLa cells were cultivated at 37°C and 5% CO_2 in MEM's Earle's with stable Glutamine (Biochrom AG, FG0325) supplemented with 10% fetal bovine serum (FBS) (Biochrom AG, S0615), 1% non-essential amino acids (PAA laboratories GmbH M11003) and 1% 2 (4-(2-hydroxyethyl)-1-piperazineethanesulfonic acid (HEPES) buffer without addition of antibiotics. HeLa cells were seeded in 35mm cell-culture dishes to a density of ca. 50% confluence. 24 h after seeding, cells were transiently transfected via calcium phosphate precipitation as described earlier [8]. 12-15 h after transfection, cells were washed twice with PBS-buffer and media was exchanged. 48 h after transfection cells were plated on the chemically modified cover glass for 15-20 h. For imaging, the medium was exchanged for medium without phenol red. For the generation of a cell line stably expressing Lifeact-EGFP, transfected cells were selected for stable neomycin resistance by cultivation in the presence of 0.8 µg/ml G418 (Calbiochem 345810). A cell clone with homogeneous and moderate expression of Lifeact-EGFP proteins were chosen and proliferated.

5.2.5 Plasmid constructs

Human expression vectors containing cmv (cytomegalo virus) promoter, which leads to high expression of the gene of interest were used. For selection and amplification in *E-coli* ampicillin resistance is encoded. The following plasmid constructs were utilized: HTP-GFP-IFNAR2, HTP-IFNAR2, fsnap-IFNAR2, AP-IFNAR1-GFP, HTP-IFNAR1, JAK1-GFP, Tyk2-GFP, STAT2-GFP and STAT1-GFP.

(HTP – HaloTag protein, GFP – green fluorescent protein, AP – acceptor peptide, fsnap – O^6-alkylguanine-DNA, IFNAR – interferon receptor, JAK – janus-activated kinase, Tyk – tyrosine kinase and STAT – Signal Transducer and Activator of Transcription).

5.2.6 Protein production, purification and labeling

IFNα2, IFNα2-YNS, IFNα2-M148A, carrying an N-terminal ybbR-tag (ybbR-IFNα2, ybbR-IFNα2-YNS and ybbR- IFNα2-M148A) were cloned by insertion of an oligonucleotide linker coding for

the ybbR peptide (DSLEFIASKLA) into the *Nde*I restriction site upstream of the corresponding genes in the plasmids pT72Cα2 [9]. These proteins and additional IFNα2 mutants: IFNα2-M148A-NLYY and IFNα2-YNS-α8tail, were expressed and purified by the same protocols established for wild-type IFNα2 [10]. YbbR-IFNα2 was labeled with ATTO-655 (^{AT655}IFNα2), ybbR-IFNα2-YNS with ATTO-655 (^{AT655}IFNα2-YNS) and ybbR-IFNα2-M148A with Dy647 (^{DY647}IFNα2-M148A) conjugated to CoA by means of the PPTase Sfp according to the protocol from the manufacturer (Covalys Biosciences). After the labeling reaction, labeled IFNα2 was further purified by size exclusion chromatography.

5.2.7 Fluorescence imaging of cell micropatterns

Fluorescence imaging of cell micropatterns was performed in a confocal laser-scanning microscope (CLSM, FluoView 1000, Olympus) equipped with an Argon ion laser (488 nm line for excitation of EGFP).

Fluorescence imaging of transmembrane micropatterns was performed using Olympus Cell^TIRFM-excellences microscope equipped with 405nm (200mW) laser, 488nm (200mW) laser, 561nm (200mW) laser and a 647nm Laser (140mW) and a back-illuminated electron multiplied (EM) CCD camera (C9100-13, Hamamatsu). A 60X objective with a numerical aperture of 1.45 (UAPON 60X/1.45, Olympus) was used for TIR excitation. The excitation beam was reflected into the objective by a quad-line dichroic beamsplitter for reflection at 405 nm, 488 nm, 568 nm and 647 nm (Di01 R405/488/561/647, Semrock). Fluorescence imaging was performed by excitation at 488 nm with power output of 2 mW and at 647 nm with a typical power output of 2.5 mW at the objective.

5.2.8 Single molecule imaging of protein-protein interactions in live cells

Single molecule fluorescence imaging at room-temperature was carried out with an inverted microscope (Olympus IX71) equipped with a single-line TIR-illumination condenser (Olympus) and a back-illuminated EM CCD camera (iXon DU897D, 512×512 pixel from Andor Technology). An argon krypton laser (C70 Spectrum, Coherent) was coupled into the microscope through a

polarization maintaining monomode fiber (KineFlex, Pointsource). The 647 nm laser line was selected by means of an acousto-optical tunable filter (AOTF, AAoptics). A 150X objective with a numerical aperture of 1.45 (UAPON 150X/1.45, Olympus) was used for TIR excitation. The excitation beam was reflected into the objective by a quad-line dichroic beamsplitter for reflection at 405 nm, 488 nm, 568 nm and 647 nm (Di01 R405/488/561/647, Semrock), and the fluorescence was detected through a quadruple bandpass filter (FF01 446/523/600/677-25, Semrock). Fluorescence imaging was performed by excitation at 647 nm with a typical power output of 2.5 mW at the objective. The camera was operated at -80°C with a typical EM gain of 300 and a frame rate of 1-32 Hz, depending on the kinetics of the interaction.

Single molecule fluorescence imaging at 37 °C was carried out using Olympus Cell^TIRFM-excellences microscope as described above. Here A 150X objective with a numerical aperture of 1.45 (UAPON 150X/1.45, Olympus) was used for TIR excitation. A frame rate of 1-32 Hz was applied, depending on the kinetics of the interaction.

All binding experiments were carried out using media complemented with oxygen scavenger [0.5mg ml^{-1} glucose oxidase (Sigma), 0.04 $mgml^{-1}$ catalase (Roche AppliedScience), 5% w/v glucose, 1 µM ascorbic acid and 1µM methyl viologene] to minimize photobleaching.

Localization and residence times of individual IFNα2 molecules were determined from trajectories obtained by the multiple target tracking algorithm (MTT) [11]. Trajectories of less than three frames were not considered in the evaluation of residence times. Histograms of the frequency of different residence times were fitted by a monoexponential decay function.

5.3 Results and discussion

5.3.1 Surface modification and patterning

Immobilization of proteins on solid supports requires preservation of the biological activity of the investigated proteins. Thus, a biocompatible platform that abrogates non-specific interactions with the support is needed. In order to address this issue, glass substrates were modified with a PEG polymer brush [12]. However, PEG brush inhibits attachment of cells to the support. For this reason, in addition to photopatternable groups, synthetic RGD peptides for

selective recognition of cell adhesion molecules (CAMs) were introduced to the system. Patterning was carried out via the polymerization of surface maleimides in the presence of maleimide-RGD (MI-RGD) moieties in solution as demonstrated in Figure 5-1 [13].

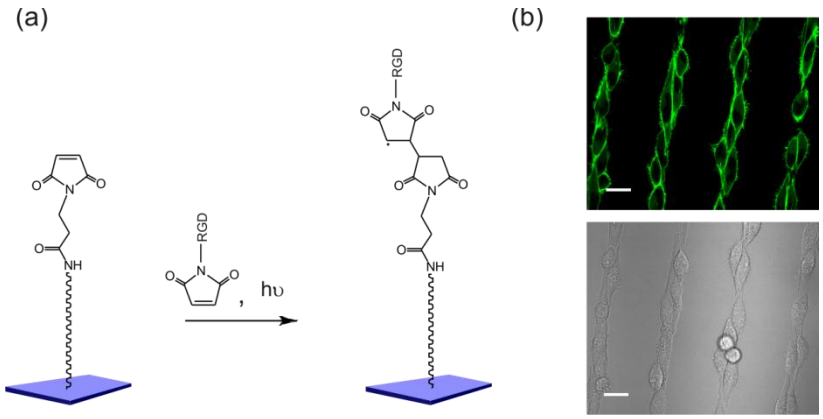

Figure 5-1. Cell adhesion and spreading in micropatterns. (a) Chemical structure in micropatterns before and after UV irradiation. (b) Top: fluorescence image of HeLa cells expressing lifeact fused to EGFP. Cells adhere and spread on RGD functionalized regions. Bottom: bright-field (BF) image of the cells. Scale bars 10 μm.

Subsequently, HeLa cells stably transfected with lifeact fused to EGFP were cultured onto the irradiated surfaces. Cell attachment and spreading along the RGD pattern (Figure 5-1b) corroborate the applicability of this method for exploring cellular processes on solid supports.

5.3.2 Immobilization of transmembrane proteins into micropatterns

Next, the binary nature of the patterning approach was exploited for selective capturing of membrane receptors directly from live cells. The free maleimide groups in the regions that were blocked by the photomask were further reacted with 500 μM HTL bearing a thiol group (Figure 5-2a,b). Then HeLa cells expressing cell-surface receptors fused to HTP were cultured on these surfaces and were selectively captured to HTL functionalized areas as depicted in Figure 5-2b. Figure 5-2c illustrates surface-immobilized receptor (IFNAR2) fused to GFP, and integrin-RGD interactions for cell attachment.

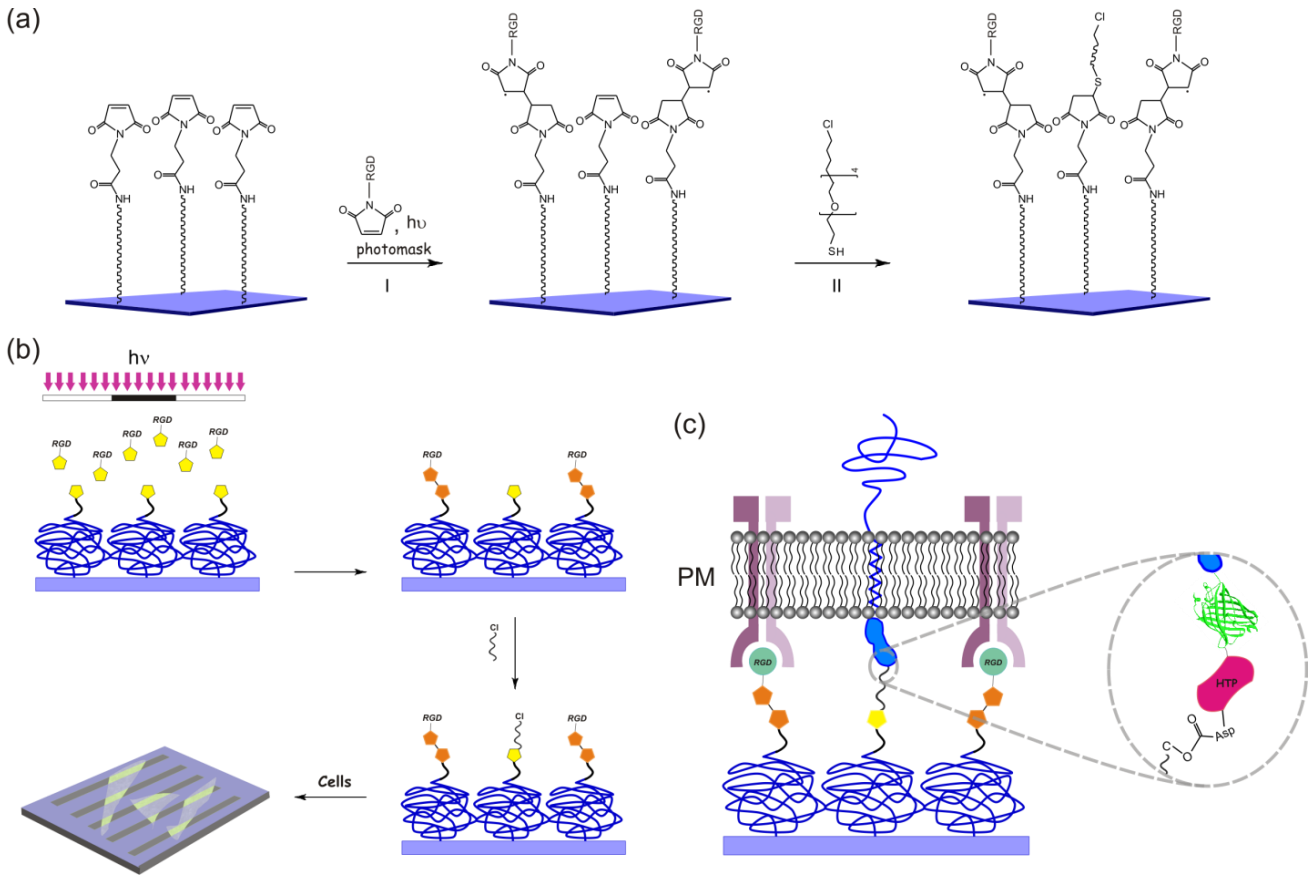

Figure 5-2. Binary micropatterning for capturing transmembrane proteins directly from live cells. (a) Chemical procedure of MI-RGD cross-linking upon UV exposure (I) and a subsequent surface functionalization of HTL moieties (II). (b) Schematic representation of the patterning strategy. (c) A cartoon of IFNAR2 fused to GFP and immobilized through HTP-HTL interaction. Cell adhesion was carried out through interaction of integrins and surface immobilized RGD upon UV exposure.

At first, HeLa cells expressing HTP-GFP-IFNAR2 were cultured on line-shaped patterns in which IFNAR2 receptor was stably bound to the HTL functionalized regions (Figure 5-3b, left image). Subsequently, the functionality of the immobilized receptor was confirmed by its interaction with 10 nM fluorescently labeled IFNα2 (^{AT655}IFNα2) as shown in Figure 5-3, central and left images.

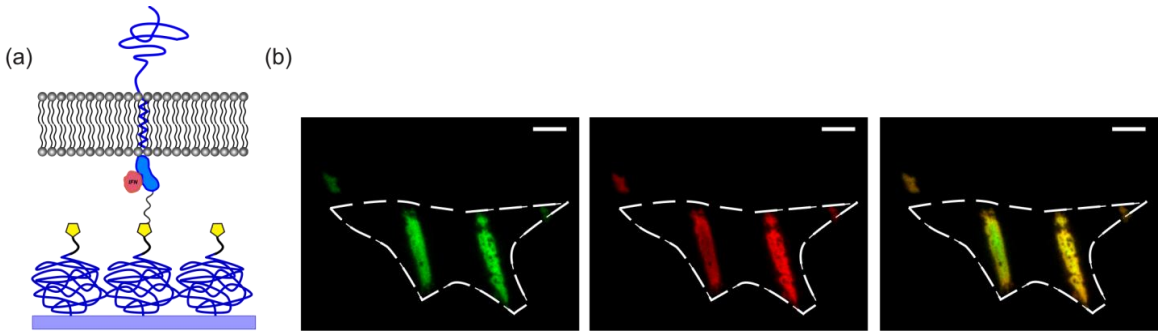

Figure 5-3. Transmembrane protein patterning. (a) Schematic representation of surface patterning of IFNAR2 using HTP-HTL interactions and integrin-RGD for cell adhesion. (b) TIRF microscopy images of patterns generated by the attachment of HTP-GFP IFNAR2 receptor to the surface (left), ^{AT655}IFNα2 interaction with the immobilized receptor (center) and overlay of these two images (right). The white line indicates the cell's border (scale bars 10 µm).

In the following experiment, HeLa cells expressing non-fluorescently labeled cell surface receptors HTP-IFNAR2 were cultured on a patterned surface. Subsequently, 10 nM ^{AT655}IFNα2 was incubated and line-shaped patterns were exposed (Figure 5-4a, left image). The presence of the complete HTL patterns was detected by staining the surface with HTP-GFP as presented in Figure 5-4a, central image. The specificity of the interaction was confirmed by a control experiment in which HeLa cells expressing IFNAR2 without HTP were cultured on a surface bearing the same line-shaped HTL patterns as shown above. First, the surface was incubated with 10 nM ^{AT655}IFNα2. Shortly after, transfected cells were detected due to the interaction of ligands with the expressed receptors. However, unlike the previous experiment, patterns of ^{AT655}IFNα2 could not be observed (Figure 5-4b, left image). The presence of HTL patterns was confirmed by staining the surface with HTP-GFP (Figure 5-4b, central image).

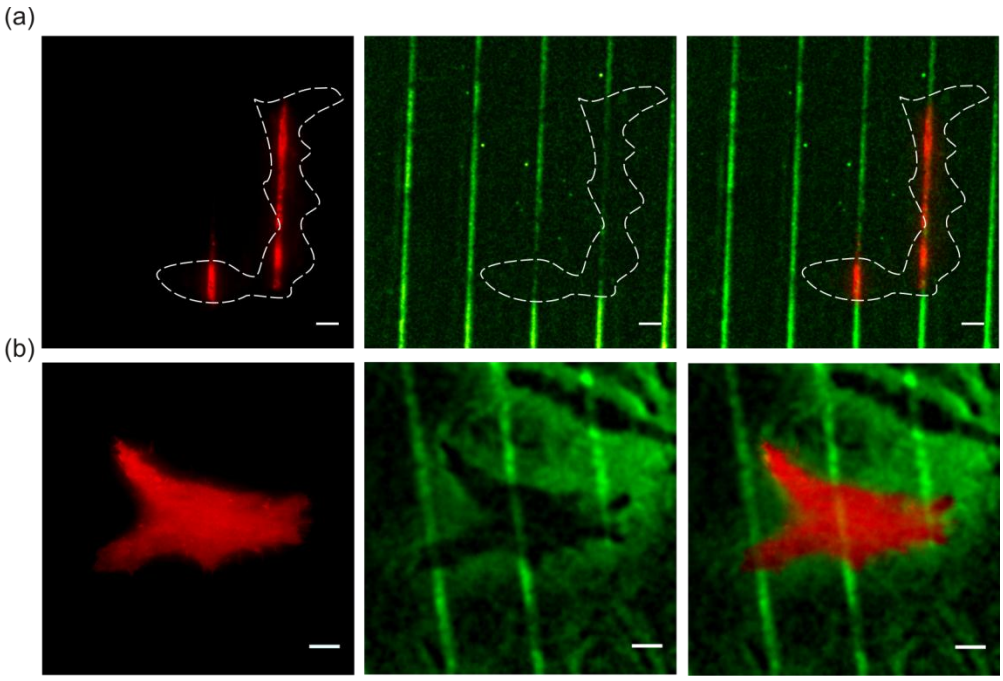

Figure 5-4. Transmembrane protein patterning. (a) TIRF microscopy images of patterns generated by the attachment of HTP-IFNAR2 receptor to the surface and a subsequent ^{AT655}IFNα2 interaction with the immobilized receptor (left). By incubation of HTP-GFP the complete patterns were exposed (center). Overlay of these two images (right). The white line indicates the cell's border (scale bars 10 µm).

So far we demonstrated the utility of this method for a qualitative characterization of ligand-receptor interactions in live cells in an ensemble manner. Next, this micropatterning method was tested as a tool for quantitative protein interaction analysis on the single molecule level.

To this end, HeLa cells expressing HTP-IFNAR2 were cultured on a patterned surface. Subsequently, surfaces were incubated with 500 pM IFNα2 mutant M148A-NLYY, which has a similar affinity to IFNAR2 as compared with IFNα2-M148A and negligible affinity to IFNAR1 as mentioned in 1.7. Enrichment of the ligands was detected on the patterned regions to which IFNAR2 receptors were attached as shown in Figure 5-5a. The interaction of the immobilized IFNAR2 with individual IFNα2-M148A-NLYY was analyzed and a dissociation rate constant of 1.52 s^{-1} was obtained from a monoexponential fit of the ligand residence time histogram (Figure 5-5b). The value obtained is in accord with values obtained *in vitro* [14, 15]. Subsequently, 1 µM IFNα2 mutant YNS-α8tail which has a stronger affinity towards IFNAR2 was added (Figure 5-5c). From the dissociation kinetics obtained during chasing, a dissociation rate constant of 1.56 s^{-1} was determined which is in perfect agreement with the rate constant obtained from the histogram of individual IFNα2-M148A-NLYY residence times.

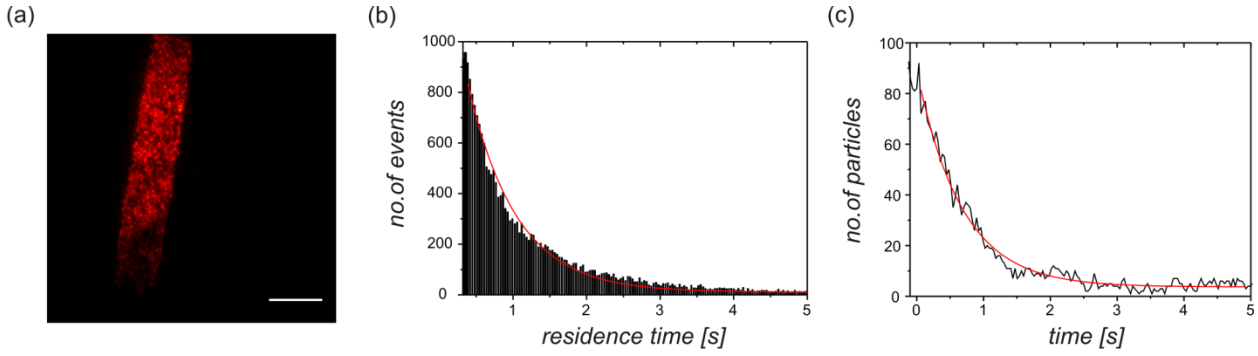

Figure 5-5. Single molecule analysis in micropatterns. (a) TIRF microscopy image of individual ^{AT655}IFNα2 molecules in a line-shaped micropattern (scale bar 10 µm). (b) Histogram of residence times of individual ^{AT655}IFNα2 molecules bound to the immobilized IFNAR2. (c) Chasing ^{AT655}IFNα2 with 1 µM unlabeled IFNα2-YNS-α8tail.

Following the results discussed above, the specificity and reversibility of ligand-receptor interactions were corroborated using surface micropatterns, thus confirming the suitability of this method for single-molecule experiments.

5.3.3 Ternary complex assembly

The patterning approach was further applied for probing ternary complex formation. Ligand binding induces the association of the two membrane receptor subunits as an initial step of signal transduction. In order to probe ternary complex formation, HeLa cells expressing both HTP-IFNAR2 and IFNAR1-GFP where cultured onto a patterned surface. Prior to ^{AT655}IFNα2 binding, IFNAR1-GFP was distributed across the cell membrane as demonstrated in Figure 5-6b (top, left image). After ligand binding (Figure 5-6b bottom, left) IFNAR1-GFP was enriched in the patterns (Figure 5-6b top right) in the regions where ^{AT655}IFNα2 was present (Figure 5-6b bottom, left). Hence, by applying our micropattern strategy, ternary complex formation can be clearly visualized. After ligand binding, cells showed a granular structure, which could be explained by endocytosis of ligand and non-immobilized receptor complexes into the cell. At the following step we tested the suitability of this technique for quantitative biophysical analysis on the single molecule level in the same system as just described. Shortly after 500 pM ^{AT655}IFNα2-M148A binding to patterns as shown in Figure 5-6d, 1 µM IFNα2-YNS-α8tail was added to the system to compete with ^{AT655}IFNα2-M148A molecules on the binding sites of the immobilized HTP-IFNAR2. After ~20 min almost all binding sites were occupied with IFNα2-YNS-

α8tail (Figure 5-6d, right image). Figure 5-6e is the dissociation curve obtained during chasing with IFNα2-YNS-α8tail, which yields a dissociation rate constant of $6.9 \times 10^{-3}\,s^{-1}$. From here, the experiments performed indicate the suitability of this patterning approach for probing interactions using single-molecule techniques in systems bearing a higher degree of complexity.

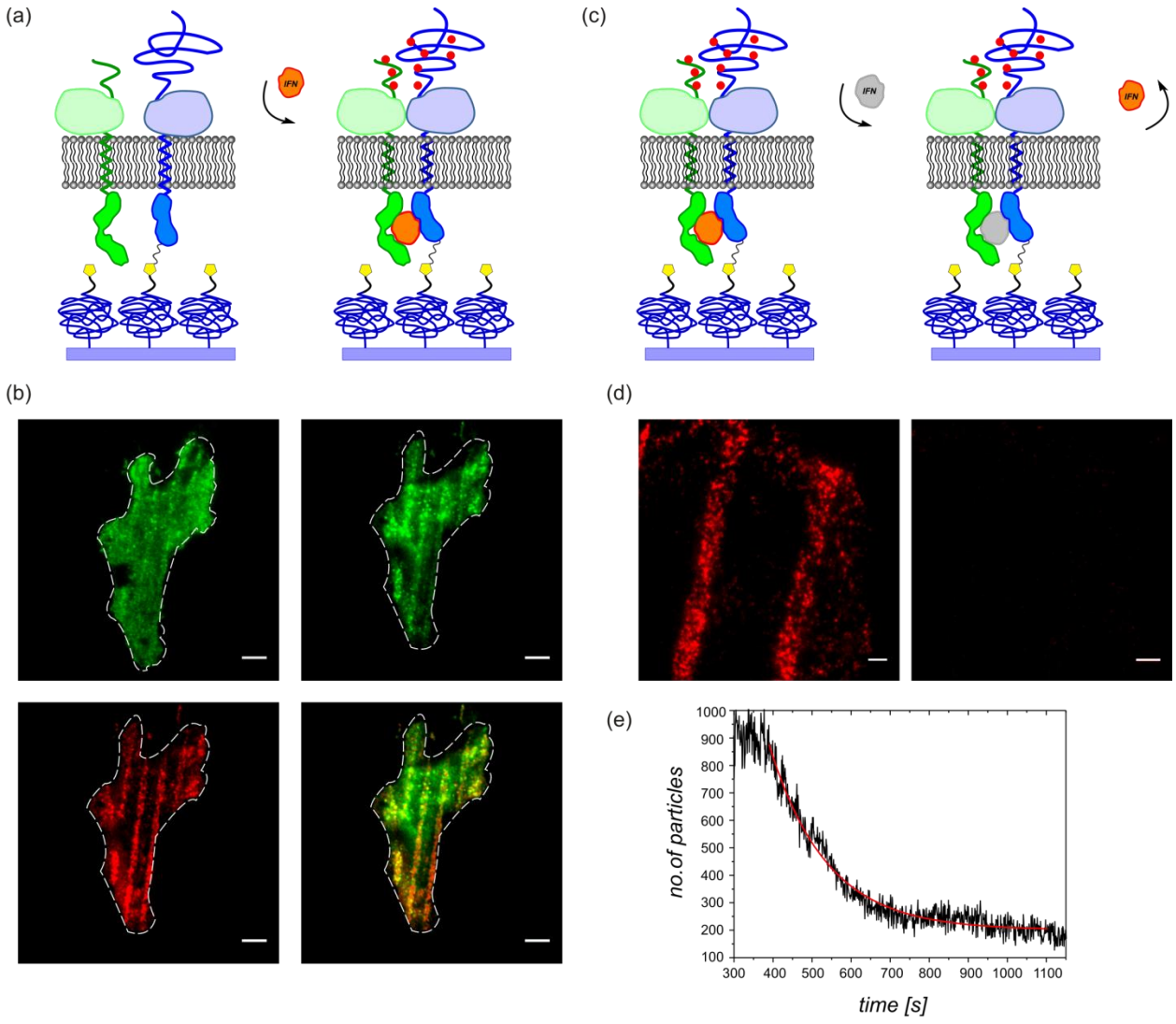

Figure 5-6. Ternary complex assembly in micropatterns. (a) Illustration of ternary complex formation induced by ^{AT655}IFNα2. (b) HTP-IFNAR2 and IFNAR1-GFP co-expressed in HeLa cells are shown. IFNAR1-GFP is spread across the cell membrane (top, left) while after ^{AT655}IFNα2 stimulation (bottom left), enrichment of IFNAR1-GFP in the pattern was observed (top, right). Overly of images after ^{AT655}IFNα2 stimulation (bottom left). Scale bars 10 µm.(c) Schemtic representation of the chasing process in which IFNα2-YNS-α8tail displaced bound ^{AT655}IFNα2 molecules. (d) TIRFM images of ^{AT655}IFNα2 molecules interact with the immobilized HTP-IFNAR2 before (left) and after (right) chasing. (e) Dissociation curve during chasing with 1 µM unlabeled IFNα2-YNS. The white line indicates the cell's border (scale bars 10 µm).

5.3.4 Cytoplasmic effector proteins

Next, we utilized the patterning approach for probing interactions of cytoplasmic effector proteins involved in JAK/STAT signaling pathways.

Protein Janus kinases

Here, we employed HeLa cells that were co-transfected with HTP-IFNAR1 and Tyk2-GFP (a member of the JAK family) for the recognition of Tyk2 towards IFNAR1 in micropatterns. The expressed Tyk2-GFP proteins were accumulated in patterns that contained the immobilized IFNAR1, before and after ^{AT647}IFNα2-YNS binding as shown in Figure 5-7b, top left and right images. Binding of ^{AT655}IFNα2-YNS molecules specifically in the patterns confirmed the presence of immobilized unlabeled HTP-IFNAR1 as shown in Figure 5-7b, bottom left image. Based on this experiment we can confirm that indeed, protein kinase Tyk2 is constitutively associated with IFNAR1 and independent on activation.

Then the nature of the interaction between IFNAR1 and Tyk2 in live cells was probed by fluorescence recovery after photobleaching (FRAP). Upon photobleaching of Tyk2-GFP a slow recovery of Tyk2-GFP from the cytoplasm was observed (Figure 5-7c). This may indicate stable interaction of the species involved, or may include contribution of both dissociation and association.

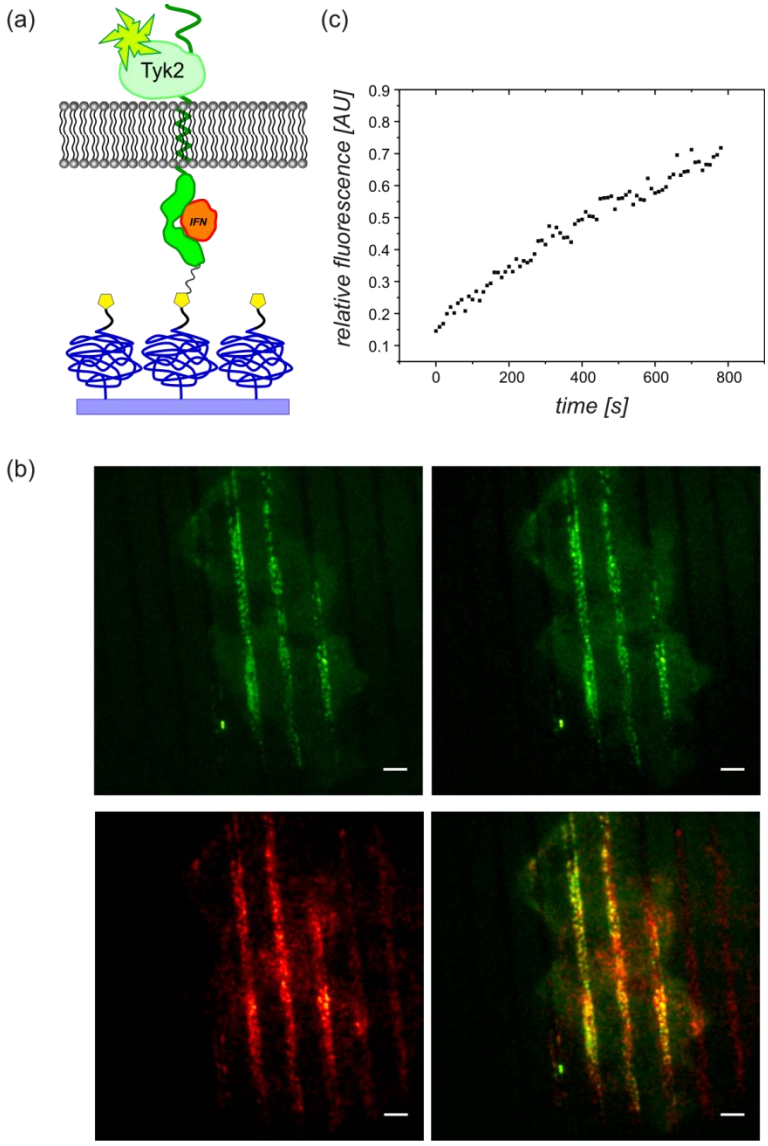

Figure 5-7. Tyk2 association to IFNα2 receptor subunit IFNAR1. (a) Illustration of IFNAR1 bound to ^{AT655}IFNα2-YNS with its extracellular domain and to Tyk2-GFP with its intracellular domain. (b) Tyk2-GFP before (top left) and after (top right) ^{AT655}IFNα2-YNS stimulation. ^{AT647}IFNα2-YNS binding to immobilized IFNAR1 (bottom, left). Overlay of Tyk2-GFP and ^{AT655}IFNα2-YNS (bottom right). Scale bars 10 µm.

Cytoplasmic transcription factors

STATs are known to be activated by JAK proteins through tyrosine phosphorylation followed by STAT dimerization and translocation to the nucleus for gene transcription. Here we probed interactions between IFNAR subunits and cytoplasmic STAT proteins in micropatterns. HeLa cells co-expressing HTP-IFNAR2 and STAT2-GFP were cultured on our line-shaped patterned surfaces. According to the TIRF images obtained after ^{AT655}IFNα2 binding, enrichment of STAT2-GFP (Figure 5-8b, left) and ^{AT655}IFNα2 (Figure 5-8b), center) in the patterns could be observed.

The overlay of these images (Figure 5-8b, right) corroborates the association of STAT2-GFP to the immobilized IFNAR2. The interaction of STAT2-GFP towards the immobilized IFNAR2 was monitored by FRAP. In contrast to the slow recovery observed for Tyk2-GFP, rapid fluorescence recovery of STAT2-GFP in the pattern was observed (Figure 5-8c, red curve), which corroborates transient interactions of STAT2 to IFNAR2. A comparison of the FRAP curves obtained for STAT2-GFP and Tyk2-GFP during 150 s is presented in Figure 5-8c. The recovery curve was fitted using a monoexponential function and a dissociation rate constant of 0.08 s^{-1} was obtained (Figure 5-8d).

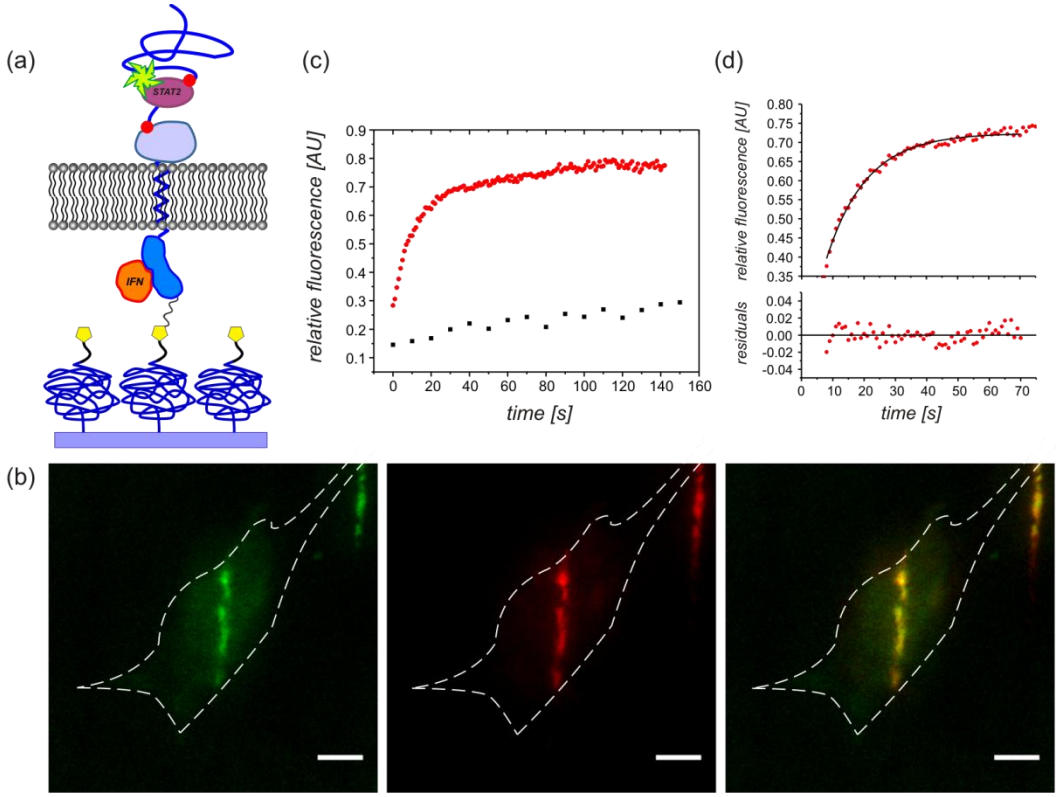

Figure 5-8. STAT2-IFNAR2 interaction characterization in micropatterned surfaces. (a) Illustration of IFNAR2 bound to ^{AT655}IFNα2 with its extracellular domain and to STAT2-GFP with its intracellular domain. (b) TIRF microscopy images of STAT2-GFP (left), ^{AT655}IFNα2 (center) and the overlay (right) after ^{AT655}IFNα2 binding. The white line indicates the cell's border (scale bars 10 µm). (c) Monitoring interaction dynamics of IFNAR2 with Tyk2 (black) and STAT2 (red) by FRAP. (d) Fitted recovery curve by a monoexponentional function assuming diffusion-uncoupled recovery [16].

At the following step we aimed to detect interactions of STAT1 with IFNAR subunits in micropatterns. To this end, HeLa cells co-transfected with HTP-IFNAR1 and STAT1-GFP were cultured on micropatterned surfaces. STAT1-GFP was shown to be distributed over the cell (in the cytoplasm) and not particularly on the line patterns (Figure 5-9b, left). Nevertheless,

^{AT655}IFNα2-YNS was specifically accumulated in the HTP-IFNAR1 patterns as shown in Figure 5-9b, center. The minor degree of STAT1-GFP which is seemingly detected in the pattern (Figure 5-9b, left) can be attributed to the strong interaction of HTP conjugated to IFNAR1 with the HTL functionalized regions, which may results in a stronger attraction of the cell membrane with the substrate in these specific regions.

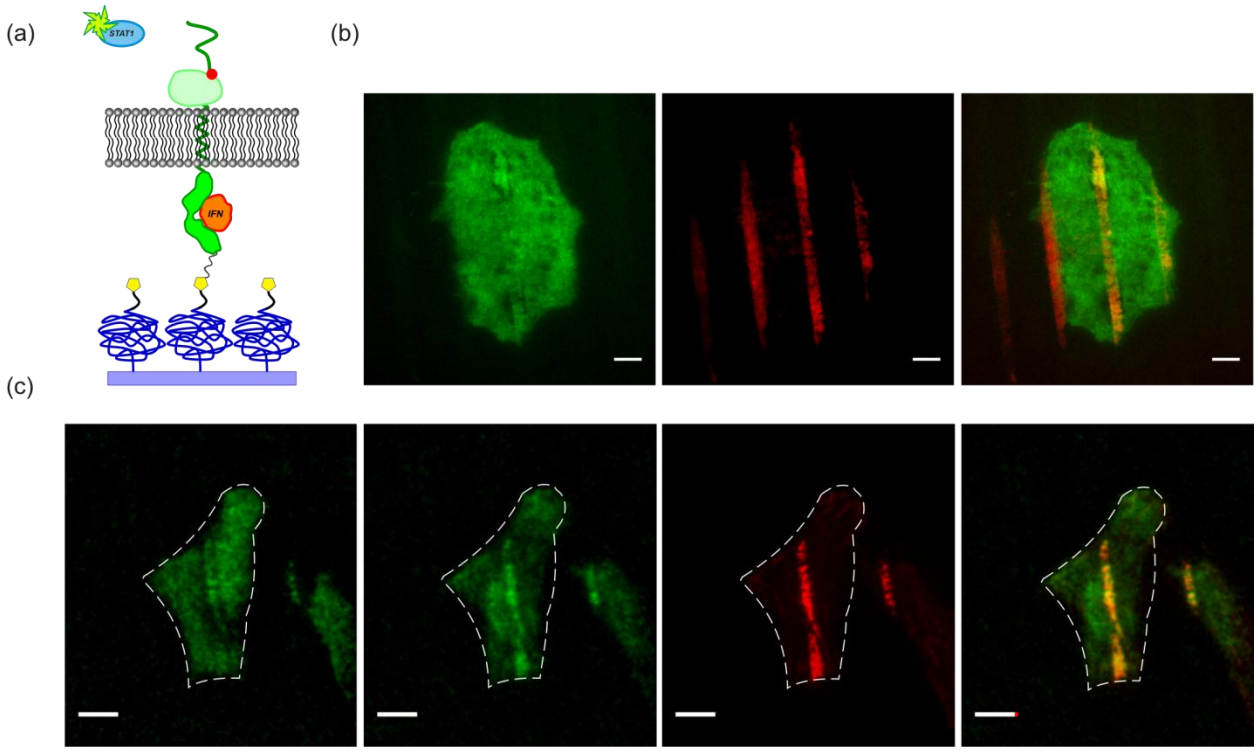

Figure 5-9. STAT1-IFNAR interaction characterization in micropatterned surfaces. (a) Illustration of IFNAR1 bound to ^{AT655}IFNα2-YNS with its extracellular domain, while STAT1-GFP is present in the cytoplasm. (b) TIRF microscopy images of STAT1-GFP (left), ^{AT655}IFNα2-YNS (center) and the overlay (right) after ^{AT655}IFNα2-YNS binding. (c) From left: STAT1-GFP before and after ^{AT655}IFNα2 stimulation. ^{AT655}IFNα2 accumulated in a line-shaped pattern where IFNAR2 was immobilized and the overlay of STAT1-GFP and ^{AT655}IFNα2 after stimulation. The white line indicates the cell's border (scale bars 10 µm).

In addition, the interaction of STAT1 and IFNAR2 in micropatterns was tested. Here we employed HeLa cells expressing HTP-IFNAR2 and STAT1-GFP, which were then cultured on a patterned surface. Prior to ^{AT655}IFNα2 binding, a very low amount of STAT1-GFP could be detected in the pattern (probably because of attraction of the membrane to the support, as mentioned above) but most of the proteins were distributed in the cytoplasm as visualized in Figure 5-9c, left image. After ^{AT655}IFNα2 stimulation, enrichment of STAT1-GFP in areas, to which HTP-IFNAR2 receptors were anchored, was observed as shown in Figure 5-9c, center-left.

Specific interaction of ^{AT655}IFNα2 with the immobilized HTP-IFNAR2 is clearly seen in Figure 5-9c, center-right.

5.4 Summary and conclusions

Cells carry out different processes to maintain their functions. The investigation of different interaction relaying upon signaling molecules binding and activation, for example, is necessary for better understanding different signaling pathways. However, the complexity of such systems together with the lack of suitable methods hampers the study of cellular processes. To address this challenge, we have developed a chemical strategy for patterning transmembrane proteins directly from live cells in order to investigate cellular responses before and after localized stimulation. This strategy is based on a biocompatible platform in combination with maleimide chemistry. Here, unique features of maleimide derivatives were exploited for binary micropatterning: (i) maleimide groups selectively react with thiols in a "click" chemistry manner and (ii) they undergo polymerization upon UV exposure in the absence of a photoinitiator and thus serve as monomers and photocatalysts simultaneously.[13] During UV irradiation MI-RGD groups were directly reacted with surface maleimides in specific regions to obtain RGD functionalized surfaces for cell adhesion. This was followed by functionalization of the previously non-irradiated regions with HTL. Transmembrane proteins fused to HTP were then selectively bound to the HTL patterns directly from live cells. This enabled us to detect ligand binding, ternary complex formation and recruitment of effector proteins simultaneously. Recognition and characterization of protein-protein interactions in live cells were proved to be highly compatible with ensemble and single molecule techniques. In addition to study interactions following the JAK/STAT signaling pathways this approach can be a highly promising towards the elucidation of versatile processes occurring at the interface of the plasma membrane.

Acknowledgement

I thank Sara Löchte for collaboration on cell culture and imaging, Oliver Beutel for single-molecule measurements and analysis and Dr. Changjiang You for MI-RGD synthesis.

5.5 References

1. Schwarzenbacher, M., et al., *Micropatterning for quantitative analysis of protein-protein interactions in living cells.* Nat Methods, 2008. **5**(12): p. 1053-60.
2. Salaita, K., et al., *Restriction of Receptor Movement Alters Cellular Response: Physical Force Sensing by EphA2.* Science, 2010. **327**(5971): p. 1380-1385.
3. Chiang, E.N., et al., *Cellular Responses to Patterned Poly(acrylic acid) Brushes.* Langmuir, 2011. **27**(11): p. 7016-7023.
4. Los, G.V., et al., *HaloTag: a novel protein labeling technology for cell imaging and protein analysis.* ACS Chem Biol, 2008. **3**(6): p. 373-82.
5. Darnell, J.E., I.M. Kerr, and G.R. Stark, *Jak-Stat Pathways and Transcriptional Activation in Response to Ifns and Other Extracellular Signaling Proteins.* Science, 1994. **264**(5164): p. 1415-1421.
6. Levy, D.E. and J.E. Darnell, *STATs: Transcriptional control and biological impact.* Nature Reviews Molecular Cell Biology, 2002. **3**(9): p. 651-662.
7. Schmitt, H.M., et al., *An integrated system for optical biomolecular interaction analysis.* Biosensors & Bioelectronics, 1997. **12**(8): p. 809-816.
8. Muster, B., et al., *Respiratory chain complexes in dynamic mitochondria display a patchy distribution in life cells.* PLoS One, 2010. **5**(7): p. e11910.
9. Piehler, J. and G. Schreiber, *Biophysical analysis of the interaction of human ifnar2 expressed in E-coli with IFN alpha 2.* J Mol Biol, 1999. **289**(1): p. 57-67.
10. Piehler, J., L.C. Roisman, and G. Schreiber, *New structural and functional aspects of the type I interferon- receptor interaction revealed by comprehensive mutational analysis of the binding interface.* Journal of Biological Chemistry, 2000. **275**(51): p. 40425-40433.
11. Serge, A., et al., *Dynamic multiple-target tracing to probe spatiotemporal cartography of cell membranes.* Nat Methods, 2008. **5**(8): p. 687-94.
12. Kaminski, W.E., A. Piehler, and G. Schmitz, *Genomic organization of the human cholesterol-responsive ABC transporter ABCA7: Tandem linkage with the minor histocompatibility antigen HA-1 gene.* Biochemical and Biophysical Research Communications, 2000. **278**(3): p. 782-789.

13. Yamada, M., I. Takase, and N. Koutou, *Photopolymerization of Maleimide and Its N-Substituted Derivatives.* Journal of Polymer Science Part B-Polymer Letters, 1968. **6**(12PB): p. 883-&.
14. Kalie, E., et al., *The Stability of the Ternary Interferon-Receptor Complex Rather than the Affinity to the Individual Subunits Dictates Differential Biological Activities.* Journal of Biological Chemistry, 2008. **283**(47): p. 32925-32936.
15. Waichman, S., et al., *Maleimide Photolithography for Single-Molecule Protein-Protein Interaction Analysis in Micropatterns.* Analytical Chemistry, 2011. **83**(2): p. 501-508.
16. Sprague, B.L. and J.G. McNally, *FRAP analysis of binding: proper and fitting.* Trends in Cell Biology, 2005. **15**(2): p. 84-91.

6 Summary

Here I have demonstrated a novel, generic and highly efficient technique for micropatterning of proteins, artificial membranes and live cells based on the photochemical features of maleimide derivatives. To this end, I utilized glass-type substrates compatible with the surface sensitive analysis techniques employed in the thesis. A coating layer of a PEG polymer brush imparted the biocompatible nature of these surfaces that were subsequently coupled with specific chemical functionalities suitable for selective immobilization and patterning of biological entities. The flexibility of this approach for diverse surface capturing groups was successfully demonstrated using affinity- and covalent-based interactions. The well established maleimide chemistry emerged to be highly suitable for probing protein interactions in a quantitative fashion using ensemble measurement techniques as well as single-molecule means.

Summing up, the following immobilization and patterning methods were developed:

I. A site-specific, covalent protein immobilization method based on enzymatic transfer reaction. A protein of interest fused to ybbR peptide tag was selectively attached to biocompatible surfaces by the transfer of a prosthetic group P-pant, from CoA to a hydroxyl group in a serine residue which is a constituent in the ybbR peptide. This reaction is catalyzed by the PPTase Sfp.

II. Functional surface micropatterning was established by utilizing the photodestruction of maleimide moieties covalently bound to a PEG coated support. The patterning approach relies upon the ability of maleimide groups to undergo polymerization upon UV exposure without the assistance of a photoinitiator. Different chemical strategies for protein capturing were demonstrated.

III. Micropatterning of polymer-supported membranes was developed by coupling hexadecyl vinyl-ether to surface maleimides upon UV irradiation. Using this approach confinement, diffusion and interactions of reconstituted membrane receptors were studied.

IV. Micropatterning of membrane receptors in surface adhered live cells was established by the polymerization of surface maleimide with maleimide carrying cell adhesive peptides. The binary nature of the patterning strategy was exploited so that after UV

treatment, free maleimides that remained were reacted with selective chemical groups for site-specific immobilization of membrane receptors directly from cells.

The systems described here were analyzed using both ensemble and single molecule techniques. Therefore the methods developed hold promise as a generic tool to identify and characterize diverse biological systems using a wide variety of techniques.

7 Appendix

7.1 Publications

1. Waichman S., Roder F., Richter C.P., Birkholz O. and Piehler J., *Quantitative diffusion and interaction analysis of individual membrane proteins confined in micropatterned polymer-supported membranes.* Submitted.

2. Roder F., Waichman S., Paterok D., Schubert R., Richter C., Liedberg B. and Piehler J., *Reconstitution of membrane proteins into polymer-supported membranes for probing diffusion and interactions by single molecule techniques.* Anal Chem., **83**, 6792–6799, (2011).

3. Waichman S., You C., Beutel O., Bhagawati M. and Piehler J., *Maleimide photolithography for single-molecule protein-protein interaction analysis in micropatterns.* Anal Chem., **2**, 501-8 (2011).

4. Waichman S., Bhagawati M., Podoplelova Y., Reichel A., Brunk, A., Paterok D. and Piehler J., *Functional immobilization and patterning of proteins by an enzymatic transfer reaction.* Anal. Chem.,**82**, 1478–1485, (2010)

5. Lafont U., Waichman S., Valvo M. and Kelder E.M., *Sol-Gel and hard template-assisted synthesis of 3D nanostructured SnO_2 electrodes.* J Nanosci. Nanotechnol. **10**, 4273-4278 (2010)

6. Waichman S., Loechte S., Beutel O., You C. and Piehler J., *lateral organization of cell surface receptors for probing cellular events.* In preparation.

7.2 List of figures

7.3 Abbreviations

ACP	Acyl carrier protein
Anp	3-amino-3-(2-nitrophenyl)-propionic acid
AFM	Atomic force microscope

B. subtilis	Bacillus subtilis
BioMEMS	biomicro-electrochemical systems
BLM	Black lipid membrane
BT-thiol	Biotin-OEG_3-undecanethiol
CAMs	Cell adhesion molecules
CoA	Coenzyme A
CP	Carrier protein
DHPE	1,2-dihexadecanoyl-*sn*-glycero-3-phosphoethanolamine
DPN	Dip-pen nanolithography
EC	Extracellular domain
ECM	Extracellular matrix
EDTA	ethylenediaminetetraacetic acid
E.coli	Escherichia coli
FA	Focal adhesion
FCS	fluorescence correlation spectroscopy
FRAP	fluorescence recovery after photobleaching
FTIR	Fourier transform infra-red
GFP	Green Fluorescent Protein
GST	Glutathione S-transferases
HDVE	Hexadecyl vinyl ether
HTP	HaloTag protein
HTL	HaloTag ligand
ID	Intracellular domain
IFN	Interferon
IFNAR	Type I interferon receptor
Ig	Immunoglobulin
JAK1	Janus-activated kinase1
ME	mercaptoethanol
MEMS	Microelectromechanical systems

MPA-NHS	3-(maleimido)propionic acid N-hydroxy-succinimide ester
µCP	Microcontact printing
MI-RGD	Maleimide-RGD
MIR	Middle infra-red
NIR	Near infra-red
Nvoc	Nitroveratryloxycatbonyl
ORF	Open Reading Frame
PCP	Peptidyl carrier protein
PEG	Poly(ethylene) glycol
PEO	polyethylene oxide
PPT	phosphopantetheinyl transfer
PPTase	Phosphopantetheinyl tranferase
PM	Plasma membrane
PSM	polymer-supported membranes
RIfS	Reflectance interference spectroscopy
SAM	Self-assembled monolayer
SAv	Streptavidin
SEM	Scanning electron microscopy
SLB	Supported lipid bilayer membrane
SOPC	1-stearoyl-2-oleoyl-*sn*-glycero-3-phosphocholine
SPM	scanning probe microscopy
SPR	Surface plasmon resonance
SMT	Single-molecule tracking
STAT	Transducer and Activator of Transcription
SUV	Small unilamellar vesicle
t-BLMs	Tethered bilayer lipid membranes
TIRF	Total internal reflection fluorescence
TM	Transmembrane
Tris-NTA	Tris-(nitrilotriacetic acid)-OEG_7-thiol

Tyk2	tyrosine-kinase2
UV	Ultra-violet
VSUV	Very small unilamellar vesicle

Curriculum vitae

Name Sharon Waichman

Contact details Beery str. 25
55900 Ganey-Tikva, Israel
E-mail: sharonw4@gmail.com
Sharon.Waichman@biologie.uni-osnabrueck.de

Education

2007-present **PhD candidate in Biophysics**
University of Osnabrück, Germany
Advisor: Prof. Jacob Piehler
Thesis title: *Photopatterning for probing protein-protein interactions in artificial model systems and live cells*

2005-2007 **M.Sc. in Nanoscience and Nanotechnology (*cum laude)***
Delft University of Technology, the Netherlands
The Catholic University of Leuven, Belgium
Advisor: Dr. Erik M Kelder
Thesis title: *Synthesis and characterization of nanoarchitectured electrode materials for Li-ion batteries*

2000-2004 **B.Sc. in Chemistry (*cum laude)***
Bar-Ilan University, Israel
Area of specialization: Physical chemistry

Declaration

I hereby declare that the presented thesis 'Photopatterning for probing protein-protein interactions in artificial model systems and live cells' was prepared entirely on my own and I have not used outside sources without declaration in the text. Any concepts or quotations applicable to these sources are clearly attributed to them. I have not attempted a promotion before.

Osnabrueck, 27th June Sharon Waichman